COMBUSTION AND EXPLOSION OF CARBON NANOFIBERS

A Dissertation

by

JIAQI ZHANG

Submitted to the Office of Graduate and Professional Studies of
Texas A&M University
in partial fulfillment of the requirements for the degree of

DOCTOR OF PHILOSOPHY

Chair of Committee,	M. Sam Mannan
Co-Chair of Committee,	Chad V. Mashuga
Committee Members,	Mustafa Akbulut
	James Holste
	Andrea Strzelec
Head of Department,	M. Nazmul Karim

May 2016

Major Subject: Chemical Engineering

ABSTRACT

Although there is a fast growth in the production and application of nanomaterials, very little research about the fire and explosion hazards associated with nanomaterials has been done. Dust explosion studies on micro-size materials show that combustible engineered nanomaterials may possess high risk for explosion because increased specific surface area of nanomaterials may improve the ignition sensitivity and explosion severity. This study focuses on combustion and explosion of carbon nanofibers (CNFs), considering its large-scale production, wide application, and various handling processes. This study characterizes the morphology of CNFs with scanning electron microscope, the particle size distributions with Spraytec and Beckman Coulter, and the thermal stability with thermogravimetric analysis. Explosibility tests are performed in a customized 36-L dust explosion vessel and a minimum ignition energy apparatus (MIKE 3). Combining the characterization tests, explosibility tests, and theoretical analysis, this study provides a good understanding about combustion and explosion risk of CNFs after different processes – milling duration, and annealing at 1500 °C or 3000 °C.

In general, this study concludes that the minimum ignition energy of CNFs is higher than 1 J, which indicates a low ignition sensitivity. Minimum explosible concentration of CNFs varies from 105 g m^{-3} to larger than 300 g m^{-3}. The maximum overpressure is about 8 bar. CNF is classified as St-1 combustible dust with a deflagration index around 100 bar m s^{-1}.

It is also found that the smaller agglomerates caused by milling process not only reduces the minimum explosible concentration (MEC), but also increases the maximum pressure increase rate $[dP/dt]_{max}$.

Besides, the annealing process, either 1500 °C or 3000 °C, improves the graphite degree of CNFs and hence decreases the explosion severity with a lower $[dP/dt]_{max}$. Additionally, the 3000 °C annealing process reduces the iron content within CNFs and hence increased MEC. It is because the pyrophoric Fe-NPs could be ignited remotely with a favorable penetration topology of CNF agglomerates and therefore promotes the heating of unburnt CNFs and facilitates the overall combustion and explosion process.

This study also modifies an estimation method for maximum overpressure and proposes a heterogeneous model explaining the influential factors.

DEDICATION

To

My parents: Caifu Zhang and Jin’e Zhang

A happy family is but an earlier heaven.

--- John Bowring

ACKNOWLEDGEMENTS

Joining Texas A&M University is a wonderful journey in my life; meeting so many lovely people on Aggie land makes this journey even more colorful. I greatly appreciate my committee chair, Dr. Mannan, for all his guidance, advice, and help through this journey. Besides offering academic advises, he also provided tremendous professional suggestions, help, and protection to his students. I am so honored and grateful to be one of his students. My great appreciation also goes to my committee co-chair, Dr. Mashuga for his support and guidance of this research. He taught me to be a better researcher with his enthusiasm, experience, and knowledge in this research area. I would like to thank my committee members Dr. Holste, Dr. Akubulut, and Dr. Strzelec, for their guidance and support throughout this research. Thanks to Dr. Yi Liu and Dr. Hao Chen for their help that added to the success of this work.

I have to thank Diana, Arthur, and Jiaojun, who gave me guidance and help for designing and performing experiments in the 36-L dust explosion vessel. Also thanks to Hallie for being in the laboratory, helping me with the experiments, and bringing happiness to the laboratory. Thanks also go to my friends and colleagues and the department faculty and staff for making my time at Texas A&M University a great experience. Special thanks also go to members of the Mary Kay O'Connor Process Safety Center, and Dr. Mashuga's group, especially to Dr. Pasman, Dr. Waldram, Valerie, Alanna, Zhe, Yizhi, Ning, Xiaohong, Ruochen, Nirupama, Yan-ru, Wen, Pranav, and Purvali. I also acknowledge Dr. Tomasz Olewski and Nepu Saha from TAMU-Qatar for supporting the TGA revalidation tests.

I need to thank MKOPSC for funding my research and supporting me as a graduate research assistant. This work was supported primarily by the MKOPSC. I also gratefully acknowledge the financial support from the National Science Foundation EAGER Program (No.1321581) and the supplemental support for "Research Experiences for Undergraduates" from this program. I also want to thank Dow Chemical for the opportunity of MIE tests.

I have to acknowledge my dearest friends, Xuanxuan and Momo, for them bringing joy to my life and offering support and help when I experience difficulties. I also need to thank my boyfriend Jean-Sebastien for his love and support.

No word is enough to express my feelings for my parents. Thanks to my mother for always believing in me. I am thankful to my father for his support and guidance. Actually, I can’t thank them enough for the unconditional, countless love they gave me.

TABLE OF CONTENTS

Page

Page

Page

LIST OF FIGURES

Page

Page

Page

LIST OF TABLES

Page

CHAPTER I

INTRODUCTION

1.1 Motivations

Among the factors influencing dust explosibility, particle size has been widely investigated. The effect of particle size on explosion behaviors was concluded emphatically as (Eckhoff, 2003): MIE tends to reduce exponentially as particle size decreases; the "plateau effect" of particle size on MEC exists, which means that the minimum explosible concentration declines with reduced particle size until reaching a limiting stage where particles are too fine; the explosion severity can be significantly enhanced by reducing the particle size.

Given the seminal work stated above, extreme explosibility of nanoparticles have been expected due to a small dimension of nanoparticles. However, some research (Eckhoff, 2012; Worsfold, Amyotte, Khan, Dastidar, & Eckhoff, 2012) have claimed that the explosibility of nanoparticles is limited by impeded dispersion and high coagulation rates.

Nevertheless, experiments indicate that nanoparticles may possess extreme hazards of fire and explosion: it was surprisingly observed that single wall carbon nanotubes (SWCNTs) caught fire when exposed to a camera's flashlight (Ajayan et al., 2002). While conducting dust explosion tests of nano-titanium and nano-iron particles, it was found that these particles melted before igniters were triggered, which made it impossible to measure explosibility through ASTM standard procedures (Wu & Wu, 2008). Meanwhile, the supporting experimental data cited for the agglomeration effect

on explosibility of nanoparticles (Worsfold et al., 2012) may be caused by different oxidation degrees as stated in the original paper (Wu, 2010).

A big quantity of carbonaceous nanomaterials are produced world widely. It was reported that more than 300 tons of carbonaceous nanomaterial (carbon nanotubes, carbon nanofibers, fullerene, and so on) were produced annually. More than 800 products involved with carbonaceous nanomaterials were produced in 2011 (Piccinno & Gottschalk, 2012). As one of the most important members, carbon nanofibers have been applied in mainly four areas, including electronic components, polymer additive, gas storage, and catalyst support material (Jong & Geus, 2000). Composites with carbon nanofibers have been applied for bumpers and fenders of automotive uses, and aircraft braking systems (Pyrograf, 2012). Different processing methods of carbon nanofibers were used for these wide applications. Milling was applied for preparing shorter CNFs (F. Liu et al., 2003) while annealing was used for improving the purity (Andrews, Jacques, Qian, & Dickey, 2001; W. Huang, Wang, Luo, & Wei, 2003). However, research efforts about the explosibility are not enough, especially for the difference of carbon nanofibers after various processing methods.

Because of the complicated properties of nanoparticles, experimental data with controlled conditions and systematic analyses on multiple factors are urgently needed.

1.2 Objectives

The objective of this study is to identify the fire and explosion risks associated with carbon nanofibers. While several engineering processes are widely applied in

producing and customizing carbon nanofibers, this research aims to identify the influential factors of dust explosion in addition to a general conclusion about carbon nanofibers' explosibility. This study also aims to invest efforts on understanding the mechanism of dust explosion of carbon nanofibers as well as modifying a method to estimate the maximum overpressure of explosion of carbonaceous material.

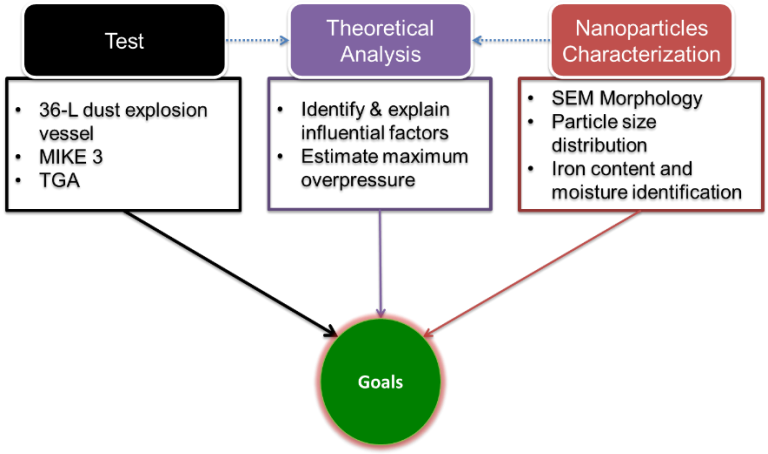

Figure 1. Study objectives

Specifically, as shown in Figure 1, the objectives of this research include:

1. Customizing and characterizing various types of carbon nanofibers. Two types of common engineering process are to apply - milling and annealing. It is also one of the objectives to understand the characterizations of these carbon nanofibers. Characterizations like iron content, moisture content, morphology, and particle distribution are needed due to their potential influence on the explosibility of carbon nanofibers. In addition, this study also aims to understand the hazard of carbon nanofibers in terms of health to protect the researchers.

2. Quantitatively measuring explosibility characteristics of these carbon nanofibers. These properties include the minimum ignition energy (MIE), minimum explosive concentration (MEC), maximum overpressure (P_{max}), and the dust explosion deflagration index (K_{St}). Besides, this study also aims to study the thermal stability (onset temperature T_{onset}, and oxidation temperature $T_{oxidation}$) of carbon nanofibers with thermogravimetric analysis (TGA).
3. Identifying and explaining the influential factors of carbon nanofibers' explosibility. This objective is to be achieved by analyzing the explosibility test results and the characterizations of various carbon nanofibers. In addition, this study will attempt to understand the mechanism of carbon nanofibers' combustion and explosion, and modify a current estimation method of the maximum overpressure of explosion of carbonaceous material.

1.3 Dissertation Organization

This dissertation is based on a current, on-going research program in the dust laboratory of the Mary Kay O'Connor Process Safety Center at Texas A&M University. Parts of the work in the dissertation were published in peer-reviewed publications.

This dissertation includes eight chapters:

Chapter I presents the motivations, objectives, and the organization of this dissertation.

Chapter II introduces the background and literature review about this research. It starts with the basics of dust explosion, such as the "dust explosion pentagon", several

dust explosion incidents dating back to 1785, and the development of standards and programs by agencies and government in the United States to prevent dust explosion incidents in several industries. Then it presents the explosibility characteristics and classifications used to describe a dust explosion behavior and rank the risk of a combustible dust, together with factors influencing these explosibility characteristics, especially the particle size. In addition, this chapter summarizes the current research results on dust explosion nanomaterials with the gaps identified. At last, the customized 36-L dust explosion vessel at Mary Kay O'Connor Process Safety Center is introduced.

Chapter III describes the material used in this research – carbon nanofibers, and their characteristics, which includes the iron content and moisture content identification, SEM morphology, and particle size distribution obtained by two different laser diffraction particle size analyzers (Malvern Spraytec and Beckman Coulter). In addition, health hazards of carbon nanofibers are also included in chapter III. To control these hazards, several personal protective equipment and other engineering controls are incorporated in the laboratory. This information is also presented in chapter III.

Chapter IV is focused on the study of thermal stability analysis of carbon nanofibers and combustion of carbon particles. Thermogravimetric analysis (TGA) is conducted for these carbon nanofibers at various conditions, such as different air atmosphere and temperature increase rates. It summarizes the thermal stabilities of these CNFs by identifying temperatures needed to react with air. In addition, the two-film model of carbon combustion is presented. This study also attempts to identify the limiting step of dust explosion of carbon particles with different diameters by theoretical

analysis. Energy conservation during the combustion of carbon particles is also discussed.

Chapter V starts with an introduction about the minimum ignition energy of different materials and energy generated by different electrostatic discharge types. With the hypothesis that the iron content may increase the ignition sensitivity and risk of carbon nanofibers, this study conducted MIE test in a MIKE 3 apparatus. The tests, observation, and results are summarized.

Chapter VI introduces a finding of this study that dust explosion of carbon nanofibers is promoted by iron nanoparticles. This study conducts a comprehensive study of identifying the minimum explosible concentration of various carbon nanofibers in the 36-L dust explosion vessel. Then it is found that MECs of carbon nanofibers with higher iron content and MECs of smaller agglomerates are much lower than others. A qualitative heterogeneous model based on heat transfer is also proposed to explain the effect of agglomerate size and Fe-NPs on combustion: smaller agglomerates with bigger specific surface area lead to faster temperature rise; pyrophoric Fe-NPs can be ignited remotely with a favorable penetration topology of CNF agglomerates and therefore promotes the heating of unburnt CNFs and facilitates the overall combustion and explosion process.

Chapter VII presents both the experimental results and the theoretical analysis about explosion violence of carbon nanofibers, such as P_{max} and K_{St}. Explosibility tests with 10 kJ ignition energy are conducted in the 36-L dust explosion vessel to identify the explosion violence at different concentrations. Influential factors are also identified. In

addition, this chapter proposes an improved estimation method for the maximum overpressure according to the two-film model of carbon combustion. The laminar burning velocity is estimated based on thin film theory. Besides, this chapter modifies the heterogeneous model proposed earlier to demonstrate the influential factors identified from experimental results.

Chapter VIII summarizes the main conclusions from the current research and provides some recommendations for future work.

CHAPTER II

BACKGROUND AND LITERATURE REVIEW[*]

2.1 Dust Explosion and its Pentagon

A dust explosion was described as *"An explosion is a gas-dynamic phenomenon characterized by such a rapid increase in system pressure that destructive forces are generated. … For a dust explosion, specifically, it is usually the rapid chemical oxidation of dust particles dispersed in air that leads to a rapid energy release which increases the temperature of the system so rapidly that a pressure increase follows."* (Cashdollar & Hertzberg, 1987).

A "fire triangle" is used to describe the three elements needed to cause a fire - fuel, oxidant, and ignition source. Similarly, the concept of "dust explosion pentagon" was proposed (Kauffman, 1982) as shown in Figure 2. These five indispensable elements are:

1. Combustible dust. It is defined as: *"a combustible particulate solid that presents a fire or deflagration hazard when suspended in air or some other oxidizing medium over a range of concentrations, regardless of particle size or shape"* (NFPA, 2012c).

[*] Part of this chapter is reprinted from "Dust explosion of Carbon Nanofibers Promoted by Iron Nanoparticles" by Zhang, J., Chen, H., Liu, Y., Elledge, H., Mashuga, C.V., & Mannan, M.S. (2015). *Industrial & Engineering Chemistry Research, 54*(15), 3989-3995, with permission from American Chemical Society

2. Ignition source. Some ignition sources for dusts are flames and direct heats, hot work, incandescent materials, hot surfaces, sparks (electrical, friction, or impact), self-heating, static electricity, and lightning (Mannan, 2005).
3. Oxygen
4. Dispersion of dust particles with sufficient quantity and concentration
5. Confinement of the dust cloud by an enclosure or partial enclosure

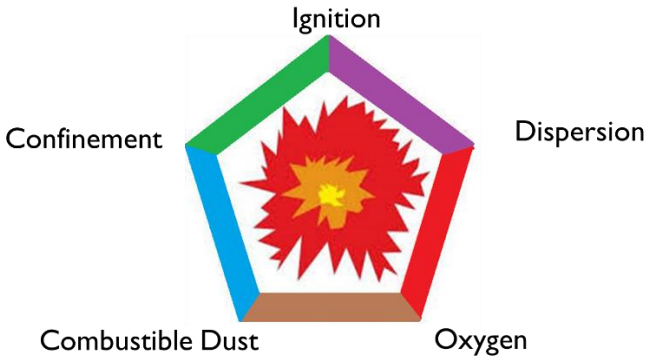

Figure 2. Dust explosion pentagon, reproduced from (Kauffman, 1982)

In an industrial dust explosion, the air disturbance and shock wave of a primary explosion brings more combustible dust into air and causes a secondary explosion. Usually, the secondary explosion is more destructive than the primary one due to the larger amount of dust involved in the explosion.

2.2 Dust Explosion Incidents and their Influence

Dust explosion incidents have a long history and serious consequences. The first recorded dust explosion occurred in Turin, Italy, on December 14, 1785 (Eckhoff, 2003). The incident occurred in a flour warehouse, where a boy was employed in stirring flour under the light of a lamp. It is believed that the explosion was initiated when the fine flour particles in the air met the fire of lamp.

During the last two centuries, dust explosion incidents keep occurring worldwide. Materials involved in these incidents are mainly corn starch, grain dust, flour, metal, coal, plastic, and wood (Mannan, 2005). A severe dust explosion incident can cause dozens of fatalities. In 1919, an explosion occurred at Cedar Rapids, Iowa. This corn explosion killed 43 people. Another corn explosion occurred in Peking, IL, in 1924, and killed 42 people.

In 1987, OSHA issued the Grain Handling Facility Standard (29 CFR 1910.272), together with several other OSHA standards to address the hazards of combustible grain dust in specific types of facility. Besides this, there is no comprehensive general industry OSHA standard to address hazards of combustible dusts.

There are several consensus standards presented by National Fire Protection Association (NFPA) applied to industries for handling combustible dusts. A few of these standards are listed below together with reference to the most recent version while the original documents were issued during 1960s to 1980s.

1. NFPA 61, Standard for the Prevention of Fires and Dust Explosions in Agricultural and Food Processing Facilities (NFPA, 2013a)

2. NFPA 484, Standard for Combustible Metals (NFPA, 2014)
3. NFPA 654, Standard for the Prevention of Fires and Dust Explosions from the Manufacturing, Processing, and Handling of Combustible Particulate Solids (NFPA, 2013b)
4. NFPA 655, Standard for Prevention of Sulfur Fires and Explosions (NFPA, 2012a)
5. NFPA 664, Standard for the Prevention of Fires and Explosions in Wood Processing and Woodworking Facilities (NFPA, 2012b)

Despite the NFPA regulations, incidents continue to occur. In 2003, three severe industrial explosions involving combustible powders occurred in the United States (Blair, 2007):

1. On January 29, 2003, an explosion and fire of fine plastic powders destroyed the West Pharmaceutical Services in Kinston, North Carolina. It killed 6 people and injured dozens.
2. On February 20, 2003, an explosion and fire of resin dust damaged the CTA Acoustics manufacturing plant in Corbin, Kentucky. It killed 7 people.
3. On October 29, 2003, explosions of aluminum dust damaged the Hayes Lemmerz manufacturing plant in Huntington, Indiana. It injured 3 people.

These intensive dust explosion incidents brought attention of the public, agencies, and government to address the hazards of combustible dusts. A special study focused on dust explosions was conducted by the U. S. Chemical Safety and Hazard Investigation Board (CSB) following these incidents. It was reported that 281

combustible dust incidents took place in the United States from 1980 to 2005, killing 119 workers and injuring 718 others (Blair, 2007). The report also recommended that *"OSHA should issue a comprehensive dust standard that applies to general industry"*. On October 19, 2007, OSHA initiated a Combustible Dust National Emphasis Program, which described policies and procedures regarding inspection of facilities that handle combustible dust. This program covered, at the minimum, the following dusts (OSHA, 2007):

- Metal dust: aluminum, magnesium
- Wood dust
- Plastic dust
- Biosolids
- Organic dust: sugar, paper, soap, and dried blood
- Dusts from certain textiles

Again, on February 7, 2008, an explosion and fire of sugar destroyed the Imperial Sugar refinery in Savannah, Georgia. It caused 14 deaths and 38 injuries (Vorderbrueggen, 2011). After this incident, OSHA decided to intensify its focus on hazards of combustible dust (OSHA, 2008). It intends to *focus on specific group that have experienced either frequent combustible dust incidents or combustible dust incidents with catastrophic consequences*. It states that facilities with combustible dusts, which are contained within dust control systems, but pose hazard of a deflagration, explosion or fire, may be covered by 29 CFR 1910.22 (housekeeping) or 29 CFR 1910.17(c) (housekeeping in storage).

With all these efforts of controlling the hazards of combustible dust, incidents are still happening. It suggests that the "battle" against combustible dust still requires efforts from industries, government, and academia. Here are several incidents that occurred in the recent past:

1. On December 9, 2010, an explosion of titanium powder occurred at New Cumberland A.L. Solutions plant in West Virginia. It fatally injured 3 people (CSB, 2011).
2. In 2011, 3 iron dust fires occurred at the Hoeganaes facility in Gallatin, TN. These incidents caused 5 fatalities (CSB, 2012).
3. On October 9, 2012, a combustible dust explosion occurred at US Ink in East Rutherford, NJ. It injured 7 workers (CSB, 2015).
4. On August 2, 2014, a metal dust explosion happened at an auto- parts factory in Kunshan, Jiangsu, China. It resulted in 146 fatalities and 95 injuries remaining hospitalizations (Nie et al., 2015).
5. On June 27, 2015, colored festival powder exploded at an outdoor music concert at the Formosa Fun Coast, Taiwan. It caused more than 500 injuries (Botelho & Wang, 2015).

2.3 Explosibility Characteristics, Classification

2.3.1 Explosibility characteristics

Important explosibility characteristics of dust suspensions are:

1. Minimum explosive concentration (MEC)

2. Minimum ignition temperature (MIT) of a dust layer or a dust cloud
3. Minimum ignition energy (MIE)
4. Limiting oxygen concentration (LOC)
5. Explosion pressure characteristics
    a. Maximum explosion pressure (P_{max})
    b. Maximum rate of pressure rise ($[dP/dt]_{max}$)
    c. Average rate of pressure rise
    d. Deflagration index (K_{St})

These characteristics are used to depict dust explosion behaviors. While other characteristics are more self-explanatory, the deflagration index may need more description. This important parameter to evaluate dust explosion was introduced by Bartknecht (Eckhoff, 2003). He reported that the "cube root law" was valid for numerous dusts in geometrically similar vessels larger than 0.04 m^3:

$$\left[\frac{dP}{dt}\right]_{max} V^{1/3} = \text{constant} \equiv K_{St} \quad (1)$$

where

P is the pressure, bar;

t is time, s;

V is the volume of space explosion confined in, m^3;

K_{St} is the deflagration index, which is the value at the optimum dust concentration, bar·m s^{-1}.

It needs to be noted that the validity of the equation above is based on the following assumptions (Abbasi & Abbasi, 2007; Eckhoff, 2003):

- Tests are performed in geometrically similar vessels
- The flame thickness is negligible when compared to the vessel radius
- The burning velocity is identical in all volumes

These characteristics are usually obtained through experimental tests. Several kinds of equipment were designed and built. Before 1980, several data have been generated from the "Hartmann tube". However, due to the wall effects of its cylindrical shape, it was not able to generate a uniform environment for dust dispersion and turbulence. Therefore, K_{St}, P_{max}, MEC, and LOC are currently tested in ISO 1 m^3 vessel and 20-L spherical vessel (Abbasi & Abbasi, 2007). MIE is usually determined through the MIKE 3 apparatus while several equipment are qualified to determine the MIT of a dust layer or a dust cloud. Detailed information about a spherical vessel and a MIKE 3 apparatus are included in Chapter VI and Chapter V respectively. Definitions, test methods, and applications of these properties are summarized in Table 1.

Table 1. Explosibility characterizations and test standards of combustible dusts

Property	ASTM standard	Description
$K_{St}=(dP/dt)_{max}V^{1/3}$	ASTM E1226 (ASTM, 2012a)	Deflagration index, measure the relative explosion severity compared to other dusts
P_{max}	ASTM E1226 (ASTM, 2012a)	Maximum overpressure, used to design enclosures and predict the severity of the consequence
MIE	ASTM E2019 (ASTM, 2013a)	Minimum ignition energy, used to predict the ease and likelihood of ignition of a dispersed dust cloud
MEC	ASTM E1515 (ASTM, 2014)	Minimum explosive concentration, used to measure the minimum amount of dust required to spread an explosion
LOC	ASTM E2931 (ASTM, 2015)	Limiting oxygen concentration, determine the least amount of oxygen required for explosion propagation through the dust cloud
MIT	ASTM E2021 (ASTM, 2013b) ASTM E1491 (ASTM, 2012b)	Minimum ignition temperature, the lowest temperature needed to trigger an explosion of a dust layer or a dust cloud

Produced based on (Dastidar, Nalda-Reyes, & Dahn, 2005)

2.3.2 Explosibility classification

There are several classifications for combustible dusts and their explosion behaviors. Two classifications based on the explosibility characteristics are described here.

Because the "cube root law" is valid for vessels with similar geometry, and the 20-L spherical vessels are widely applied for explosibility tests, the classification method based on the K_{St} value is adopted. Table 2 describes the dust explosion class and explosion features in each class.

Table 2. Explosibility classification based on K_{St} value

K_{St} (bar ·m s^{-1})	Dust explosion class	Explosion features
0	St 0	No explosion
0< K_{St}<200	St 1	Weak
200<K_{St}<300	St 2	Strong
300<K_{St}	St 3	Very strong

Another index was developed by the Bureau of Mines to compare the explosibility of other combustible dusts with Pittsburgh coal. It includes both explosion severity characteristics (ES) and explosion/ignition sensitivity characteristics (IS). Parameters like $[dP/dt]_{max}$ and P_{max} are used to describe ES while MIE, MIT, and MEC are applied for IS. The index is calculated by the following equations (Abbasi & Abbasi, 2007):

$$IE=IS\times ES \tag{2}$$

$$IS=\frac{\left(MIT\times MIE\times MEC\right)_{Pc}}{\left(MIT\times MIE\times MEC\right)_{sample}} \tag{3}$$

$$ES=\frac{\left(MEP\times MRPR\right)_{Pc}}{\left(MEP\times MRPR\right)_{sample}} \tag{4}$$

where

MEP is the maximum explosion pressure, P_{max};

MRPR is the maximum rate of pressure rise, $[dP/dt]_{max}$;

Pc means Pittsburgh coal.

It can be found that the second classification is more comprehensive by including most of the explosibility characterizations. However, it also means it needs almost all the explosibility tests to properly classify a kind of combustible dust. Hence, the application of these classifications should be chosen flexibly.

2.3.3 Influential factors (particle size) of explosibility

There are several factors affecting dust explosibility. These factors can be the properties of the combustible dust or the environment when explosion occurs. For example, chemical composition, particle size, and moisture content of combustible dust can affect the explosibility (Cashdollar, 2000; Eckhoff, 2003; Mannan, 2005). In addition, the explosibility of certain combustible dust changes with the presence of various oxygen concentrations, inert gases and inert dusts, and flammable gases (Dastidar et al., 2005; Dastidar, 2005; Jiang, Liu, & Mannan, 2014; Jiang, Liu, Mashuga, & Mannan, 2015). The conditions, like ignition temperature and turbulence of the dust cloud when explosion occurs, also matter (Amyotte, Chippett, & Pegg, 1988; Bradley, Lau, & Lawes, 1992; Cashdollar, 2000; van der Wel, van Veen, Lemkowitz, Scarlett, & van Wingerden, 1992), which are also identified (Abbasi & Abbasi, 2007). Among these factors, particle size is one of the factors where literature focuses on. In general, the decrease of particle size can increase the fire and explosion risk of combustible dusts by lowering the MIE and MEC but increasing the value of P_{max} and K_{st}.

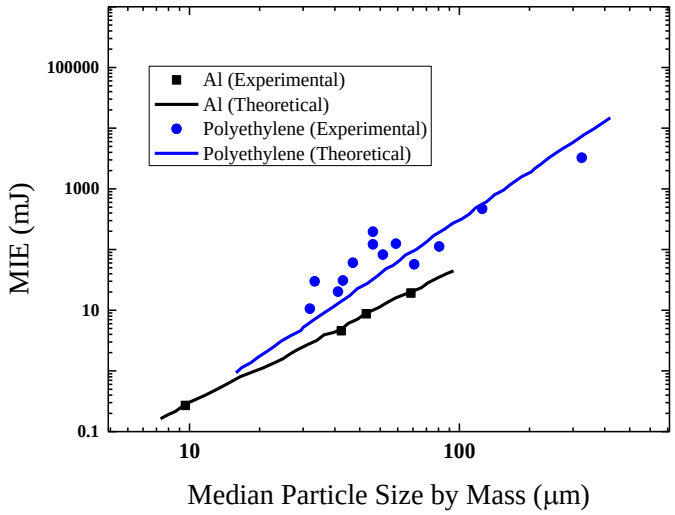

Figure 3. Minimum electric spark ignition energy of clouds in the air as functions of median particle size and theoretical line (reproduced from (Eckhoff, 2003))

MIE is the most sensitive parameter affected by decrease in particle diameter. As shown in Figure 3, experimental results show that MIE of polyethylene decreases from 1000 mJ to 10 mJ when mean particle size decreases from 100 μm to 25 μm; MIE of aluminum particle decreases from 10 mJ to less than 1 mJ when its median particle size decreases from 50 μm to 10 μm (Bartknecht, 1987). Based on these results, a theoretical relation between MIE and mean particle diameter (d) was obtained for polyethylene as below (Kalkert & Schecker, 1979):

$$\text{MIE} \propto d^3 \tag{5}$$

Another theoretical analysis was conducted based on the following assumptions:

- MIE is the energy needed to sustain ignition of a given dust cloud
- The gas follows the ideal gas law

- Particles are spherical

Then the relation between particle size and MIE depends on the controlling step of explosion process (Bouillard, Vignes, Dufaud, Perrin, & Thomas, 2010):

When it is in the kinetically controlled regime:

$$\text{MIE} \propto d^3 \tag{6}$$

When it is in the diffusion controlled regime:

$$\text{MIE} \propto d^{1.5} \tag{7}$$

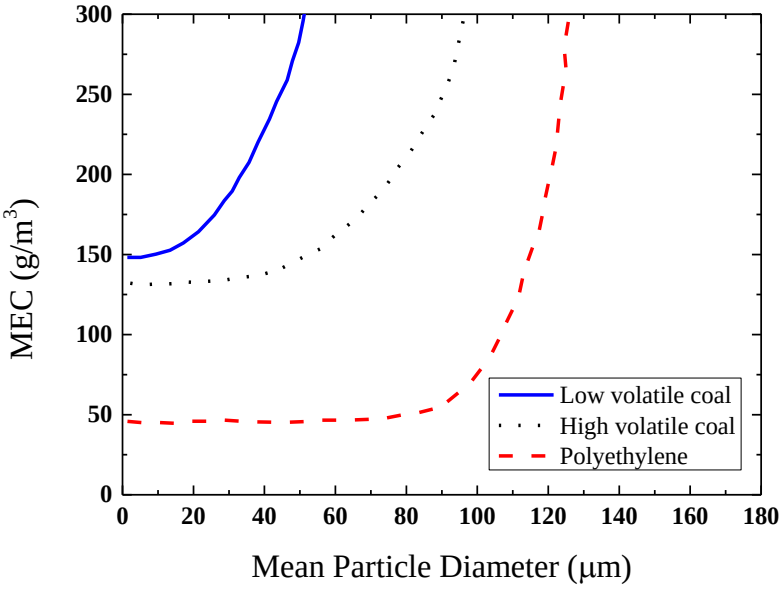

Figure 4. Influence of mean particle diameter on MEC (reproduced from (Eckhoff, 2003))

Particles with smaller diameters also have a lower MEC to cause a dust explosion. However, the MEC remains the same when the diameter reaches a certain

limit. It is called the “plateau effect”. As shown in Figure 4, this limit of diameter varies among different combustible dusts. For example, it is about 80 μm for polyethylene, but 10 μm for low volatile coal (Cashdollar & Hertzberg, 1987).

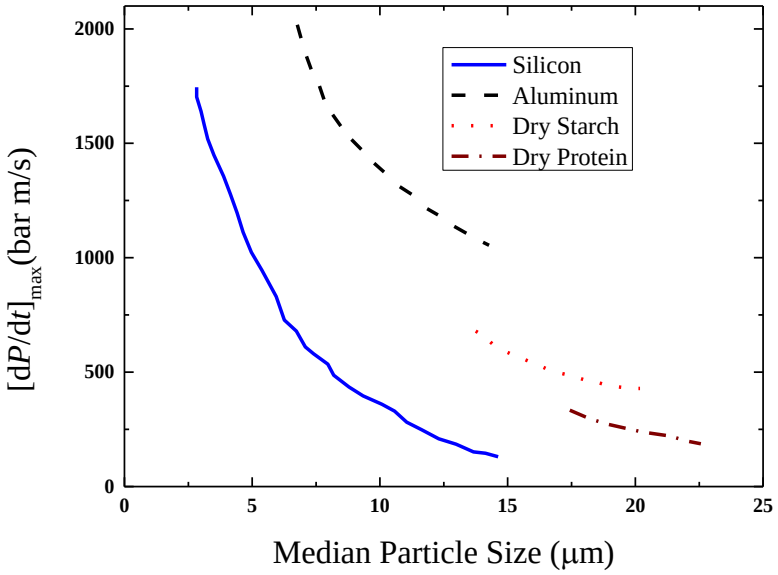

Figure 5. Influence of particle size on $[dP/dt]_{max}$ (reproduced from (Eckhoff, 2003))

When particle size or the specific surface area goes down, the explosion violence increases. This effect was supported by experimental results of silicon, aluminum, starch, and protein (Eckhoff, Parker, & Gruvin, 1986). A linear relation correlation was found between specific surface area and maximum rate of pressure rise for aluminum dust (Bartknecht, 1987).

2.4 Current Studies on Dust Explosion of Nanomaterials

Based on the trends of micro-particles, combustible nanoparticles were expected to have extreme ignition sensitivities and explosion severities (Eckhoff, 2003). The question whether dust explosion risks are enhanced when handling nanoparticles compared with micro-size particles was raised in about 2010. Many studies about dust explosion of nanomaterials, especially metal nanoparticles and carbonaceous particles have been performed.

A small-scale test apparatus was built and applied for testing the explosibility characteristics of several nanomaterials (Holbrow et al., 2010) together with a modified Kuhner MIKE 3 test apparatus. These nanomaterials include aluminum nanoparticles, iron nanoparticles, zinc nanoparticles, copper nanoparticles, carbon nanofibers, and carbon nanotubes. MIE, P_{max}, and K_{St} values of these nanomaterials were reported. It was concluded that P_{max} and K_{St} of nanoparticles were similar to conventional micro-scale powders, while MIE of some nanoparticles were much lower.

A theoretical analysis was conducted by Dr. Eckhoff based on inter-particle cohesion forces, fast coagulation process, and flame propagation mechanism (Eckhoff, 2011, 2012). It is concluded that the ignition sensitivities and explosion severity of nanoparticles may be limited by the unsatisfied dispersibility and fast coagulation rate. In addition, the combustion of volatiles becomes the rate controlling process for smaller particles (<10 μm), which means the size does not have influence any more. The cause of the reported low MIEs of some nanoparticles is not clear. The small primary particle

size or the high reactivity of nanomaterials can contribute to this phenomena (Eckhoff, 2011, 2012).

A study on explosion characteristics of aluminum nanopowders (35 nm and 100 nm) was performed (Wu, 2010). Values of P_{max}, $K_{St,}$ MEC, and MIE were obtained from a 20-L apparatus and a 1.2 L Hartmann apparatus. After comparing with the values of 40 μm aluminum particles, it was concluded that both the P_{max} and K_{St} increased while the MIE decreased. Hence, the dry milling process which can break particles down to nanoscales presents a high risk of dust explosion for aluminum production process.

In addition, analytical models were developed to explain the dependency of the combustion times with the particle diameter (Bouillard et al., 2010). Based on these models, the MIT and MIE decrease as the particles become smaller, which means nanoparticles may possess high risk of combustion and explosion. It was also predicted that there is no big variation of MECs as particle size changes.

Explosibility of micron- and nano-size titanium powders was also studied (Boilard, Amyotte, Khan, Dastidar, & Eckhoff, 2013). It was found that nano-titanium was much more sensitive than micron-titanium, so that even low spark energies can cause explosions. In addition, this high sensitivity makes it impossible to apply the traditional explosion test procedure to test the explosibility of nano-titanium particles.

Another explosibility study of metal nanoparticles was performed (Krietsch, Scheid, Schmidt, & Krause, 2015). Compared to the micro-size particles, most nanoparticles do not show a more critical burning behavior nor explosion severity. However, copper becomes flammable when it goes down to nano-scales. In addition, due

to the shear force of the dispersion process nanoparticles with high ignition sensitivities may react with air before triggering the igniters, which makes it impossible to apply the standardized methods for explosibility tests (ASTM, 2012a, 2014).

Most recently, several carbonaceous nanoparticles were studied: fullerene, single wall carbon nanotubes (SWCNTs), carbon black, multi-wall carbon nanotubes (MWCNTs), graphene, carbon nanofibers (CNFs), and graphite (Turkevich, Dastidar, Hachmeister, & Lim, 2015). Properties like MEC, MIE, MIT, P_{max} and K_{St} were measured. The results showed that the MECs of carbonaceous nanoparticles were comparable to the MECs of micro-size carbon particles, such as coals, carbon blacks, and graphite. In addition, these materials can be classified as St-1 explosion class except for fullerene, which lies on the border of St-1 and St-2. The explosion susceptibility is enhanced for carbonaceous nanoparticles considering their lower MIEs than the graphite.

Therefore, it can be found that within the last five years, much of the efforts to understand the combustion and explosion risk of nanomaterials were investigated through experimental tests, theoretical analyses, analytical models, and even equipment design and construction. Due to the variation in nanomaterial properties, equipment size and shape, and experimental conditions, there are still conflicting results among these experiments. In general, the fire and explosion risks of nanomaterials are summarized as:

- Nanoparticles, especially metal nanoparticles, possess much lower MIEs than micro-size particles, even lower than 1 mJ. It indicates that high ignition sensitivities are expected for nanoparticles. Smaller primary particle size or

improved reactivity may contribute to this. Therefore, efforts are still needed to explore the reason for the lower MIEs.

- Enhanced explosion violence is obtained in some nanoparticle experiments while others showed similar values of P_{max} and K_{St} as micro-size particles. This disagreement may be caused by different chemical properties of the materials tested in addition to their particle size difference.
- No significant change was presented for MECs. A "plateau" effect is expected when particle size is reduced to nanoscales.
- To better understand the fire and explosion risk of nanomaterials, more information and characterizations are needed due to nanoparticles' complex properties.

2.5 36-L Dust Explosion Vessel

2.5.1 The 36-L dust explosion vessel

A customized 36-L dust explosion vessel was built in the Mary Kay O'Connor Process Safety Center, Department of Chemical Engineering, at Texas A&M University (Castellanos, Carreto-Vazquez, et al., 2014; Castellanos, Lewandowski, et al., 2014).

Figure 6. The 36-L dust explosion vessel

As shown in Figure 6, the 36-L dust explosion test apparatus consists of:

- An explosion chamber: a semi-spherical vessel made of stainless steel and a capacity of 36-L, as well as a MAWP (Maximum Allowable Work Pressure) of 1000 psia (6.9 MPa);
- A dispersion system: the apparatus is equipped with a compressed air reservoir made of stainless steel, has a design pressure of 1800 psia (12.4 MPa), a dust storage container with overall dimensions of 2*8 in (diameter, *h*), and a nozzle (installed inside the explosion chamber) to spray the dust;
- Ignition system (top-right of Figure 6): consists of chemical igniters placed at the center of the chamber and can be triggered by an electrical spark;

- Vacuum system: consists of a vacuum pump with a capacity of 0.0017 psia (11.7 Pa), a manual valve, and a filter with element nominal pore size of 60 μm (for micro-size particles) or 0.5 μm (for nano-size particles);
- Control unit (bottom-right of Figure 6): consists of a control box that can be operated in manual or automatic operation mode. It also has a data acquisition and analysis system which can collect pressure data (P vs. t and [dP/dt] vs. t) by pressure transducers, and a computer with Lab View software to show the pressure data to the operators;
- Vent line: depressurizes the explosion chamber after every test;
- Extraction line: extracts the particles out to the atmosphere;
- Hybrid gas mixture lines: can mix fuel, nitrogen, and air to perform a hybrid mixture test.

This equipment is capable of determining the explosion characteristics of combustible dusts, including maximum explosion pressure (P_{max}), maximum rate of pressure rise ($[dP/dt]_{max}$), deflagration index (K_{St}), minimum explosible concentration (MEC), and limiting oxygen concentration (LOC).

A schematic diagram of the vessel is shown in Figure 7. The control unit, the extraction line, and the hybrid mixture lines are not included.

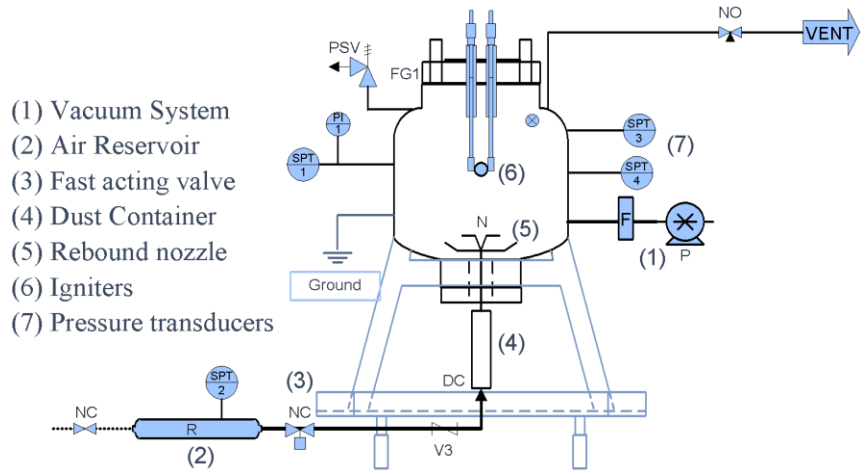

Figure 7. Schematic diagram of 36-L dust explosion vessel (Castellanos, Carreto-Vazquez, et al., 2014; Castellanos, Lewandowski, et al., 2014)

For a typical pure dust test, the vertical dispersion method is employed. The general operation procedure is:

Step 1: Load dust samples into the dust container, which is located below the vessel;

Step 2: Close the vessel after installing the igniters and the nozzle;

Step 3: Purge compressed air into the air reservoir;

Step 4: Vacuum the vessel with the vacuum system;

Step 5: Open the fast acting valve (item 3 in Figure 7), which is between the air reservoir and the dust container. The reservoir pressure disperses the sample into the vessel from the bottom.

Step 6: The igniters will be triggered by the LabVIEW program automatically after a certain period of time. The LabVIEW program also catches the signals from the pressure transducer and converts them into a pressure versus time profile.

To compare with commercial equipment, there are three dispersion nozzles widely used in standard 20-L dust explosion chambers: perforated ring, rebound, and Dahoe. Considering the dust plugging issues with the annular holes of perforated ring nozzles (Amyotte, 2013), a rebound nozzle was selected for the dispersion process in our 36-L dust explosion chamber. In order to obtain the same dispersion behavior as the standard 20-L dust explosion chamber, three significant factors – the pressure in the air reservoir, the vacuum level of the vessel, and the ignition time delay - were calibrated. Explosibility tests were performed in this customized equipment to participate the international round robin testing. The results showed a good agreement with other testing equipment, which ensured the repeatability and credibility of this customized equipment (Castellanos, Carreto-Vazquez, et al., 2014; Castellanos, Lewandowski, et al., 2014).

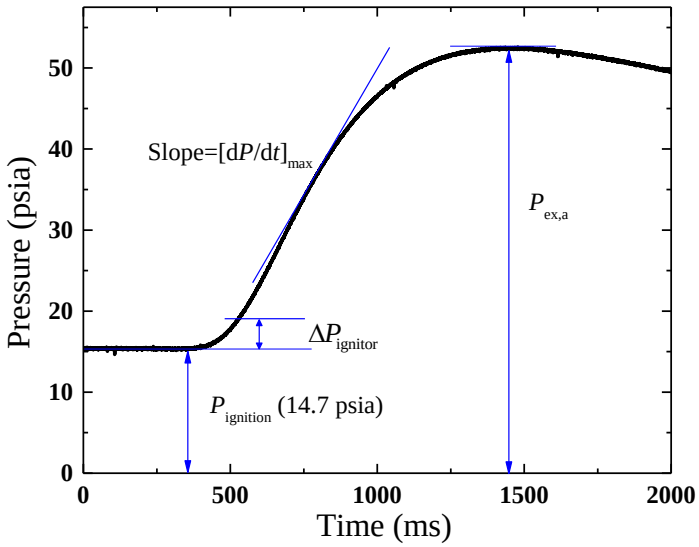

Figure 8. A typical pressure-time profile

A typical pressure profile with essential parameters is plotted in Figure 8. $P_{ignition}$ is the absolute pressure when the ignitor is activated. $P_{ignition}$ depends on Step 3, the compressed air stored in the air reservoir, and Step 4, the pressure inside the vessel after the vacuum process. Calibration was performed based on the volume ratio between the vessel and the air reservoir, and the capability of the fast acting valve, to ensure the ignition occurs at atmospheric pressure (101.325 KPa). Therefore, in every test, the air reservoir is compressed to 300 psia (2.1 MPa) while the vessel is vacuumed to 10.3 psia (71 KPa), as specified in the standard operating procedure.

$P_{ex,a}$ is the maximum explosion pressure (absolute pressure) reached during a single deflagration. The main contributors to $P_{ex,a}$ are the energy released from the

chemical igniters and the combustible dust. $\Delta P_{\text{ignitor}}$ is the pressure rise in the chamber due to the occupied energy of the ignitor in the air at atmospheric pressure. This is also the absolute pressure value of $P_{\text{ex, ignitior}}$ and is measured by triggering an ignitor without loading any dust sample.

$[dP/dt]_{max}$ is the maximum slope that can be found in a pressure profile. The LabVIEW program will search for it and will change the $[dP/dt]$ search time to 25 ms if the explosion is very weak.

2.5.2 Highlights of process safety analysis

A comprehensive process safety analysis (PSA) was conducted and approved by the Department of Chemical Engineering, and the Office of Engineering Safety of Texas A&M University.

The high pressure produced during the tests is one potential physical hazard. During the test, the dust explosion of carbonaceous material may produce maximum pressures around 10 bars (1 MPa). The 36-L vessel is capable of handling those pressures because it was designed and fabricated in accordance with the ASME Boiler and Pressure Vessel Code, Section VIII. The current 36-L vessel was hydrostatically tested at 1,500 psi (10.3 MPa) and therefore its MAWP is 1,000 psia (6.9 MPa). The air reservoir is able to support pressures up to 1,800 psia (12.4 MPa), and pipelines and connections are made of stainless steel (SS 316) that are able to support pressures up to 2,200 psi (15.2 MPa).

Another possible scenario is that the vacuum indicator could become damaged during an explosion and be the source of release for the high pressure due to its MAWP of 30 psi (206.8 KPa). To control this hazard, a valve was installed between the vacuum indicator and the 36-L vessel. During every test, the operator must close the valve. This step is included in the standard operating procedure.

CHAPTER III

CARBON NANOFIBER CHARCTERIZATION*

3.1 Carbon Nanofibers

The CNFs used in this study were obtained from Pyrograf Products, Inc., an affiliate of Applied Sciences, Inc. Carbon nanofibers, also known as Stacked-Cup Carbon Nanotubes, have a unique morphology in which graphene planes are canted from the fibers axis, resulting in exposed edge planes on the interior and exterior surfaces of the fibers (Monthioux, Noé, & Dussault, 2007).

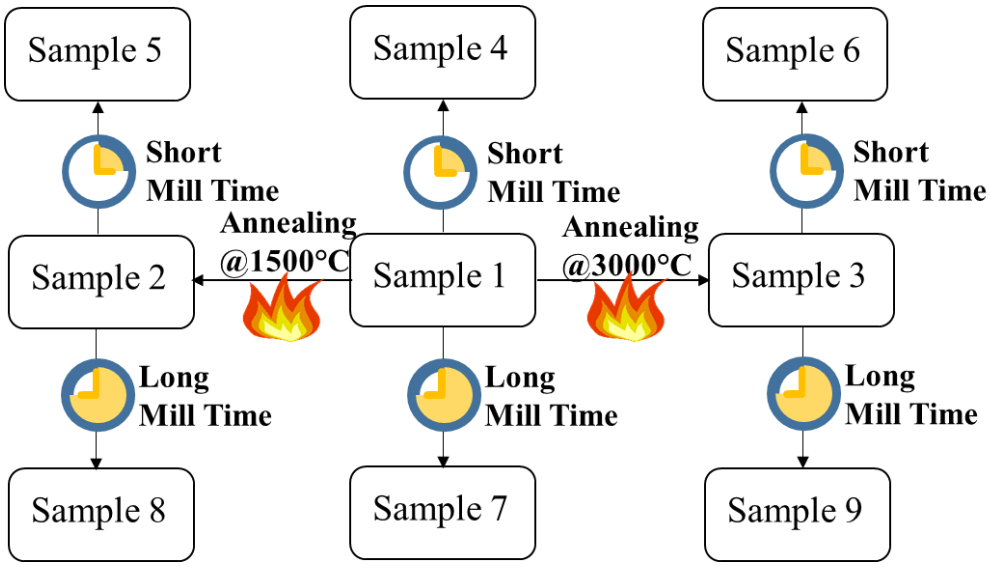

Figure 9. CNF sample preparation process

* Part of this chapter is reprinted from "Dust explosion of Carbon Nanofibers Promoted by Iron Nanoparticles" by Zhang, J., Chen, H., Liu, Y., Elledge, H., Mashuga, C.V., & Mannan, M.S. (2015). *Industrial & Engineering Chemistry Research, 54*(15), 3989-3995, with permission from American Chemical Society

Nine CNF samples were investigated in this study. Sample 1 was produced via chemical vapor deposition on iron catalysts. Samples 2 and 3 were obtained from sample 1 by annealing in an inert atmosphere (nitrogen) at 1500 ℃ and 3000 ℃ respectively. Samples 4, 5, and 6 were obtained respectively from samples 1, 2, and 3 by mechanical milling, with bulk densities increased from 21 kg m^{-3} to 125 kg m^{-3}. Samples 7, 8, and 9 were obtained from samples 1, 2, and 3 by applying longer mechanical milling, with bulk density further increased to 190 kg m^{-3}. The detailed sample preparation process was shown in Figure 9.

3.2 Iron Nanoparticles and Iron Content

The annealing process is usually employed to make materials more crystallized and stable by reordering or eliminating frustrations or unsaturated bonds. Moreover, some impurities could be removed by the annealing process, for example, iron nanoparticles which were used as a catalyst to produce carbon nanofibers. Previous research shows that iron nanoparticles, whose diameters were similar to these carbon nanotubes, existed both at nanotube tips and inside the cores (Andrews et al., 2001).

Iron content was identified according to the ASTM E 394 (ASTM, 2004), as shown in Table 3. The Fe content in the CNFs was around 1.4% for the raw product. After annealing at 1500 ℃, the Fe content slightly reduced to 1.2% and further annealing at 3000 ℃ significantly reduced Fe content to around 100 ppm. The results of the iron content are summarized in Table 3.

Table 3. Iron content of CNFs

Sample	Iron content (by weight)
1, 4, & 7	~1.4%
2, 5, & 8	~1.2%
3, 6, & 9	~ 100 ppm

3.3 Moisture Content

Moisture plays an important role in explosibility (Mannan, 2005). The moisture content of samples 1, 2, and 3 was identified by drying the samples for several hours at 100 ℃. One gram of each sample was subject to weight measurement in the identification process and the corresponding results are shown in Table 4. Maximum variance during the whole process was identified as smaller than or equal to 5%, which indicates that CNFs are of poor hydroscopicity.

Table 4. Moisture content identification

Sample #		**1**	**2**	**3**
Original weight (g)		1.00	1.00	1.00
100 ℃ Drying	**30 mins**	0.96	1.00	0.95
	2 hours	0.95	0.98	0.96
	6 hours	0.96	1.00	0.96
Maximum variance		5 %	2 %	5 %

To ensure moisture content of each sample is identical as received, all the CNFs were well sealed. To remove the variance of moisture content caused by the handling process, the dried out samples were exposed to the lab conditions for two and half hours, which is longer than normal operation. No significant weight change was found. As a result, tests of the same material were considered as repeatable in terms of moisture content.

3.4 SEM Morphology

3.4.1 SEM morphology before dispersion

The sample morphology observed by the Scanning Electronic Microscope (SEM), showed that instead of existing as individual fibers, CNFs tend to agglomerate together and form micro-sized ellipsoid agglomerates. In addition, SEM images of samples 1, 2, and 3 were indistinguishable. Therefore, SEM image of sample 1 (Figure 10-A1) was chosen as a representative for no mill samples (samples 1, 2, and 3) to avoid redundancies. Similarly, SEM images of sample 4 (Figure 10-A2) and sample 7 (Figure 10-A3) were chosen as representatives for short mill time samples (samples 4, 5, and 6) and long mill time samples (samples 7, 8, and 9) respectively. Comparison among these images shows that the milling process effectively reduced the CNF agglomeration size from approximately 30 μm to less than 10 μm. Longer mill time produces smaller agglomerates.

In addition, individual separated fibers were observed after dispersing CNFs in a 90% isopropyl alcohol solution (Figures 10-B1, 10-B2 and 10-B3 were representatives

for no mill samples, short mill time samples, and long mill time samples, respectively). The diameters of the fibers were found to be around 100 nm and the lengths were found to be 10-30 μm. Moreover, comparison among images 10-B1, 10-B2, and 10-B3 showed that the milling process also reduced the length of a considerable portion of fibers from about 10 μm to 5 μm or even shorter, although long fibers still existed. The reduced length to diameter ratio may contribute to the smaller agglomerates after the milling process.

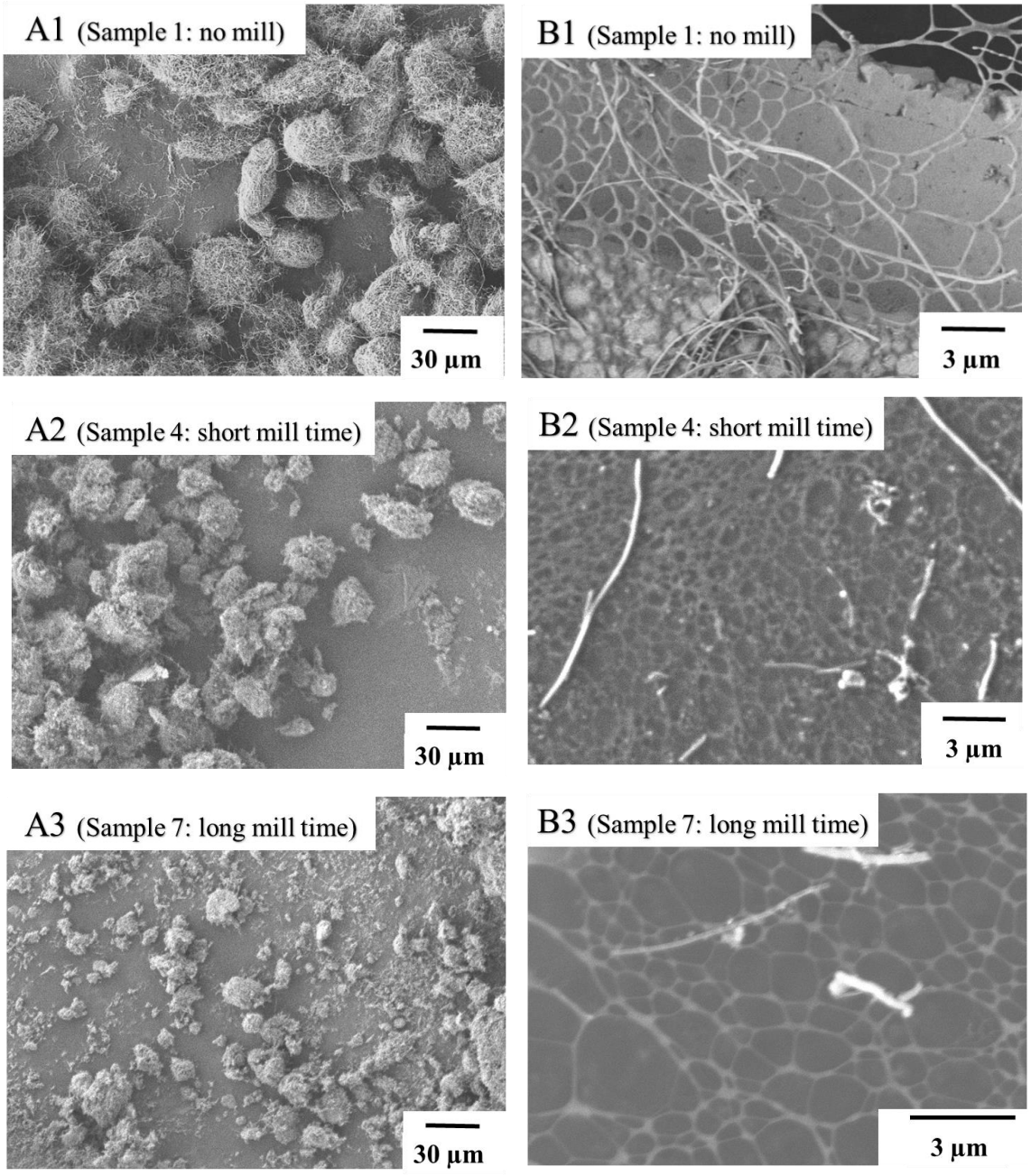

Figure 10. SEM images of CNF agglomerates (non-annealed): (A1) sample 1, (A2) sample 4, (A3) sample 7; and individual CNF fibers (non-annealed): (B1) sample 1, (B2) sample 4, (B3) sample 7

3.4.2 SEM morphology after dispersion

The morphology of the carbon nanofibers after dispersion through the 36-L dust explosion vessel was also studied. Sticky tapes were hung in the center of the vessel to capture CNFs. Samples were dispersed according to the standard operating procedure, which ensured that carbon nanofibers were well dispersed in the vessel. However, the ignitors were not triggered. Then the carbon nanofibers caught by the sticky tape were taken for SEM study. Figure 11 and Figure 12 show the results of sample 1 and sample 7 respectively.

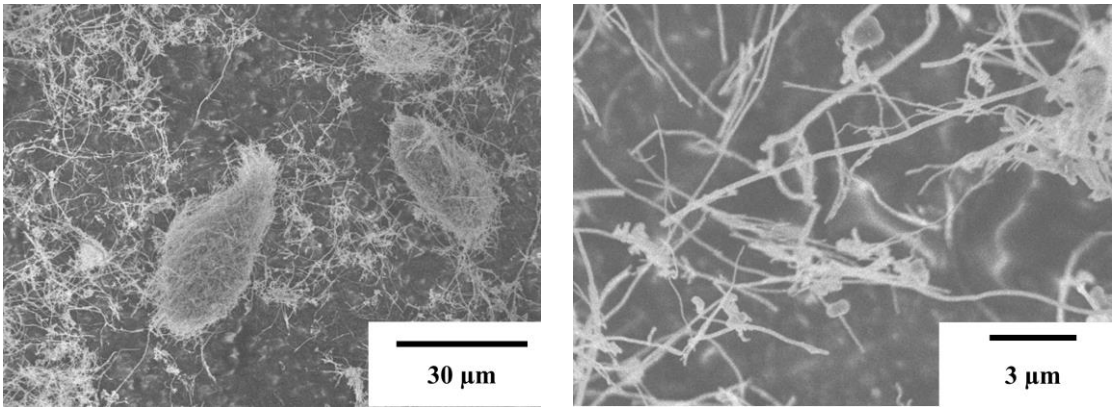

(A) (B)

Figure 11. SEM morphology of non-milled CNFs (sample 1) after dispersion at different magnitude

Figure 11 (A) presents the SEM morphology of non-milled CNFs at a magnitude of 1000. It was found that many of the agglomerates were broken after the dispersion.

Those carbon nanofibers existed as single fibers loosely attached to others. However, it also showed that some large agglomerates, such as those with a diameter of 30 μm, still exist. Figure 11 (B) presents the SEM morphology of non-milled CNFs at a magnitude of 6500, focusing on the length of single fibers. It was found that most of the fibers were still the same length as before dispersion. Therefore, a brief conclusion can be made that dispersion process breaks the agglomerates but does not break the single fibers into shorter ones.

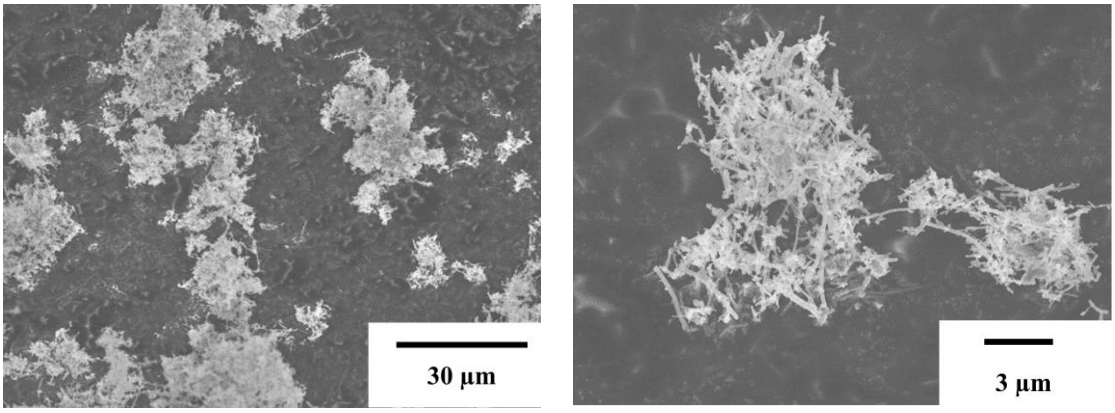

(A) (B)

Figure 12. SEM morphology of long time milled CNFs (sample 7) after dispersion at different magnitude

Figure 12 (A) presents the SEM morphology of long time milled CNFs at a magnitude of 900. It was found that most of the CNFs remained agglomerates with diameters similar to those before dispersion. Figure 12 (B) presents the SEM morphology of long time milled CNFs at a magnitude of 5500, focusing on the structure

of the agglomerates remaining after dispersion. It was found that the fibers within an agglomerate were much looser after dispersion.

Therefore, it was found that the dispersion process in explosibility testing changed the morphology of CNFs by breaking some larger agglomerates and loosening the primary agglomerates. However, to comprehensively study the effect of dispersion, more study is needed to quantitatively describe the forces during the dispersion process.

3.5 Particle Size Distribution

3.5.1 Particle size distribution obtained from Malvern Spaytec

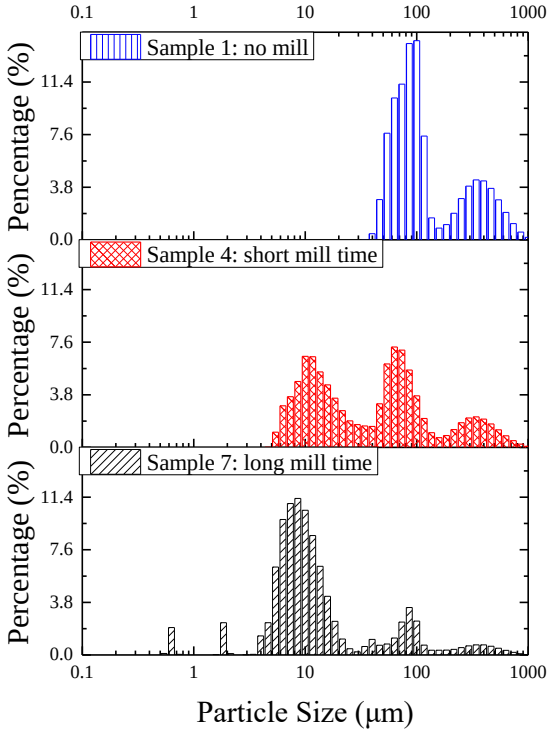

Figure 13. Number based particle size distribution for samples 1, 4 and 7 from Spraytec

Particle size distribution of CNF agglomerates were analyzed by Spraytec (Malvern Inc.), based on the correlation between particle size and light diffraction pattern. The instrument is composed of two functional modules: the Transmitter and Receiver. The Transmitter uses a He-Ne (Helium-Neon) Laser with a wavelength of 632.8 nm to pass through the dispersed particles. Optics in the Receiver module detect the light diffraction pattern produced by the spray, converting the light detected into electrical signals, which can be further processed and analyzed. Figure 13 shows the results of number-based particle size distribution of agglomerate samples 1, 4, and 7.

Most particles are larger than 30 μm before milling. After milling for a certain amount of time, many particles were broken into smaller ones of around 10 μm. Further milling time leads to the formation of more particles smaller than 10 μm. Meanwhile, the milling process widened the CNF agglomerates particle size range due to the generation of smaller particles and co-existence of large particles.

In addition, all the samples show multi-modal distribution behavior rather than a normal distribution. The milling process also increases the number of modals. It is possible that the CNFs form not only primary agglomerates, but also secondary, or even tertiary agglomerates. It also explains the size differences in sample 1 between SEM observation and Spraytec results. When mounting samples on conductive tape for SEM measurement, the shear force of the mounting action breaks the secondary agglomerates, leaving mostly primary agglomerates.

Based on previous work, it is likely that the dispersion process for MEC determination, which uses forced compressed air pressure as high as 2 MPa, may break

some secondary or larger agglomerates but probably not break primary agglomerates (F. Liu et al., 2003; Y. Liu et al., 2008; Y. Liu, Gao, Qian, Wang, & Wei, 2011).

3.5.2 Particle size distribution obtained from Beckman Coulter

In this study, the particle size distributions of samples 1, 4, and 7 represent unmilled, short milling time, and long milling time CNFs, respectively. Particle size analysis was performed with a Beckman Coulter (LS 13320) utilizing polarization intensity differential scattering (PIDS) technology and its tornado dry powder system. The surface area percentage based particle size distributions (D3,2) and volume percentage based particle size distributions (D4,3) were investigated, as shown in Figures 14-A and 14-B respectively. Both figures indicate the same general trend that CNFs formed micro-size agglomerates and the milling process efficiently reduced their agglomerate sizes. It can also be observed that the short-time milling efficiently reduced the agglomerate sizes by about 10 times, in which the milling process broke the tertiary agglomerates and partially secondary agglomerates, while produced more secondary and possibly primary agglomerates (J. Zhang et al., 2015). Also, the long-time milling process only reduced the agglomerate size slightly as compared to the short milling times.

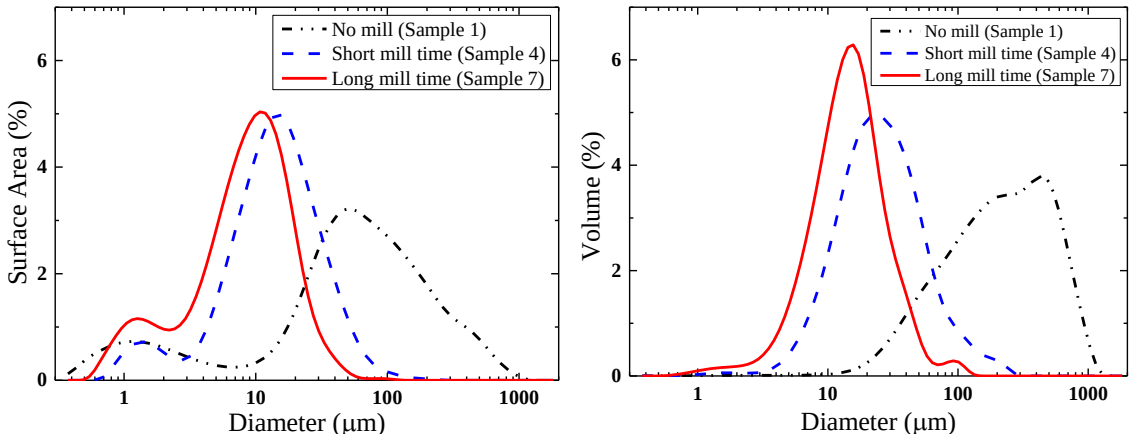

(A) (B)

Figure 14. Particle size distribution: (A) Surface area percentage; (B) Volume percentage

When compared with the volume percentage based particle size distribution, which is a unimodal distribution, the surface area percentage based particle size distribution is a bimodal distribution, which interestingly reveals the existence of agglomerates smaller than 5 μm with modes at about 2 μm.

Table 5 summarizes the properties of these CNF samples.

Table 5. Descriptions of CNF samples

Sample	Sample Description				
	Milling Time	**Anneal (°C)**	**Agglomerate Size Range**	**Iron Removal**	**Improved Graphite Perfection?**
1	No	None	20-500 μm	No	No
2	No	1500	20-500 μm	No	Yes
3	No	3000	20-500 μm	Yes	Yes
4	Short	None	5-70 μm	No	No
5	Short	1500	5-70 μm	No	Yes
6	Short	3000	5-70 μm	Yes	Yes
7	Long	None	3-40 μm	No	No
8	Long	1500	3-40 μm	No	Yes
9	Long	3000	3-40 μm	Yes	Yes

3.6 Hazards of Carbon Nanofibers

According to the carbon nanofibers Safety Data Sheet (SDS), there are three routes of exposure to CNFs, which may cause health issues:

1. Skin contact. Carbon nanofibers and their associated dust/shards may cause temporary irritation of the skin, especially for skin with wound.
2. Inhalation. Carbon nanofibers and their associated dust/shards may cause temporary irritation of the nasal passages, throat, upper respiratory tract, or gastrointestinal tract. In addition, carbon nanofibers are considered respirable fibers, because their length to cross-sectional width ratio is greater than 3. These

respirable fibers can reach and remain in the bronchial tubes or alveoli of the operators and may cause lung damage or disease.

3. Eye contact. Carbon nanofibers and their associated dust/shards may cause temporary irritation of the eyes.

Based on these three potential paths, this study used the proper personal protective equipment and other engineering control to protect the operators, other personnel inside the laboratory, and the environment around the building. Suggestions from the SDS, NIOSH (the National Institute for Occupational Safety and Health), and carbon nanofiber handling experts were incorporated.

3.6.1 Personal protective equipment

According to these possible routes of exposure, this study identified three pieces of basic personal protection equipment: respirators (half-face respirators with goggles or full-face respirators), gloves, and lab coats.

For the respirators, the SDS of carbon nanofibers recommended NIOSH certified air-purifying, tight-fitting full-face respirators equipped with N-100, P-100, or R-100 filters with an APF (assigned protection factor) of 50 or greater. NIOSH recommended choosing the respirator based on the REL (recommended exposure limit) of carbon nanofibers, which is 7 $\mu g \cdot m^{-3}$. If the concentration inside the laboratory is lower than 50 times the REL, it is recommended to have respirators with P-100 filters. If the concentration of carbon nanofibers is higher than 50 times the REL, but lower than 100 times the REL, then pressure demand supplied air respirators equipped with a full face

piece are required. Respirator masks with a protection class FFP3 or FFP2 are recommended by international experts working on carbonaceous nanomaterial explosions.

Table 6 summarizes several mask types with their polydisperse aerosol test results. Considering only small amounts of dust are used in the test and the mask test results, this study chose P-100 full-face respirators for protecting the operators from airborne carbon nanofibers.

Table 6. Mask types

Approval	**Type**	**Polydisperse aerosol test (%)**
NIOSH	N95	0.565-0.703
NIOSH	P100	0.0034-0.0222
CE	FFP2	0.270-0.505
CE	FFP3	0.0098-0.0144

Reproduced from (Rengasamy et al., 2009)

For hand protection, molded nitrile gloves impervious to nanomaterials were recommended in the SDS, and they have passed ASTM standard F739 (ASTM, 2012c). The same suggestions were offered by NIOSH and the experts.

For body protection, the SDS recommended full body protective clothing impervious to nanomaterials, which also passed ASTM standard F739 (ASTM, 2012c). Similarly, air-tight fabrics made of nonwoven textiles were recommended by the experts as laboratory coat materials and so disposable lab coats were chosen.

The author with fully equipped PPEs is shown in Figure 15.

Figure 15. Fully equipped PPEs

3.6.2 Other engineering controls

As for the other engineering controls in the laboratory to protect both the environment and the personnel inside, this study installed the following:

- The main explosion vessel is located inside an enclosed chamber, which is equipped with local exhaust ventilation systems. In addition, to capture the carbon nanofibers before they leave the building through the ventilation system, a high efficiency particulate air (HEPA) filter is installed in the ventilation system.

- Weighing the dry bulk CNFs is performed inside a small glove box chamber.
- After the experiment, the working area is cleaned with a HEPA-filtered vacuum, whose bags and filters are replaced according to the manufacturer's recommendation.

CHAPTER IV

THERMAL STABILITY AND COMBUSTION OF CARBON NANOFIBERS

4.1 Introduction

Minimum ignition temperature (MIT) is an important characteristic of combustible dust. The standard hot-surface ignition temperature test (ASTM E 2021) requires a certain dust layer thickness to ensure identical heat exchange with the atmosphere (ASTM, 2013b). The MIT of a dust cloud (ASTM E 1491) requires well dispersed dust particles in a test vessel (ASTM, 2012b). Both of them need a large amount of samples. For example, 100 g – 400 g is needed for MIT of a dust cloud. In order to determine the comparative thermal stability of these CNFs with a smaller amount of material and to ensure improved repeatability, this study conducted thermogravimetric analysis (TGA).

4.2 Thermogravimetric Analysis (TGA) of CNFs

4.2.1 Test method and conditions

The physical and chemical properties of CNFs were measured as a function of increasing temperature up to 1000 ℃. Two important parameters were identified from the thermogravimetric curves and their derivatives, *i.e.*, detected onset temperature of weight loss (T_{onset}) when CNFs start to react with air, and the oxidation temperature ($T_{oxidation}$), which was the temperature of maximum weight loss rate (Oner, 2007). As shown in Figure 16, from the thermogravimetric derivative curve, T_{onset} was determined as the intersection of the horizontal line y=0 and the tangent line when CNFs start to

react with air. In addition, the $T_{oxidation}$ was determined as the intersection of the tangent lines on both sides of the weight loss rate peak.

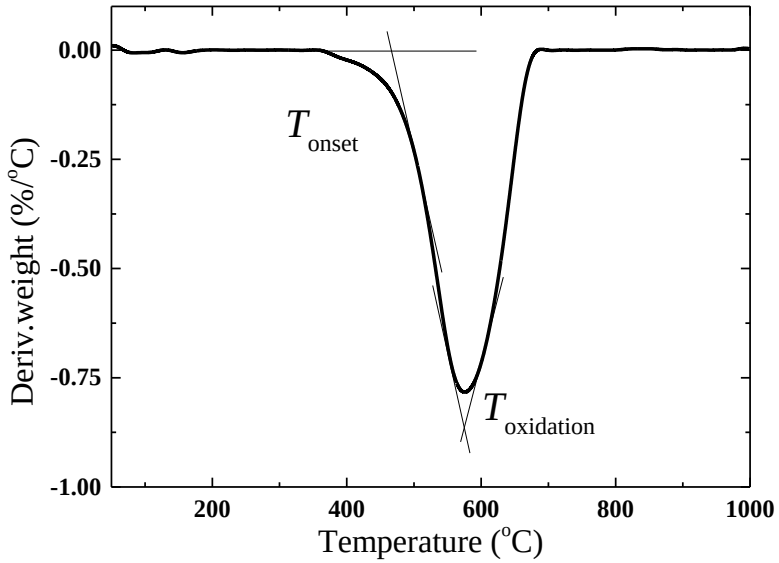

Figure 16. Determination of the onset temperature and the temperature of maximum oxidation rate

Although neither of them were equal to the MIT, these characterization temperatures provided insights into the thermal stability of the CNFs. Three scenarios with variable atmosphere and heating rates were examined as shown in Table 7.

Table 7. TGA test conditions

Test Series #	Sample	Atmosphere	Temperature Ramp
1	Sample 3	Nitrogen	5 ℃ min^{-1}
2	Samples 1, 4, 7	Air	5 ℃ min^{-1}
3	Samples 1-9	Air	20 ℃ min^{-1}

4.2.2 Test results

One sample (sample 3) was first tested in a nitrogen atmosphere with a flow rate of 60 cm^3 min^{-1} and a temperature increase rate of 5 ℃ min^{-1}. Shown as the green line in Figure 17, it demonstrates no observable weight loss up to 1000 ℃, which indicates CNFs possess a high thermal stability in an inert nitrogen atmosphere and there was no detected thermal decomposition or vaporization up to 1000 ℃.

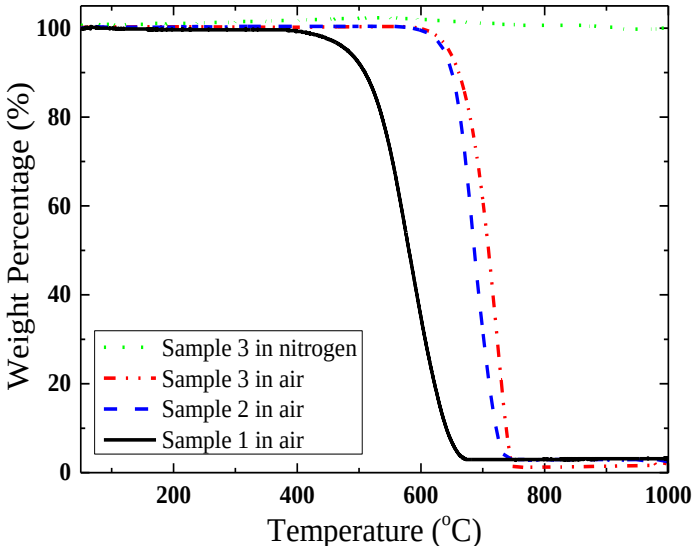

Figure 17. Thermogravimetric curves for CNFs (samples 1-3) using a heating rate of 5 ℃ min^{-1} in air or nitrogen

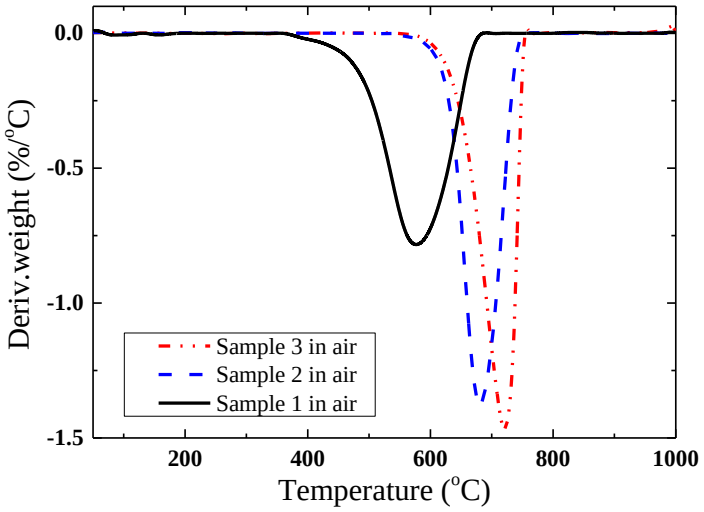

Figure 18. Thermogravimetric derivatives for CNFs (samples 1-3) using a heating rate of 5 ℃ min^{-1} in air or nitrogen

Samples 1-3 (non-annealed, 1500 ℃ annealed, and 3000 ℃ annealed) were tested in an air atmosphere with a temperature increase rate of 5 ℃ min^{-1} to evaluate the effect of the annealing process on thermal stability. Figures 17 and 18 show their weight loss percentages and their derivatives as a function of temperature respectively. In general, only oxidation of carbon was observed at temperatures higher than 450 ℃, which means all of these CNFs are highly thermal-stable in air below 450 ℃.

Finally, these samples were tested with a high temperature increase rate of 20 ℃ min^{-1} to simulate the combustion process of CNFs with air on a hot surface. The thermogravimetric curves and their corresponding derivatives were shown in Figure 19.

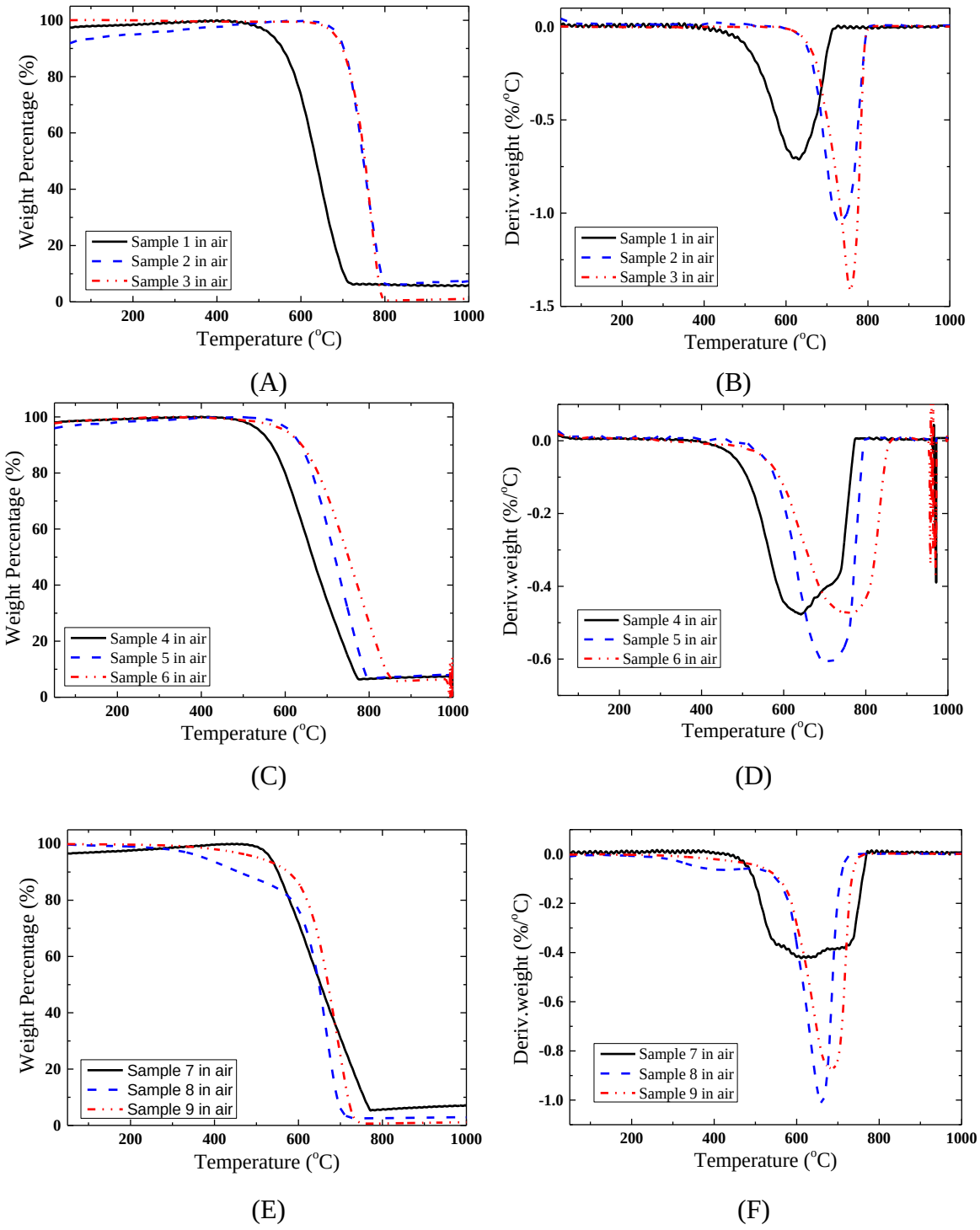

Figure 19. Thermogravimetric curves (left) and derivatives for CNFs (right) with temperature increase rate of 20 ℃ min^{-1} in air

In this study, characterization temperatures - T_{onset} and $T_{oxidation}$ - were determined from the derivatives, as described in Figure 16. Results at different temperature increase rates are listed in Table 8 with estimation errors of ±5°C.

Table 8. T_{onset} and $T_{oxidation}$ of CNF samples

Sample	5 °C min^{-1}		20 °C min^{-1}	
	T_{onset} (°C)	$T_{oxidation}$ (°C)	T_{onset} (°C)	$T_{oxidation}$ (°C)
1	480 ± 5	580 ± 5	520 ± 5	640 ± 5
2	620 ± 5	680 ± 5	670 ± 5	740 ± 5
3	650 ± 5	720 ± 5	680 ± 5	765 ± 5
4	-	-	500 ± 5	650 ± 5
5	-	-	580 ± 5	710 ± 5
6	-	-	600 ± 5	780 ± 5
7	-	-	490 ± 5	650 ± 5
8	-	-	570 ± 5	660 ± 5
9	-	-	590 ± 5	680 ± 5

Table 8 shows higher characterization temperatures were found when samples were tested with higher temperature increase rates (5 vs. 20 °C min^{-1}). The thermal stability of CNFs was significantly improved after annealing. T_{onset} and $T_{oxidation}$ of unmilled CNFs increased by about 150 °C after annealing (samples 2 and 3 versus sample 1), while T_{onset} and $T_{oxidation}$ of milled CNFs increased by about 100 °C after annealing (samples 5 and 6 versus sample 4; samples 8 and 9 versus sample 7). In addition, oxidation of annealed CNFs occurred at a narrower temperature range. CNF annealing at 1500 °C and 3000 °C showed nearly identical promotion of the annealing effects, which corroborates the effect of different annealing temperatures found by other researchers on improving the graphite perfection (W. Huang et al., 2003). Therefore, it

can be concluded that improved graphite perfection after annealing helped increase the T_{onset} and $T_{oxidation}$ when reacting with air.

Additionally, comparison of non-annealed samples 1, 4, and 7 indicated that the milling process had a slight effect on their thermal stability. For annealed samples, the milling process will have a significant effect on the thermal stability (sample 5 and 8 versus sample 2; sample 6 and 9 versus sample 3), and cause reduction of the onset temperatures by 80-100 ℃. However, the duration of milling is only a negligible factor in reducing the onset temperature.

4.3 Combustion of Carbon Particles

4.3.1 Two-film model

In the classic two-film model, proposed by Burke and Schumann (Burke & Schumann, 1931), developed by Held (Held, 1961), and supported by experiments involving large particles (Graaf & Brennst-Warme-Kraft, 1965), final combustion takes place in an outer layer, but the formed carbon dioxide attacks the carbon surface according to this reaction:

$$C + CO_2 \rightarrow 2CO \qquad \text{(R1)}$$

The CO generated at the surface diffuses outward and is consumed at a flame sheet where it meets an inward-diffusing flow of O_2 and reacts with stoichiometric proportions:

$$CO + \frac{1}{2}O_2 \rightarrow CO_2 \qquad \text{(R2)}$$

Figure 20 shows the mass flow at the carbon surface and the flame sheet for this model.

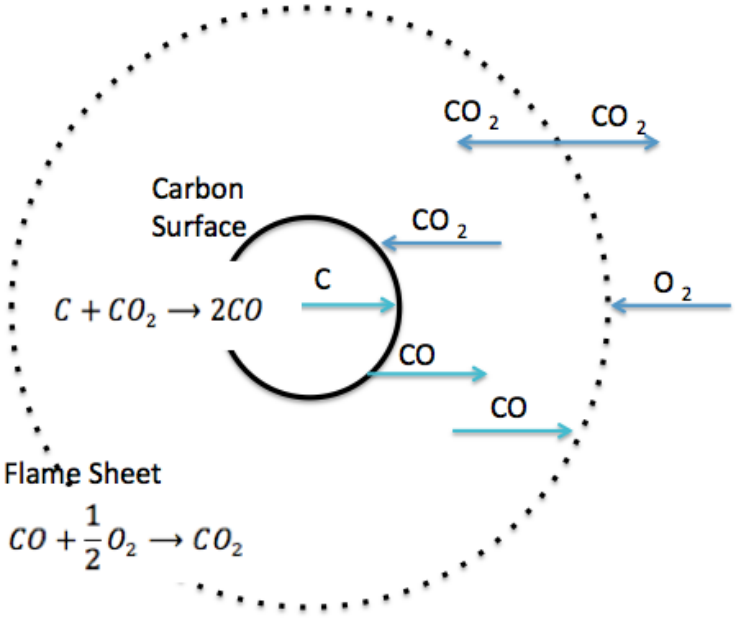

Figure 20. Mass flow at the carbon surface and the flame sheet of two-film model, reproduced from (Turns, 2000)

4.3.2 Limiting step of dust explosion of carbonaceous material

The diffusion of oxygen and the reaction on the particle surface are two main parts of the combustion process. Either of them can be the limiting step. The following section will compare the combustion time of a single particle to identify the limiting step for the combustion of particles we are studying. The following section illustrates the calculation example for a 30 μm particle with 1500 K surface temperature. For diffusion, the air comes from the unburnt zone, therefore, a temperature of 300 K and a pressure of

101.3 kPa is used in the calculation. For the reaction, since it occurs on the hot particle surface, a temperature of 1500 K and a pressure of 516.7 kPa is used.

The collision integral of air, Ω_D, is a function of temperature and intermolecular potential field for one molecule of A (Oxygen) and one molecule of B (Nitrogen). It can be approximated by the following expression (Neufeld, Jansen, & Aziz, 1972):

$$\Omega_D = \frac{a}{\left(T^*\right)^b} + \frac{c}{\exp\left(dT^*\right)} + \frac{e}{\exp(fT^*)} + \frac{g}{\exp\left(hT^*\right)} \tag{8}$$

The parameters in this equation are listed in Table 9:

Table 9. Parameters for collision integral (Graaf & Brennst-Warme-Kraft, 1965)

Parameter	Value	Parameter	Value
T^*	$\frac{kT}{\varepsilon_{AB}}$	e	1.03587
a	1.06036	f	1.52996
b	0.15610	g	1.76474
c	0.19300	h	3.89411
d	0.47635	$\frac{\varepsilon_{AB}}{k}$, K (for air)	97

The temperature of air coming to the particle surface is assumed as 300 K.

The diffusivity of air can be determined by using the Wilke and Lee Method (Keane, Leng, & Prausnitz, 1985):

$$D_{AB} = \frac{\left[3.03 - \left(\frac{0.98}{M_{AB}^{1/2}}\right)\right]\left(10^{-3}\right)T^{3/2}}{PM_{AB}^{1/2}\sigma_{AB}^{2}\Omega_{D}} \quad (9)$$

D_{AB} : Diffusion coefficient, $cm^2\ s^{-1}$

M_A, M_B : Molecular weights of A and B, respectively

T: Temperature, K

P: Pressure, bar

σ_{AB} : "Collision diameter," a Lennard-Jones parameter, angstrom

Ω_D : Diffusion collision integral, dimensionless

If the reaction is controlled by a diffusion step, then the combustion time, τ_b, can be calculated (Bouillard et al., 2010)

$$\tau_b = \frac{\rho_s d_p^2 \left(MW_{O_2} \big/ 2MW_C\right)}{8\rho_g D_{O_2}\left(Y_{O_{2,\infty}}\right)} \quad (10)$$

ρ_s, ρ_g : Density of solid particle and air, $kg\ m^{-3}$

d_p : Diameter of particle

$Y_{O_{2,\infty}}$: Oxygen mass fraction in air, 0.233

MW_{O_2}, MW_C : Molecular weight of oxygen and carbon

If the reaction is controlled by a surface reaction step, then the combustion time can be calculated (Bouillard et al., 2010):

$$\tau_b = \frac{\rho_s d_p}{2k_1\left(P_{tot}MW_{gas}/RT_s\right)\left(MW_C/MW_{O_2}\right)Y_{O_2,s}} \tag{11}$$

$$k_1 = 3.007\times10^5 \times \exp\left(-\frac{17966}{T_s}\right) \tag{12}$$

k_1 : Kinetic constant of combustion, m s^{-1}

T_s : Temperature at the particle surface

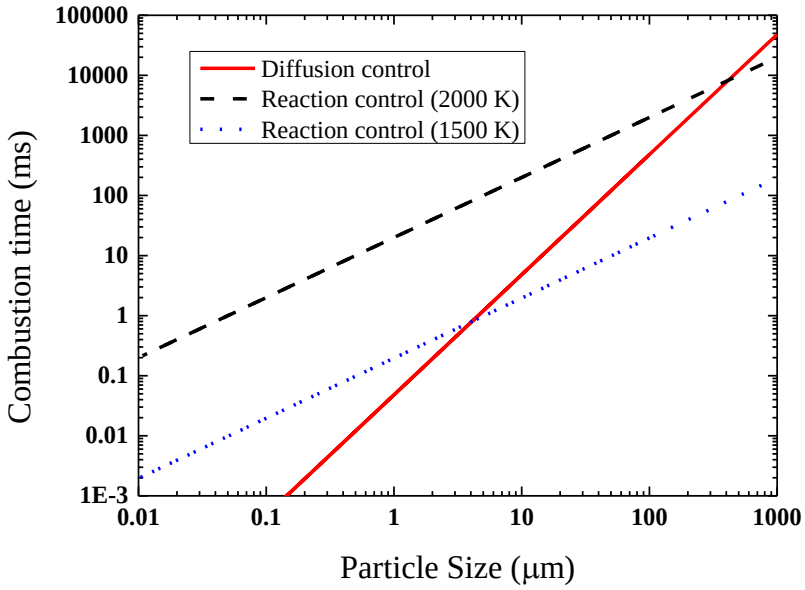

Figure 21. Combustion time for different particle sizes

This study repeated this calculation for a wide range of particle sizes at the temperatures of 1500 K and 2000 K, since the temperature will significantly impact the surface reaction rate. The results are summarized in Figure 21. These calculation results match the experimental data of carbon particles smaller than 10 μm and larger than 100 μm (Bouillard et al., 2010) within a reasonable deviation, which supports the validity of this calculation. Both the experiments and calculation show that for carbon particles smaller than 10 μm, the combustion process is controlled by the surface reaction. Also with the particle size shrinking, the difference between reaction rates and diffusion rates becomes larger. This is reasonable because the required diffusion path of oxygen is much shorter. The diffusion control becomes the limiting step for carbon particles larger than 100 μm.

For our target particles - those between 10 μm and 100 μm - experimental data are currently not available. However, the calculation shows that it is difficult to state that there is a dominant step since the differences between combustion times are not apparent. Also, without knowing the exact surface temperature, it is impossible to find the more important control step, the diffusion or the reaction.

However, no matter which step is limiting the combustion process, the surface area plays an important role. The relationship between the combustion rates in terms of carbon for a single particle, $\dot{m}_c$, and particle size, d_p, can be written as (Holbrow et al., 2010):

$$\dot{m}_c \propto d_p^2 \tag{13}$$

Then, the combustion rate for a certain dust cloud, $\dot{M}_c$, can be expressed as:

$$\dot{M}_c \propto \frac{1}{d_p} \tag{14}$$

For larger particles, whose combustion process is limited by diffusion, the relationship can be expressed as (Holbrow et al., 2010):

$$\dot{m}_c \propto d_p \tag{15}$$

Then,

$$\dot{M}_c \propto \frac{1}{d_p^2} \tag{16}$$

According to equation (14) and equation (16), further study of the combustion rate and particle size is needed to figure out how the reaction and diffusion cooperate in controlling the combustion mechanism.

4.3.3 Energy conservation

A coal particle combustion in air was studied to determine the relationship between particle temperature and time in a furnace of known temperature. The following equations were proposed based on these assumptions:

- The particle was a perfect and homogeneous sphere;
- The temperature of the particle was uniform;
- Either the diameter or the density of the particle remained constant;

- The furnace and the particle were black and gray bodies, respectively;
- The particle was in permanent thermal equilibrium with the gas and walls of the furnace.

$$\frac{dC_{\mathrm{p}}\rho_{\mathrm{c}}}{6}\frac{\mathrm{d}T_{\mathrm{p}}}{\mathrm{d}t} = H_{\mathrm{r}} + H_{\mathrm{c}} + H_{\mathrm{q}} \tag{17}$$

where

C_{p} is the specific heat capacity of the particle;

T_{p} is the temperature of the particle;

ρ_{c} is the density of the particle;

d is the diameter of the particle;

H_{r} is the radiative heat flux received by the particle per unit time. It is determined according to the following equation:

$$H_{\mathrm{r}} = E\tau\left(T_{\mathrm{f}}^4 - T_{\mathrm{p}}^4\right) \tag{18}$$

where

E is the total emissivity of the coal;

τ is the Stefan-Boltzmann constant;

T_{f} is the flame temperature.

H_{c} is the convective heat flux received by the particle per unit time. It is determined according to the following equation:

$$H_{\mathrm{c}} = h_{\mathrm{c}}\left(T_{\mathrm{g}} - T_{\mathrm{p}}\right) \tag{19}$$

where

T_g is the temperature of gas around the particle;

h_c is the convective heat transfer coefficient between the particle and the gas determined from the Nusselt number.

H_q is the heat of reaction per unit time:

$$H_q = AW\frac{\pi}{4}d^2 \tag{20}$$

where

W is the rate of de-volatilization per unit of particle surface area;

A is a constant.

CHAPTER V

MINIMUM IGNITION ENERGY OF CARBON NANOFIBERS

5.1 Introduction

There are several kinds of ignition sources, for example, mechanical sparks, smoldering particles, mechanical heating, static electricity, hot surfaces, fires, auto ignition, and so on (Bartknecht, 2012). Among all these ignition sources, the electrostatic discharges play an important role in causing dust explosion incidents. Minimum ignition energy is the lowest energy value of a high-voltage capacitor discharge required to ignite the most flammable dust/air mixture.

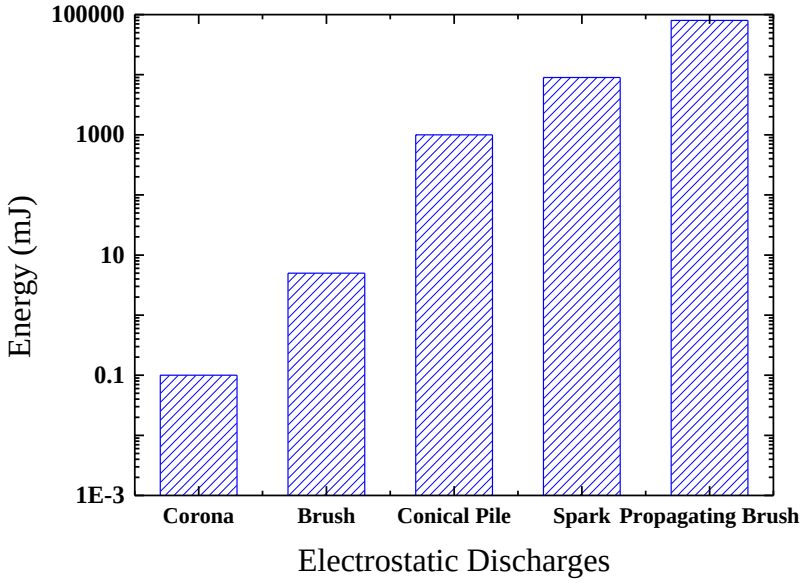

Figure 22. Energy generated by electrostatic discharges (Glor, 1985)

A charged object can be discharged to the ground or to an oppositely charged object by six methods: spark, propagating brush, conical pile, brush, lightning-like, and corona discharges (Crowl & Louvar, 2001). Figure 22 summarized the energy generated by different types of electrostatic discharges. While typical MIE for powder is between 0.1 and 100,000 mJ, all these discharge types except corona has the potential to ignite a combustible dust cloud.

When it comes to the risk of dust cloud ignition by static electricity, the possibility of occurrence of these discharge models should be considered. Possible discharge models were investigated for typical dust handling processes, for example, filling silos and large containers. The occurrence of conical pile discharge shows its importance while possibilities of other models were either removed or significantly low. For example, conductive materials of construction are grounded and no insulating internal coatings are applied, and thus spark and propagating brush discharges can be excluded (Glor, 2001).

Since the samples are composed of graphite and Fe-NPs, MIEs of carbon material and Fe-NPs are listed in Table 10. Carbon materials with different volatile components and graphite perfection need different quantities of ignition energy to initiate an explosion. In general, carbon material needs MIE higher than 20 mJ. For carbon nanotubes, which are very similar to CNFs, the MIE is higher than 1,000 mJ. While the MIEs of Fe-NPs are reported below 1 mJ, even at the low concentration of 600 mg in a 2 L tube (Wu, Chang, & Hsiao, 2009), the possibility of Fe-NPs' effect on decreasing the MIEs of CNFs exist. If this occurs, it means that CNFs with iron

nanoparticles can be ignited by the conical pile or brush discharges, and the risk of igniting CNFs is significantly increased. Therefore, MIE tests of Sample 7, which has the highest iron content, were conducted.

Table 10. MIEs of carbon materials and iron nanoparticles

Material		**MIE**
Carbon Material	Coal	40 mJ (Haase, 1977)
	Coal, Pittsburgh	250 mJ (Haase, 1977)
	Charcoal	20 mJ (Haase, 1977)
	Carbon Nanotubes (CNT)	>1 J (Babrauskas, 2003)
	Carbon Black	>1 J (Babrauskas, 2003)
Iron Nanoparticles	Fe (15nm)	<1 mJ (Wu et al., 2009)
	Fe (35nm)	< 1 mJ (Wu et al., 2009)
	Fe (65nm)	< 1 mJ (Wu et al., 2009)

5.2 MIE Test Apparatus

MIE tests were performed in the minimum ignition energy apparatus (MIKE 3), which is shown in Figure 23, at Dow Chemical in Freeport, Texas. This apparatus is a modified Hartmann-tube with a volume of 1.2 L. There is a dust dispersion system at the bottom of MIKE 3. A certain amount of dust can be dispersed inside the tube by 7 bar compressed air.

Figure 23. MIKE 3 apparatus

Table 11. MIE test variables

Level	Concentration [mg]	Ignition Energy [mJ]	Delay Time [ms]	Test Number	Inductance [mH]
1	150	1	60	5	0
2	300	3	90	10	1
3	600	10	120	20	
4	900	30	150		
5	1200	100	180		
6	1500	300			
7	1800	1000			
8	2400				
9	3000				
10	3600				

Two electrodes are installed at the middle part of the tube and can release test energies of 1000, 300, 100, 30, 3, and 1 mJ. Tests are performed by changing the mass levels (concentration) and energy level. By definition, MIE data refer to protracted capacitor discharges. These are generally more incentive than purely capacitive discharges. The results obtained under such conditions (with inductance) can be applied to operational conditions only if the capacitors in plant installations are also discharged via an inductance. If the incendivity of electrical discharges - especially of electrostatic discharges - with regard to dust/air mixtures is to be assessed, the minimum ignition energy must also be determined without an inductance in the discharge circuit. Therefore, tests can be performed both with and without inductance. The test variables of MIKE 3 are summarized in Table 11.

The two values determined are the lowest energy value (W2) at which ignition occurred and the energy (W1) at which at least 10 successive experiments were conducted without observing ignition. According to ASTM E-2019 Standard Test Method for Minimum Ignition Energy of a Dust Cloud in Air (ASTM, 2013a), the MIE is determined between these two values:

$$W1<MIE<W2 \tag{21}$$

5.3 Test and Result

In this study, tests were performed at a low mass level of 900 mg and at a high mass level of 2400 mg with the highest available energy level (1000 mJ). While tests can

be performed both with (1 mH) and without inductance, this study chose to test with inductance so the results would be conservative.

The detailed test conditions and observations are listed in Table 12 below.

Table 12. MIE test conditions and observations

Test Series	Test Condition			Test Number	Observation	Conclusion
	Mass mg	Energy mJ	Inductance mH			
1	900	1000	1	10	Black dust cloud only	MIE > 1000 mJ
2	2400	1000	1	10	Black dust cloud only	

During the tests, it was observed that the black CNF cloud filled the whole vertical tube and no sign of light was observed after the spark was released from the electrodes. Therefore, the MIE was determined to be above 1000 mJ. CNFs need relatively high initial energy to be ignited, which means it is safe from electrostatic discharge.

CHAPTER VI

PROMOTED DUST EXPLOSION OF CARBON NANOFIBERS BY IRON NANOPARTICLES[*]

6.1 Synopsis

Dust explosions, especially a fine particle explosion, are hazards with severe consequences, which have caused significant loss of life and property damage in several industries. Minimum explosive concentration (MEC) is one of the important parameters used to evaluate the dust combustion and explosion risks, and helps design corresponding safeguards in industry. Although there has been a tremendous boost in the application of nano-materials in the past two decades, the efforts to evaluate the safety boundaries of nano-materials are not sufficient; *e.g*., the experimental evaluation of their MECs is very scarce. To fill this gap, MEC tests of several commercially available carbon nanofibers were conducted in this study by following ASTM standards. The results obtained demonstrate that a reduction in particle size by a mechanical-milling process could decrease MEC, while an annealing process (1500 ℃ or 3000 ℃) could increase MEC, and thus lower the explosion risk. Agglomeration, particle size, and existence of metal nano-particles (*i.e*., nano iron particles) all contribute to changes in the MEC, which were not disclosed in previous studies for MEC estimation. To describe the effect of these factors more accurately, a heterogeneous model based on a dynamic

[*] Part of this chapter is reprinted from "Dust explosion of Carbon Nanofibers Promoted by Iron Nanoparticles" by Zhang, J., Chen, H., Liu, Y., Elledge, H., Mashuga, C.V., & Mannan, M.S. (2015). *Industrial & Engineering Chemistry Research, 54*(15), 3989-3995, with permission from American Chemical Society

perspective is proposed to evaluate the influences of those factors on the heat transfer process and ultimately the explosibility of nano-materials. Detailed analyses of the mechanisms affecting the combustion and explosion process were also performed in this study.

6.2 Introduction

Dust explosion or unintended dust combustion can have dire consequences in the process industries. According to a 2006 U.S. Chemical Safety and Hazard Investigation Board report, 281 combustible dust incidents occurred in the United States from 1980 to 2005, which killed 119 workers and injured 718 others (Blair, 2007). Most recently, a metal dust explosion in an auto- parts factory in Kunshan, Jiangsu, China on August 2, 2014 resulted in 146 fatalities and 95 injuries (Nie et al., 2015). The incident investigation team reports that the combustible dust involved in this incident was aluminum powder, and the dust explosion was triggered by heat release from a reaction between aluminum powder and water due to the corrosion of dust collectors (SAWS, 2014). After this incident, the CSB emphasized the importance of paying attention to the dangers of combustible dust (Moure-Eraso, 2014). In the past two decades, nanomaterials have drawn many researchers' attention due to their excellent mechanical or electrical properties, which are now better understood. Although the associated health hazards have been widely studied, more work continues. However, the physical hazards, *i.e.*, the fire and explosion hazards, are somewhat overlooked. In order to prevent and

mitigate nano particle dust explosions, it is essential to have a better understanding of the explosion behaviors of these promising materials.

Dust explosion is usually affected by the following factors (Mannan, 2005): chemical composition, particle size, moisture content, oxygen concentration, and concentration of inert gas and/or inert dust. The effect of particle size on explosion behaviors is well established for common materials (Eckhoff, 2003). The minimum ignition energy (MIE) of dust particles tends to reduce exponentially as particle size decreases, and the explosion severity is often significantly enhanced by reducing the particle size. According to this theory, nanoparticles will show different explosion behaviors compared with regular micro-dusts due to the extremely small particle size. This concept was supported by several experimental observations, for example, nano-titanium and nano-iron particles were found oxidized and released lots of energy due to the shear force in the dispersion process (Wu & Wu, 2008). This suggests the extremely high ignition sensitivity of metal nanoparticles. In addition, single wall carbon nanotubes (SWCNTs) were found to catch fire when exposed to a camera's flashlight (Ajayan et al., 2002), which was attributed to the pyrophoric oxidation of iron nanoparticles (Smits, Wincheski, & Namkung, 2003). However, counter to these observations, it was found that an explosion of 200 nm aluminum particles was stronger than that of 100 nm particles. Different oxidation degrees of nano-aluminum particles and different agglomerate size, which are very important to metal dust hazard assessment, were attributed to this discrepancy from previous theory (Wu, 2010). Some research (Eckhoff, 2011, 2012; Worsfold et al., 2012) also found that the explosibility of nanoparticles was

limited by impeded dispersion and high coagulation rates. Therefore, more experimental efforts should be devoted to understanding the true hazards of these nanomaterials.

Moreover, explosion behaviors of a mixture of two different types of nanomaterials have not been studied. Some metal nanoparticles are usually contained in carbon-nanomaterials during synthesis and application processes. Metal nanoparticles act as a catalyst in synthesizing these carbon nanomaterials, and the content of metal nanoparticles in the product can be very high depending on the synthesis conditions. Even after purification, the content of residual metal nanoparticles can still be around 1%. The metal nanoparticles, usually well dispersed in synthesized products, may show different behaviors from an aggregate of metal nanoparticles, although the content is low.

By experimentally identifying and analyzing MECs of different CNFs (Carbon Nano-fibers) in terms of agglomerate size and iron nano-particle (Fe-NPs) content, this work

- Validated the previous “rule of thumb”
- Disclosed Fe-NPs’s promotion effect on CNFs’ explosibility
- Proposed a heterogeneous model based on a dynamic perspective to evaluate the influences of agglomerate size and Fe-NPs on the heat transfer process and ultimately the explosibility of nano-materials

6.3 MEC Test

According to ASTM E1515 (ASTM, 2007), MEC is the minimum concentration of a dust-air mixture that will propagate a deflagration in a near spherical closed vessel of 20-L or greater volume. To avoid the effect of overdriving, a 2.5 kJ ignition energy is used for every MEC test. After running tests by increasing dust concentrations step by step, there are two alternatives to determine the MEC of combustible dust. The first method is to plot the pressure rise as a function of concentration. The pressure rise is defined as (ASTM, 2007):

$$\text{Pressure rise} = P_{\text{ex,a}} - P_{\text{ignition}} - \Delta P_{\text{ignitor}} \tag{22}$$

where $P_{\text{ex,a}}$ is the maximum explosion pressure reached during a single deflagration; P_{ignition} is the absolute pressure when the ignitor is activated (typically 101.325 KPa); and $\Delta P_{\text{ignitor}}$ is the pressure rise in the chamber due to the occupied energy of the ignitor in air at atmospheric pressure, which is also the absolute pressure value of $P_{\text{ex,ignitor}}$ and measured by triggering an ignitor without loading any dust sample. These parameters are identified through pressure-time profiles obtained from tests as illustrated in Figure 8 in Section 2.5.1. Then the MEC is the lowest concentration (ASTM, 2007) for which

$$\text{Pressure rise} = P_{\text{ex,a}} - P_{\text{ignition}} - \Delta P_{\text{ignitor}} \geq 1 \text{ bar, gauge} \tag{23}$$

Another alternative is to plot the pressure ratio (PR) as a function of concentration. The pressure ratio is defined as (ASTM, 2007):

$$\mathrm{PR} = \left(P_{\mathrm{ex,a}} - \Delta P_{\mathrm{ignitor}} \right) / P_{\mathrm{ignition}} \quad (24)$$

Then the MEC is defined as the lowest concentration for which

$$\mathrm{PR} \geq 2 \quad (25)$$

It is recommended to repeat the test at concentrations, when PRs are close to 2. The MEC is usually rounded to the nearest 5 g m^{-3} or 10%, whichever is larger. For this study, the PR method was applied.

6.4 Results and Discussion

A blank test was first run with a 2.5 kJ ignitor. The pressure rise of this igniter in the 36-L dust explosion vessel was identified as 0.20 bar. The various concentration of samples 1-3 of CNFs were tested in the 36-L dust explosion vessel. Table 13 listed the values of $P_{\mathrm{ex,a}}$ and PR of samples 1-3 at concentration of 300 g m^{-3}. Therefore, samples 1-3 did not explode at concentrations up to 300 g m^{-3}. Therefore, the MECs of sample 1, 2, and 3 were identified to be larger than 300 g m^{-3}, which was because the low bulk density of CNFs and the limited volume of the dust container restrain the tests to higher dust concentrations.

Table 13. $P_{\mathrm{ex,a}}$ and PR of samples 1-3 at concentration of 300 g m^{-3}

Sample #	$\boldsymbol{P_{\mathrm{ex,a}}}$	**PR**
1	1.59	1.24
2	1.52	1.19
3	1.49	1.21

The short-time milled CNFs, samples 4-6, were also tested at various concentrations. Figure 24 - 26 show the pressure ratios as a function of concentration of samples 4 - 6 respectively.

In Figure 24, which is for sample 4, a line was drawn to connect the average value of PR at 250 g m^{-3} and the average value of PR at 200 g m^{-3}. Its cross point with the line PR=2 was identified as the MEC, which is 210 g m^{-3}. A similar process was conducted for samples 5 and 6. The MEC of sample 5 was identified as 210 g m^{-3}, while the MEC of sample 6 was larger than 300 g m^{-3}.

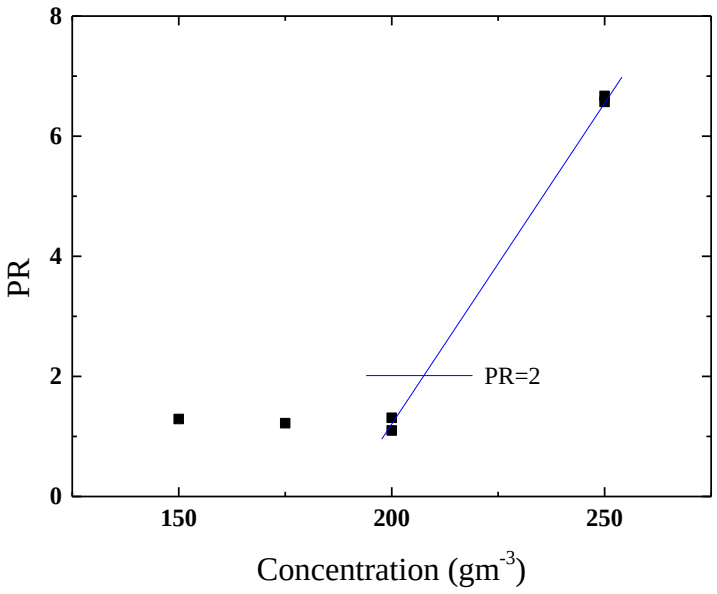

Figure 24. PR as a function of concentration for sample 4

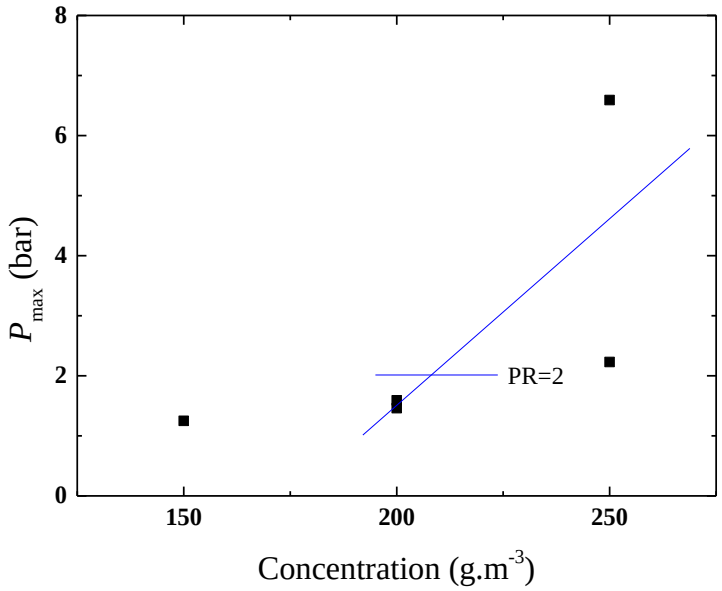

Figure 25. PR as a function of concentration for sample 5

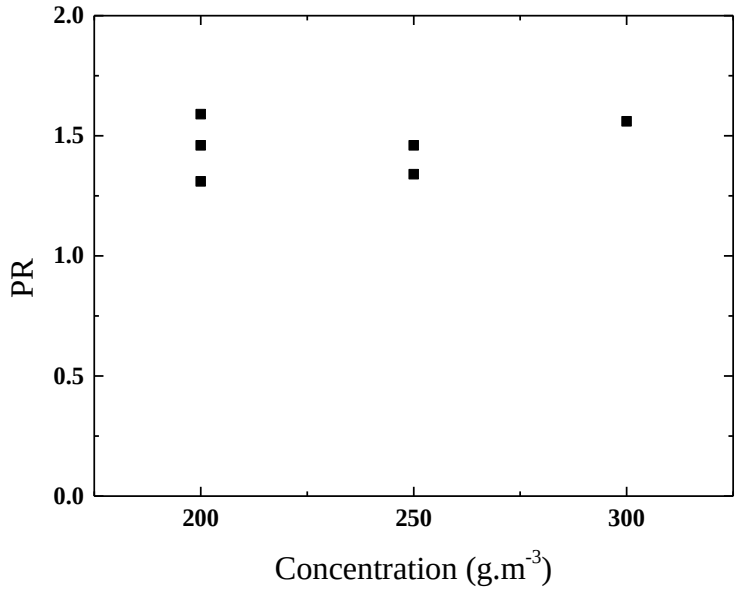

Figure 26. PR as a function of concentration for sample 6

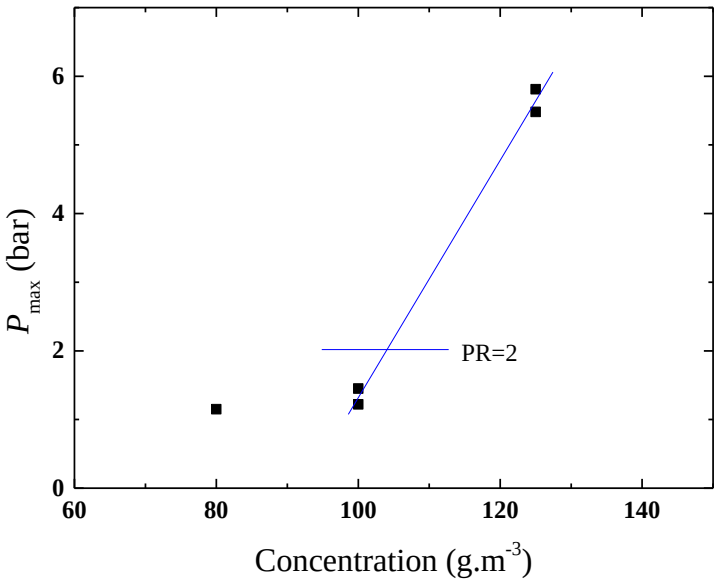

Figure 27. PR as a function of concentration for Sample 7

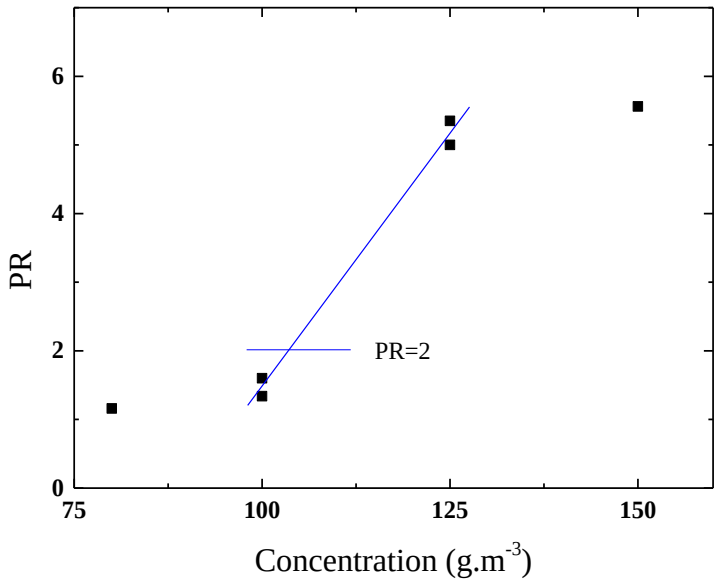

Figure 28. PR as a function of concentration for sample 8

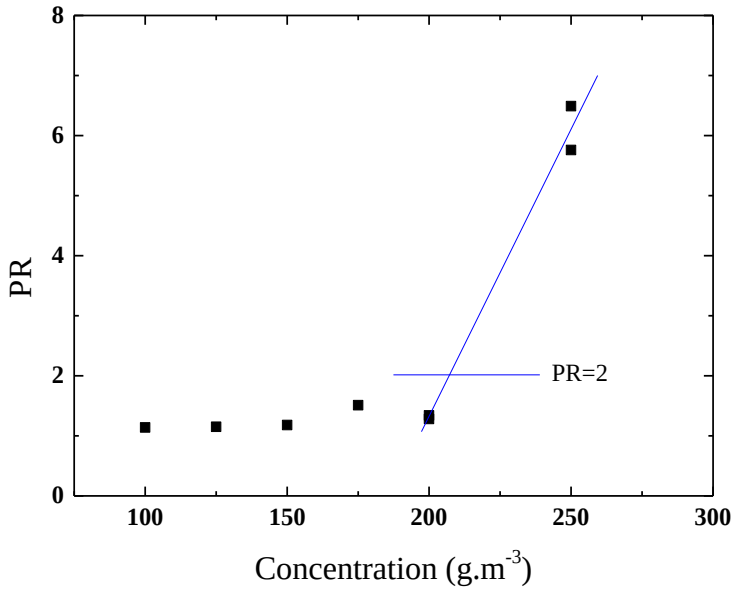

Figure 29. PR as a function of concentration for sample 9

MEC tests were also conducted for samples 7-9 at various concentrations. The PRs as a function of concentration were plotted in Figures 27-29 respectively. Similar method was applied to determine the MECs for these samples. MECs were identified as 105 g m^{-3} for samples 7 and 8, while MEC for sample 9 was 210 g m^{-3}.

These identified MECs were summarized in Table 14, together with their process method and iron content identified in Section 3.2.

Table 14. MECs of CNFs

Sample	MEC ($g\ m^{-3}$)	Sample Description		
		Mill	Annealing temperature (℃)	Iron content
1	>300	No	No	1.4%
2	>300	No	1500	1.2%
3	>300	No	3000	100 ppm
4	210	Short time	No	1.4%
5	210	Short time	1500	1.2%
6	>300	Short time	3000	100 ppm
7	105	Long time	No	1.4%
8	105	Long time	1500	1.2%
9	210	Long time	3000	100 ppm

Table 15. MECs of various carbon material

Carbon Material	MEC ($g\ m^{-3}$)
Carbon	Stoichiometric concentration: 111 $g\ m^{-3}$
Pittsburgh high volatile coal	60 (Cashdollar, 1996)
Graphite Dust 4 μm	70 (Denkevits & Dorofeev, 2005)
Graphite Dust 25-32 μm	100 (Denkevits & Dorofeev, 2005)
Graphite Dust 40-45 μm	120 (Denkevits & Dorofeev, 2005)

As listed in Table 15, the stoichiometric concentration for the combustion of carbon ($C+O_2=CO_2$) in air is calculated to be about 111 $g\ m^{-3}$ on a gram carbon basis; The MEC of Pittsburgh high volatile coal was reported as low as 60 $g\ m^{-3}$ (Cashdollar, 1996). MECs of CNFs are larger than that of the volatile coal or even larger than the stoichiometric concentration for the combustion of carbon, indicating that CNFs are not

very reactive. This is reasonable, since the crystallized carbon atoms in CNF are more stable than in amorphous carbon. In addition, MECs of some graphite dust (4 μm – 45 μm) were found between 70 g m^{-3} and 120 g m^{-3} (Denkevits & Dorofeev, 2005). While MECs of CNFs are similar to these graphite dusts, it supports the hypothesis that the size of agglomerates rather than that of single nanoparticles can be used as an index to estimate CNFs' explosibility.

As expected, MECs are found to decrease after the milling process. No mill samples 1, 2 and 3 have MECs higher than 300 g m^{-3}, while short mill time samples 4, 5 and 6 have lower MECs than no mill samples, and long mill time samples 7, 8 and 9 have the lowest MECs. These results match the known trends of particle size: the smaller the particle, the lower the MEC; and in general, wider particle size distribution leads to higher explosibility (Castellanos, Carreto-Vazquez, et al., 2014). These findings indicate the milling process could increase the explosion risks of CNFs. Given that the milling method is widely used in customizing CNFs and other nano-materials but seldom studied for safety concerns, more attention should be given to this hazard.

From Table 14, it is interesting to find that the MECs are also affected by the annealing process. Annealing at 1500 ℃ did not change the MECs; however, the MECs of CNFs increase significantly after annealing at 3000 ℃.

Improved graphite perfection after annealing may hinder the kinetics of the CNF-oxygen reaction in the combustion process resulting in a decrease in the explosibility of CNFs. It was shown that high-temperature annealing of multi-walled carbon nanotubes can lead to an increased graphite perfection (Andrews et al., 2001; W. Huang et al.,

2003). However, Raman spectra results show that the graphite perfection were significantly improved after annealing at 1500 ℃, while the improvement of graphite perfection was not apparent when the annealing temperature increased from 1500 ℃ to a higher temperature (W. Huang et al., 2003). Therefore, the contradiction between graphite perfection and MECs indicates that the improved graphite perfection is not the influential factor.

On the other hand, Table 14 shows that iron content plays an important role in affecting the MECs of CNFs. Pyrophoric oxidation of iron particles was found to attribute to the ignition phenomena of SWCNTs exposed to a camera flashlight (Smits et al., 2003). From Table 14, it is observed that among samples with identical particle size distribution, *i.e.*, the group of samples 1/2/3, 4/5/6, and 7/8/9, only samples with lower iron content (samples 6 and 9) show higher MEC than other samples in the same group. It is not obvious for sample 3, since we are not able to obtain the exact MECs due to its low density.

6.5 Mechanism of CNFs Dust Explosion Promoted by Iron Nanoparticles

To better show the effect of iron on explosibility of CNFs, a diagram (Figure 30) was developed according to the explosion behaviors of gas/dust mixtures (Garcia-Agreda & Benedetto, 2011). Dimensionless Fe content (Fe Concentration/MEC_{iron}) and dimensionless carbon content (Carbon Concentration/MEC_{carbon}) are expressed respectively in the x- and y-axis. The black dash diagonal indicates that the mixtures of two components have independent effect (no interaction) on explosibility. Mixtures in

the right-upper area have antagonistic effect on explosibility while mixtures in the left-lower area have synergistic effect. To generate the explosion line of CNF - Fe-NPs, the MEC of sample 9 was treated as the MEC for pure CNFs. MEC for iron nanoparticles are reported as 500 g m^{-3} for 15 nm particles, 125 g m^{-3} for 35 nm particles, and 500 g m^{-3} for 65 nm particles (Wu & Wu, 2008). The lowest concentration, 125 g m^{-3}, was selected as the MEC for pure iron nanoparticles in this work. The red and blue points were obtained based on the experimental result of samples 7 and 8. They have 1.4% and 1.2% iron content, and are in the left-lower area away from the dash line. The synergistic effect is self-evident between iron nanoparticles and carbon nanofibers.

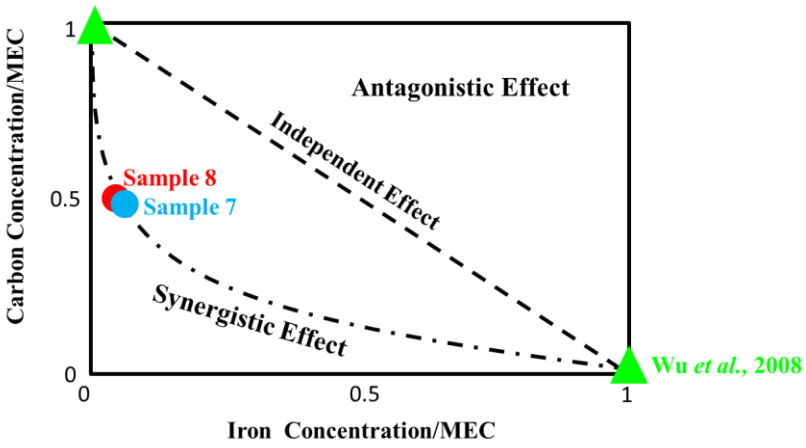

Figure 30. Experimental results of explosion regimes in the iron/carbon concentration

Therefore, it can be hypothesized that high iron content reduces CNFs' minimum concentrations needed for causing a dust explosion, thus possessing a higher risk of explosion during the handling process.

Since iron is widely used as a catalyst in producing CNFs or CNTs and may not be completely removed due to the high cost of annealing, this discovery can be very valuable for safety protection in CNF manufacturing industries. This study has shown CNFs have variable fire and explosion risks depending on the processing and treating methods. These hazards were not sufficiently evaluated before, and neglect of this potential hazard may lead to undesired incidents.

There are three possible assumptions in promoting the dust explosion by iron nanoparticles, and their relevance with this study is discussed below:

(1) Iron burns as fuel? MEC of iron nanoparticles are reported as 500 g m^{-3} for 15 nm particles, 125 g m^{-3} for 35 nm particles, and 500 g m^{-3} for 65 nm particles (Wu & Wu, 2008). Our Fe-NP concentration in the mixture is only about 1.5 g m^{-3}, which is far below the known MEC of pure Fe-NP. On a percentage basis, iron is not expected to influence the mixture MEC. Thus, the possibility of iron particles burning directly as a dust can be excluded as a cause of iron improving explosibility of CNFs.

(2) Iron acts as catalyst for the carbon-oxygen reaction? The real processes involved in carbon combustion are very complicated. However, several models were developed, depending on the assumptions made for both the surface and gas-phase chemistry to provide insight into the real processes: one-film model, two-film model, and continuous-film model (Turns, 2000). In these models, for carbon particles with different sizes, temperatures, and pressures, the limiting step can be either diffusion, kinetic reaction on the surface, or both. However, no research has found Fe-NPs possess functions of elevating oxygen diffusion or kinetically increasing surface reaction rates

for the carbon-oxygen reaction. On the other hand, the reported pyrophorosity of Fe-NPs provides an explanation for promoting dust explosion as explained below.

(3) Pyrophoric Fe-NPs trigger the ignition of CNFs and facilitate the propagation of combustion? This assumption is very likely since previous experience showed that CNTs with iron can be ignited around 300 ℃ in air while pure CNTs cannot. In addition, several studies discussed the special effect of iron nanoparticles (Fe-NPs): the phenomena of a camera flash igniting SWCNTs was attributed to the pyrophoric nature of fine Fe particles within the nanotube bundles (Ajayan et al., 2002); iron (on the surface) helps catalyze the boron (core) oxidation at room temperature (Wang, 2012); the addition of metal nanoparticles (either Ni or Fe) can lower the ignition temperature of aerosols by as much as 150 ℃ (Ma, Liu, Aronhime, & Zachariah, 2011).

One possible explanation is illustrated in Figure 31 regarding the Fe-NPs effect of triggering the ignition of CNFs.

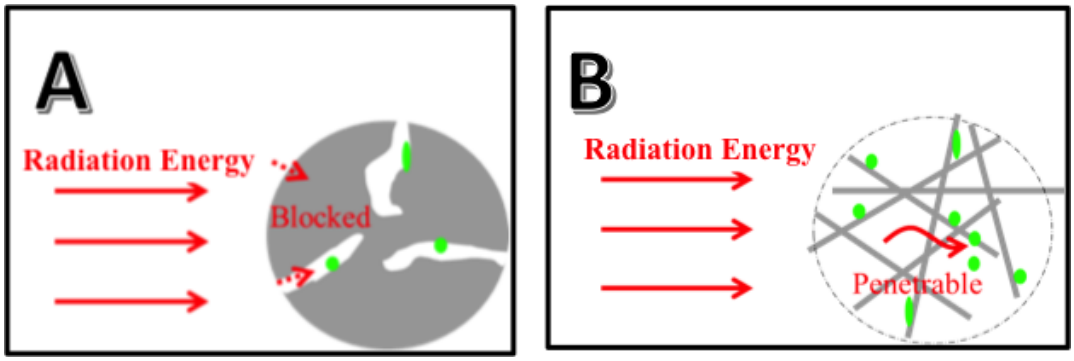

Figure 31. Radiation energy path in A: Conventional bulky particles; B: Nano-fiber agglomerates

Figure 31 shows the radiation energy path for both conventional bulky particles and nano-fiber agglomerates. The grey parts denote carbon material while the smaller green spheres denote Fe-NPs. For the conventional particles, most radiation energy is blocked/adsorbed by the bulky carbon materials, which will impede Fe-NPs to be accessible to the radiation. But the case is different for CNFs. The topology of CNF agglomerates is favorable for radiation energy to penetrate through the interstices and reach Fe-NPs. In addition, the lower thermal conductivity of iron - 80 $W \cdot m^{-1} K^{-1}$ - relatively insulates the heat, while heat tends to dissipate in CNFs with a higher thermal conductivity (6600 $W \cdot m^{-1} K^{-1}$ for SWCNTs and 200 $W \cdot m^{-1} K^{-1}$ for CNFs). With the penetrable topology of the CNF agglomerates to radiation energy, and the lower heat dissipation of Fe-NPs, along with its pyrophoric properties, Fe-NPs could cause "remote" ignition and serve as an additional source of ignition for the surrounding CNFs, which ultimately promotes the combustion of local CNFs as well as the propagation of combustion.

6.6 A Heterogeneous Model Explaining the Influence of Agglomerate Size and Fe-NPs on the Heat Transfer Process of Dust Explosion

As listed in Table 14, MECs are significantly different among similar CNF samples. While possible influential factors are agglomerate size and Fe-NPs, it is interesting to find out the limiting step in determining the MECs and propose a reasonable model for CNFs accordingly. Several potential factors affecting the combustion process are summarized in Table 16:

Table 16. Potential factors affecting combustion process

	Potential Factors	
1	Thermodynamics	Energy balance (enthalpy change)
2	Intrinsic reaction kinetics	Graphite perfection of CNFs
3	Transport process	Mass transfer; Heat transfer

Energy balance only depends on the change of thermodynamic states before and after the reaction. If energy balance is the determining factor of MECs, then it is predictable that MECs of samples with identical chemical composition, for example samples 1, 4 and 7, should be the same when all the tests were performed under the same controlled conditions (*e.g.*, temperature, pressure, reactants, ignition source, and amount of time after the fast acting valve closed). However, this prediction is contradictory to the experimental results listed in Table 14, which indicates that the thermodynamics of the reaction (or energy balance) is not the dominating factor.

The intrinsic reaction kinetics, which is different from the so-called apparent kinetics, excludes the effects of mass or heat transport phenomena. While particle size has no effect on intrinsic reaction kinetics, it only depends on the reactivity of reactants, temperature, pressure, and catalyst. In this study, the only factor that can affect the intrinsic reaction kinetics is the graphite perfection of CNFs. Thus, if the intrinsic reaction kinetics is the dominating factor, the MECs should be the same for samples 1, 4, 7 (also similar to samples 2, 5, 8 or samples 3, 6, 9) since they have the same graphite perfection. However, the MECs of these samples vary quite a bit. This inconsistency

between prediction and experimental observation could exclude the intrinsic reaction kinetics as the governing factor.

Furthermore, if the transport process (either the mass or heat transfer process) is the limiting step for MECs, then samples with identical agglomerate size and morphology, such as samples 7, 8 and 9 (also similar to samples 1, 2, 3 or samples 4, 5, 6), should possess very similar MECs unless factors that can affect the transport process are involved. Based on previous analysis about how Fe-NPs trigger the ignition of CNFs and facilitate the propagation of combustion, it is obvious that Fe-NPs help remove the limitation of heat transfer of CNFs and consequently decrease the MECs of CNFs. Thus, heat transfer process is the most credible limiting factor.

Since both heat transfer and mass transfer usually exhibit similar behaviors, our conclusion that heat transfer is the control step for this explosion process may seem peculiar. A qualitative heterogeneous model as illustrated in Figure 32 was proposed to help explain how heat transfer process controls the combustion and explosion process, and how the iron nanoparticles or the agglomerate size affect the heat transfer process in the combustion process.

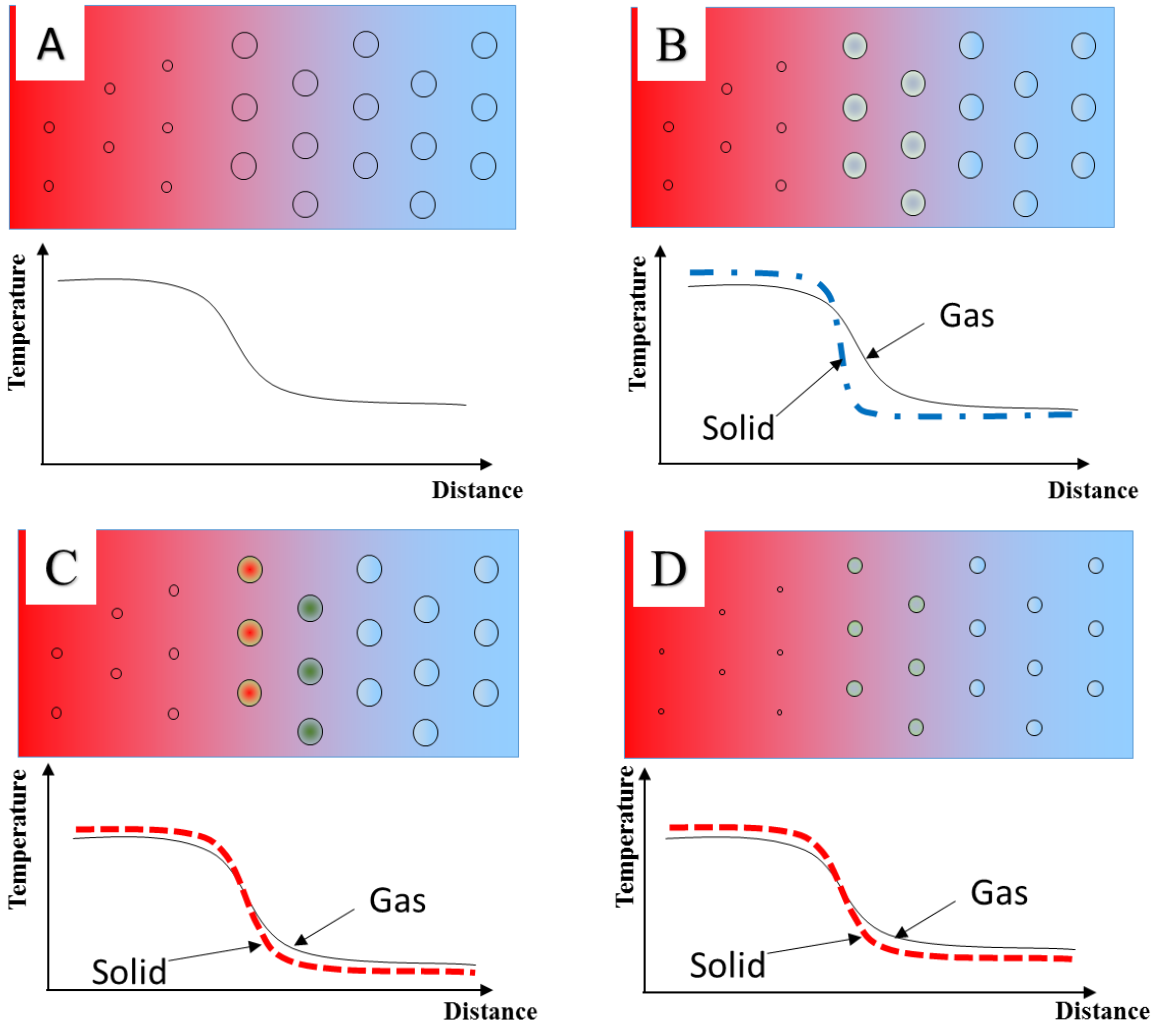

Figure 32. Dust explosion model: (A) Semi-Homogenous model; (B) Heterogeneous model; and the explications for (C): Effect of Fe-NPs by the proposed heterogeneous model; (D): Effect of dust particle size; Color darkness indicates temperature magnitude; Temperature profile: solid line for gas; dash lines for solid; X distance from flame

In Figure 32, the circles represent dust particles – the particle size in burnt areas is smaller than that in unburnt areas, because part of each particle was burned. The background colors represent the temperature: red means high temperature (burnt area) and blue means low temperature (unburnt area). The corresponding temperature-distance

profiles are also shown for each model or scenario in Figure 32. Figure 32 (A) is a semi-homogenous model used as the background group, ignoring the temperature difference between gas and solid particles. Figure 32 (B) is a heterogeneous model, taking into account the differences in the physical properties (temperature, specific heat capacity, density, *etc*.) of gas and solid particles. Usually the dust temperature is higher than the gas temperature in the burnt area because heat is generated from the combustion of dust fuel in the burnt area, while the dust temperature is lower than the gas temperature in the unburnt area close to the flame front.

As discussed earlier, Fe-NPs can serve as ignition sources for nearby carbon materials due to access to heat radiation. By incorporating the effect of Fe-NPs into the heterogeneous model, Figure 32 (C) was obtained. Since Fe-NPs attach to the surface of CNFs, the temperature increase of solid particles not only comes from the heat convection from gas phase to solid in the unburnt area, but also comes from the contribution of Fe-NPs ignition due to heat radiation. Therefore, the temperature of the solids with Fe-NP attached to the surface is closer to the gas temperature compared to the heterogeneous model, which do not consider the effect of Fe-NPs. Accordingly, the temperature profile in Figure 32 (C) is less steep compared with that in Figure 32 (B) in the zone between burnt and unburnt dust.

It is the same for the agglomerate size effect. The temperature profile is much smoother for smaller agglomerates, since the bigger specific surface area of smaller agglomerates and lower thermal inertia leads to faster temperature increase, as shown in Figure 32 (D).

From these analyses, we could find that the promoted heat transfer process by iron content and small agglomerate size could accelerate the temperature increase of solid particles before the flame front, resulting in enhanced explosibility of CNFs.

6.7 Conclusion

This research identified the MECs for various CNFs after different treatments: short/long milling periods and variable annealing temperatures. Relatively high MECs show that CNFs are not very explosive. However, their explosibility can be significantly increased if milled or the presence of other metal nanoparticles, even in small amounts. It shows that the agglomerate size rather than the size of a single fiber determines the explosibility, and smaller CNF agglomerates together with metal nano particles could influence the explosion significantly. CNFs are also a good study material to disclose the mechanism of dust explosion because of controllable agglomerate size and Fe content. A qualitative heterogeneous model based on heat transfer was also proposed to explain the effect of agglomerate size and Fe-NPs on combustion: smaller agglomerates with bigger specific surface area leads to faster temperature rise; pyrophoric Fe-NPs can be ignited remotely with a favorable penetration topology of CNF agglomerates, and therefore promote the heating of unburnt CNFs and facilitate the overall combustion and explosion process.

CHAPTER VII

CARBON NANOFIBER EXPLOSION VIOLENCE

7.1 Synopsis

Due to tremendous efforts in experimental explosion characterizations of combustible dust and better understanding of their influential factors, modern industry can design better safeguards to prevent and mitigate dust explosions. For example, the maximum over-pressure (P_{max}) and the deflagration index (K_{st}, which is the value of $[dP/dt]_{max}V^{1/3}$ at optimum dust concentration) are important characterizations used to evaluate dust explosion violence and help design proper safeguards in industry. However, when it comes to nanomaterials, research on their explosion characterizations are still coming into focus despite ever expanding production and applications. Engineered nanomaterials can have a variety of unique properties after various production and processing methods, making it difficult to analyze the reported experimental data and identify explosion factors. In this study, explosibility tests of nine commercially available carbon nanofibers (CNFs) were conducted in a customized 36-L dust explosion vessel. Test results demonstrated that a mechanical-milling process commonly used on CNFs could increase the deflagration index. While another common process, annealing, could decrease the explosion violence due to a significant influence on the deflagration index and modest influence on maximum overpressure. The effects of three influential factors - dust concentration, graphite perfection, and agglomerate size - were analyzed. In addition, this study proposed an improved method for estimating the

maximum overpressure from dust explosion as well as a demonstration of influential factors on $[dP/dt]_{max}V^{1/3}$.

7.2 Introduction

It has been more than two centuries since the first recorded dust explosion in Turin, Italy, on December 14, 1785 (Eckhoff, 2003). Tremendous efforts have focused on understanding, preventing and mitigating dust explosions. Properties of combustible dusts such as minimum explosive concentration (MEC), dust deflagration index (K_{St}), maximum explosion overpressure (P_{max}), and minimum ignition energy (MIE) are standard evaluation parameters for dust explosion, according to the American Society for Testing and Materials (ASTM) standards (ASTM, 2012a, 2013a, 2014, 2015). MIE and MEC predict the ease and likelihood of ignition of a dispersed dust cloud, while P_{max} and K_{St} measure the explosion severity of a dust explosion (Dastidar et al., 2005). Also developed were several National Fire Protection Association (NFPA) standards focused on industrial dusts (NFPA, 2012a, 2012b, 2013a, 2013b, 2014). However, dust explosion incidents occur not only in industrial facilities but under innocuous circumstances. For example, colored festival powder exploded at an outdoor music concert at the Formosa Fun Coast in Taiwan, on June 27, 2015, and caused more than 500 injuries (Botelho & Wang, 2015).

To date, no industrial incidents related to nanomaterials have been reported. However, laboratory incidents are appearing in newspaper and literature. For example, on February 14, 2008, a nanostructured energetic material exploded in a laboratory at

Military University of Technology in Warsaw, Poland, and a graduate student, lost both hands and an eye (Kemsley, 2008). A possible cause was the increased risk of electrostatic built up due to the trending of nanoparticles to agglomerate due to their larger specific surface area. In addition, an explosion of polyaniline nanomaterials was reported at Tianjin University in China. The victim sustained burn wounds to his hands, face, neck, and hair. The accumulation of a strong oxidant on large surface areas was attributed as the cause for the incident (H. Zhang, Wang, Zhang, Wang, & Wang, 2011). Increased specific surface areas of nanoparticles can also spike the risk of dust explosion according to the trend identified from micro-size particle explosions. MIE tends to reduce exponentially as particle size decreases; the "plateau effect" of particle size on MEC exists, which means that the minimum explosible concentration declines with reduced particle size until reaching a limiting stage where particles are too fine. In general, the explosion severity can be significantly enhanced by reducing particle size (Eckhoff, 2003). Therefore, more research was proposed to better understand the ignition behavior of nanomaterials, as well as the effects of agglomeration on combustion (particularly with respect to P_{max} and K_{St}) (Worsfold et al., 2012).

Dust explosions are complicated processes that are not fully understood. Explosion behaviors of micro-size particles can be impacted by chemical composition, particle size (both the median size and the polydispersity (Castellanos, Carreto-Vazquez, et al., 2014)), moisture content, oxygen concentration, gas atmosphere (Jiang et al., 2014, 2015), and inert dust concentration (Mannan, 2005). When it comes to engineering nanomaterials, the explosion behaviors become more complicated since various

processing and production methods can have unique impacts on the materials, which can potentially affect their explosion behavior. Currently, research focuses on explosions of metal nanoparticles and carbonaceous nanoparticles (Y. Huang, Risha, Yang, & Yetter, 2007; Turkevich et al., 2015; Vignes et al., 2009; Worsfold et al., 2012; Wu, 2010). Astonishing results show high potential for nanomaterials to initiate explosions and combustion. For example, the MEC of CNFs is significantly reduced by pyrophoric iron nanoparticles, which remain inside after their production (J. Zhang et al., 2015). Other examples include the flammability of nano-sized copper (Krietsch et al., 2015) and titanium nanoparticles exploding during dispersion, even with nitrogen as the compressed gas (Boilard et al., 2013).

Despite these remarkable findings, the differences in explosion severity between micro-size and nano-size particles are modest. Research on the explosion behaviors of metallic nano powders found they generally react similarly and do not possess a more intense burning behavior or higher explosion severity than dusts in the lower micron range (Krietsch et al., 2015). Research on carbonaceous nanoparticles showed that most of them were in Dust Explosion Class St-1, with minimal variation (Turkevich et al., 2015). However, there are still some experimental differences between the nano and lower micro particles that need to be recognized. For example, fullerene nanoparticles developed a stronger explosion than other carbonaceous nanoparticles, and its deflagration index is located at the border of St-1/St-2 (Turkevich et al., 2015).

While the annealing process in an inert atmosphere and mechanical milling are widely used in industries, this research aims at studying the influences of these processes

on explosion severity (P_{max} and K_{St}). Explosibility tests of nine commercially available CNFs were conducted in a customized 36-L dust explosion vessel. The effects of three influential factors – dust concentration, graphite degree, and agglomerate size - were analyzed. The CNFs were characterized with respect to particle size distribution and thermogravimetric analysis.

7.3 P_{max} and K_{St} Tests in a 36-L Dust Explosion Vessel

A customized 36-L dust explosion vessel, which has been calibrated against the standard 20-L vessel (Castellanos, Skjold, van Wingerden, Eckhoff, & Mannan, 2013) was employed to test explosibility of CNFs by following the ASTM E 1226 Standard Test Method for Explosibility of Dust Clouds (ASTM, 2012a). The standard operating procedure began with loading CNF samples into the dust container (located below the chamber), followed by installing a rebound nozzle between the dust container and the vessel. A pair of 5 kJ chemical igniters were installed in the center of the chamber. The sealed chamber was evacuated to 10.3 psia (71 KPa) while a reservoir was supplied with compressed air to 300 psig (2.07 MPa). Then a fast acting valve between the compressed air reservoir and dust container was opened for 50 ms to allow the compressed air to disperse CNF samples through the rebound nozzle, forming a uniform dust cloud inside the chamber while achieving to atmospheric pressure. Chemical igniters were programmed to ignite 25 ms after dispersion. The pressure evolution was recorded by pressure transducers installed on the vessel. The maximum pressure (P_{ex}), maximum

pressure increase rate ($[dP/dt]_{max}$), and the deflagration index (K_{St}) were determined by a LabVIEW program developed in-house.

7.4 Explosibility of CNFs

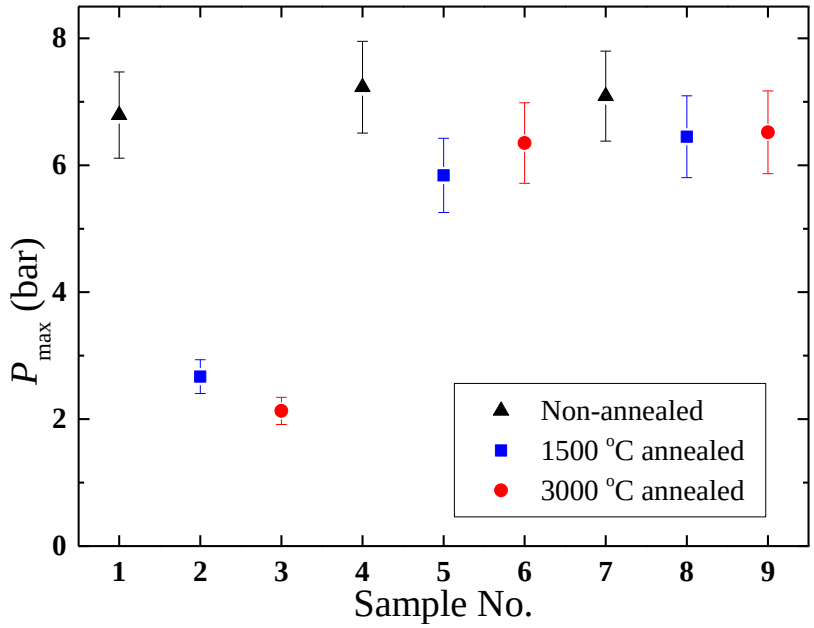

Figure 33. P_{max} of CNFs at a lean fuel concentration (125 g m^{-3})

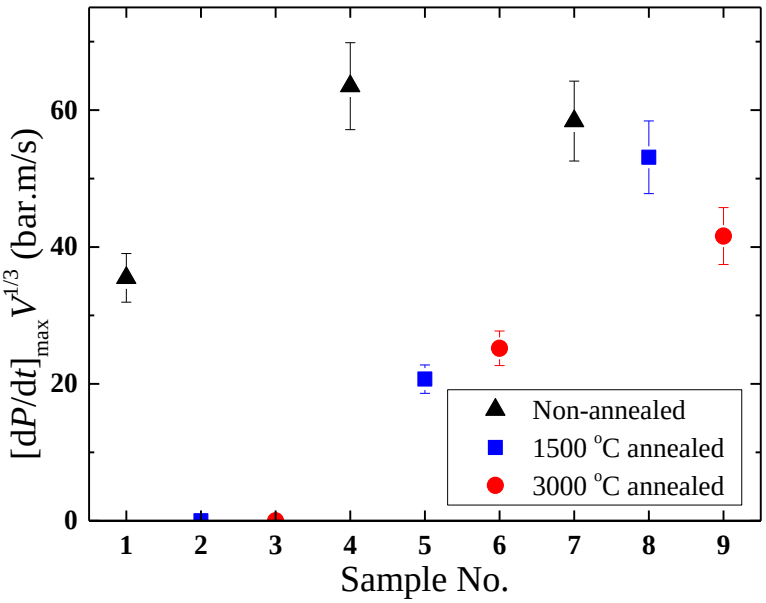

Figure 34. $[dP/dt]_{max}V^{1/3}$ of CNFs at a lean fuel concentration (125 g m^{-3})

Explosibility tests of these nine samples were first conducted at a low CNF concentration of 125 g m^{-3}, which is about the stoichiometric concentration (110 g m^{-3} for $C + O_2 = CO_2$). The concentration was also below most of their MECs determined earlier (J. Zhang et al., 2015). However, due to the higher ignition energy (10 kJ instead of 2.5 kJ used for MEC determination), most of the samples overcame the limitation of heat transfer (as previously mentioned) and formed a deflagration. Their maximum overpressures P_{max} (bar) and $[dP/dt]_{max}V^{1/3}$ (bar m s^{-1}) were plotted in Figures 33 and 34 respectively. For samples 2 and 3, their pressure ratios (PR) were calculated by equation (24), and are smaller than 2. It indicated the overpressures shown in Figure 33 were mainly caused by the ignitors rather than the CNFs. Therefore, their values of $[dP/dt]_{max}V^{1/3}$ were plotted as 0 in Figure 34 to indicate no CNF explosion.

The effect of annealing on the CNFs' explosibility was studied by comparing the P_{max} and $[dP/dt]_{max}V^{1/3}$ created by non-annealed samples and their corresponding annealed samples. Among the unmilled CNFs (samples 1-3), non-annealed CNFs exploded (sample 1) while annealed ones (samples 2 and 3) did not. Although all the short mill time CNFs (samples 4-6) exploded, the non-annealed CNFs (sample 4) formed a much higher $[dP/dt]_{max}$. Again, all the long mill time CNFs exploded while the non-annealed CNFs (sample 7) formed higher $[dP/dt]_{max.}$ Therefore, it could be concluded that the non-annealed samples have higher explosibility. In addition, suppressed explosibility was observed on the improved graphite perfection after annealing, of which negligible differences exist between 1500°C and 3000°C annealed samples, similar to that found by TGA.

This study also compared the P_{max} and $[dP/dt]_{max}V^{1/3}$ created by unmilled samples and their corresponding milled samples to study the effect of the milling process on CNFs' explosibility. While samples 2 and 3 did not explode at the given conditions, all of their corresponding milled samples formed notable deflagrations. Once the CNFs exploded, values of P_{max} were quite close while the values of $[dP/dt]_{max}$ $V^{1/3}$ had significant variability. The long mill time CNFs created much higher $[dP/dt]_{max}$ $V^{1/3}$ than the short mill time CNFs. Therefore, it could be concluded that milled samples (smaller agglomerates) have higher explosibility with higher $[dP/dt]_{max}V^{1/3}$.

Sample 7, which formed the strongest explosion at 125 g m^{-3}, was then tested at higher concentrations up to 1000 g m^{-3}. Figures 35 and 36 show the maximum overpressure P_{max} and the $[dP/dt]_{max}V^{1/3}$ as a function of concentration. A 10% deviation

is included in Figures 35 and 36 due to equipment accuracy. It can be found that the maximum overpressure is about 8 bar and that the deflagration index, which is the maximum value of $[dP/dt]_{max}V^{1/3}$ through the concentration range, is about 100 bar ṁ s^{-1}. Therefore, the combustible dust CNFs can be rated as St-Class 1 based on the St classifications for dust explosions (Abbasi & Abbasi, 2007).

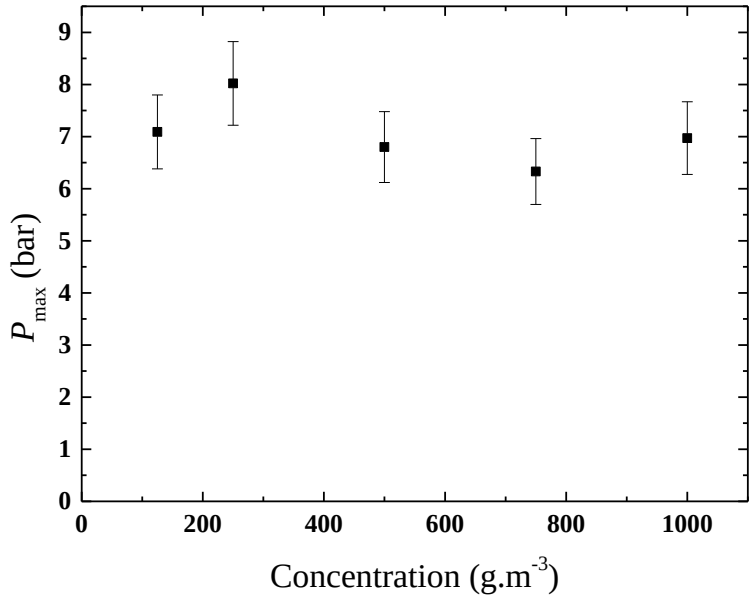

Figure 35. P_{max} of sample 7 at various concentrations up to 1000 g ṁ$^{-3}$

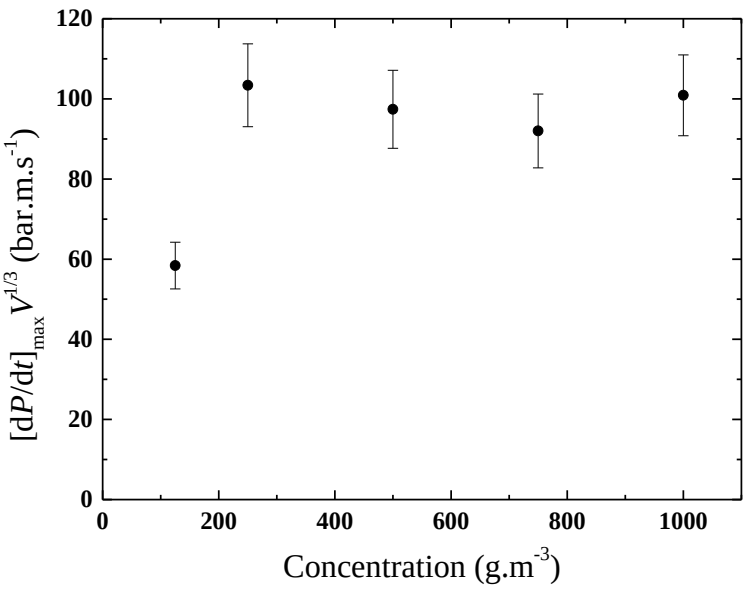

Figure 36. $[dP/dt]_{max}V^{1/3}$ of sample 7 at various concentrations up to 1000 g m^{-3}

As shown in Figures 35 and 36, the maximum overpressure and pressure increase rate reach their maximum values at the concentration of 250 g m^{-3}. Extra loading of CNFs have slight effects on lowering the values of $[dP/dt]_{max}V^{1/3}$ and P_{max}. However, these effects are still insignificant for having a rich limit. These results match previous findings in that there is an absence of a "normal" rich limit which is the characteristic of all dusts, and is a reflection of the phase heterogeneity of the reacting system (Hertzberg, Zlochower, & Cashdollar, 1988).

7.5 Effect of Ignition Energy

It is suggested in the test standard (ASTM, 2014) that a weak ignition source, for example 2.5 kJ, should be used to initiate an explosion without overdriving. When

identifying the violence of a dust explosion, it is suggested to use a strong ignition source to have a fully developed deflagration (ASTM, 2012a). However, ignition energy selection varies worldwide. In Europe, a dust is classified as 'not explosible' if it cannot be exploded in a wide concentration range with ignition energy of 1–2 kJ (Denkevits & Dorofeev, 2005; VDI-Richtlinien, 1990).

This study selected a few tests performed with the same material at the same concentration but with different ignition energy (2.5 kJ or 10 kJ) to show its effect. The results were summarized in Table 17.

Samples 1 and 9, which are carbon nanofibers with high MECs, did not explode with an ignition energy of 2.5 kJ at a concentration of 125 g m^{-3}. However, a pair of stronger igniters with 10 kJ triggered the explosions. Sample 1 produced a deflagration with the maximum overpressure of 6.79 bar and the deflagration index of 35.5 bar $m\ s^{-1}$; sample 9 formed a deflagration with the maximum overpressure of 6.52 bar and the deflagration index of 41.6 bar $m\ s^{-1}$.

Samples 4, 7, and 8, which are carbon nanofibers with low MECs, exploded with an ignition energy of 2.5 kJ at concentrations of 125 g m^{-3} or 250 g m^{-3}. When these samples were ignited by stronger igniters (10 kJ), stronger deflagrations formed. For samples 7 and 8, the values of maximum overpressure P_{max} at 125 g m^{-3} slightly increased after triggering the stronger igniters (10 kJ). However, for sample 4, the stronger igniter did not form a higher maximum overpressure at 250 g m^{-3}. Therefore, the promotion effect on maximum overpressure of igniters may only work for low concentrations. However, this hypothesis needs more experimental results for validation.

Table 17. Effect of igniters

Sample	Concentration (g m^{-3})	Igniter	Explosible?	P_{max} (bar)	K_{St} (bar m s^{-1})
1	125	2.5 kJ	No	--	--
		10 kJ	Yes	6.79	35.5
9	125	2.5 kJ	No	--	--
		10 kJ	Yes	6.52	41.6
4	250	2.5 kJ	Yes	7.42	38.8
		2.5 kJ	Yes	7.60	43.1
		10 kJ	Yes	7.41	69.0
7	125	2.5 kJ	Yes	6.6	28.4
		2.5 kJ	Yes	6.08	18.23
		10 kJ	Yes	7.09	58.4
8	125	2.5 kJ	Yes	5.88	14.36
		10 kJ	Yes	7.23	63.5

In addition, stronger igniters promoted the values of $[dP/dt]_{max}V^{1/3}$ for samples 4, 7, and 8 at concentrations of 125 g m^{-3} and 250 g m^{-3}. This promotion effect was more obvious for samples 7 and 8 at low concentration of 125 g m^{-3}. As shown in Table 17, igniters with 10 kJ increased their values of $[dP/dt]_{max}V^{1/3}$ by more than 300%. For sample 4, stronger igniters also increased the value of $[dP/dt]_{max}V^{1/3}$ by about 50% at a concentration of 250 g m^{-3}.

7.5 Modified Estimation Method for CNF Explosion's Maximum Overpressure

Based on the ideal gas law, the pressure rise during an explosion inside the constant volume vessel is caused by the increased amount of gas and the temperature rise of the gas, which is heated by the combustion heat of CNFs.

$$V = \frac{N_0 R T_0}{P_0} = \frac{N_f R T_f}{P_f} = \text{constant} \tag{26}$$

where:

V is the constant volume of the vessel (m^{-3});

subscript of "0" and "f" refer to the initial and final states of a test;

N is the total molar number of gases;

T is temperature (K);

P is pressure (Pa).

An estimation model was proposed from the equilibrium thermodynamics of the reaction $C+0.5O_2 \rightarrow CO$. It was divided into two regimes (Turkevich et al., 2015):

For concentration lower than the stoichiometric concentration (Turkevich et al., 2015):

$$\frac{P_m}{P_i} = \alpha \times \left(\frac{N_{O_2}}{N_{air}} \right) \times \left[1 + \frac{2\Delta h}{c_{air} T_i} \right] \tag{27}$$

For concentration higher than the stoichiometric concentration (Turkevich et al., 2015):

$$\frac{P_{\mathrm{m}}}{P_{\mathrm{i}}}=\left(\frac{N_{\mathrm{O_2}}}{N_{\mathrm{air}}}\right)\times\left\{1+\frac{2\Delta h}{c_{\mathrm{air}}T_{\mathrm{i}}}\times\left[1+2\left(\alpha-1\right)\times\left(\frac{c_{\mathrm{carbon}}}{c_{\mathrm{v,air}}}\right)\times\frac{N_{\mathrm{O_2}}}{N_{\mathrm{air}}+N_{\mathrm{O_2}}}\right]^{-1}\right\} \quad (28)$$

where:

$c_{\mathrm{v,air}}$ is the capacity of air of constant volume 20.85 J·mol^{-1}·K^{-1} at normal conditions;

c_{carbon} is the capacity of carbon 8.53 J·mol^{-1}·K^{-1} at normal conditions;

Δh is the enthalpy of reaction 110.5 kJ·mol^{-1};

α is the ratio of tested concentration of CNFs and the stoichiometric concentration;

T_{i} is the initial temperature 300 K.

In this model, parameters like the heat capacity of the gas mixture, unburnt carbon solid, and enthalpy of reaction were considered. It demonstrated that P_{max} increases with higher concentration of CNFs until it reaches the optimum concentration (*i.e.*, 250 g·m^{-3}, which is close to its stoichiometric concentration in air, 220 g·m^{-3}). After that, extra unburned CNFs absorb the energy released from the combustion reaction, reducing the P_{max}.

A comparison was made between these experimental data and the estimated overpressure by this model. Agreement was observed at high CNF concentrations, such as those larger than the stoichiometric concentration of reaction $C+0.5O_2 \rightarrow CO$, which is 220 g·m^{-3}. However, overpressures were generally underestimated at concentrations lower than the stoichiometric concentration. For example, the overpressure calculated at

a concentration of 125 g·m^{-3} is 4.34 bar, which is much lower than the experimental result, 7.09 $\pm$ 0.71 bar.

The assumption that only carbon monoxide was produced in the explosion may contribute to the underestimation. While CNF concentration of 125 g·m^{-3} was lower than 220 g·m^{-3} indicating the air is in excess for the combustion reaction, the produced carbon monoxide reacted with the excess oxygen molecules in the surrounding environment, forming carbon dioxide. This process was demonstrated by the two-film model of carbon combustion (Turns, 2000), as shown in Figure 20 in Section 4.3.1.

In this two-film model, the carbon surface is attacked by CO_2 according to the reaction $C+CO_2 \rightarrow 2CO$. The CO produced at the surface diffuses outward and is consumed at a flame sheet where it meets an inward-diffusion flow of O_2 in stoichiometric proportions. The global reaction $CO+0.5O_2 \rightarrow CO_2$ is assumed to be infinitely fast; thus both CO and O_2 are identically zero at the flame sheet.

It appears that there were at least two reactions between oxygen and carbon when there is extra oxygen remaining after attacking all the carbon particles:

$$C+O_2 \rightarrow CO_2 \qquad \Delta h_1=393.5 \text{ kJ·mol}^{-1};\ \Delta N_1=0 \tag{R1}$$

$$C+0.5O_2 \rightarrow CO \qquad \Delta h_2=110.5 \text{ kJ·mol}^{-1};\ \Delta N_2=0.5 \tag{R2}$$

The high amount of heat released from reaction (R1), Δh_1 made up the increased number of moles in reaction (R2), ΔN_2. Thus, the equation can be modified to

$$\frac{P_{\mathrm{m}}}{P_{\mathrm{i}}} = \alpha \times \left(\frac{N_{\mathrm{O_2}}}{N_{\mathrm{air}}} \right) \times \left\{ \beta \times \left(1 + \frac{\Delta h_1}{c_{\mathrm{air}} T_{\mathrm{i}}} \right) + (1-\beta) \times \left(1 + \frac{2\Delta h_2}{c_{\mathrm{air}} T} \right) \right\} \tag{29}$$

Here β is the portion of CNFs producing carbon dioxide while (1-β) is the portion of CNFs producing carbon monoxide. With the assumption that extra oxygen and carbon monoxide will produce carbon dioxide, the value of β can be determined:

$$\beta = \begin{cases} 1 & \text{when } c_{CNF} < 110 \text{ g} \cdot \text{m}^{-3} \\ \dfrac{220}{c_{CNF}} - 1 & \text{when } 110 \text{ g} \cdot \text{m}^{-3} < c_{CNF} < 220 \text{ g} \cdot \text{m}^{-3} \\ 0 & \text{when } c_{CNF} > 220 \text{ g} \cdot \text{m}^{-3} \end{cases} \tag{30}$$

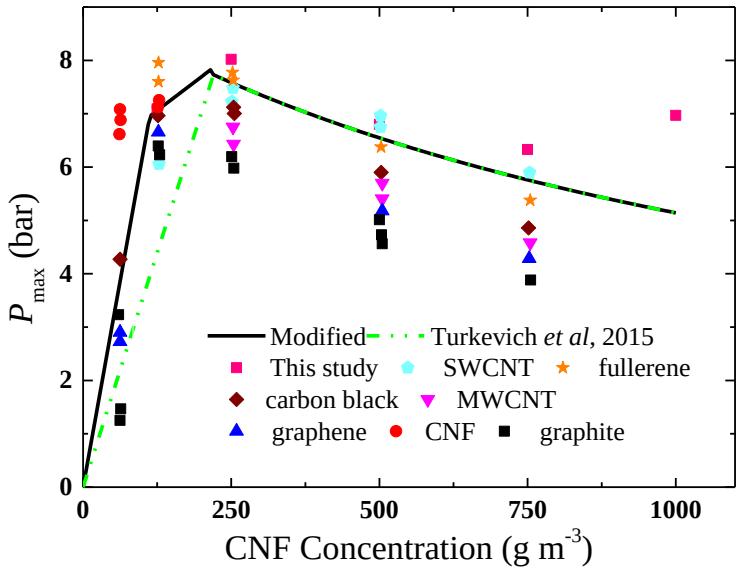

Figure 37. Maximum overpressure estimation

The estimated P_{max} values via this improved approach and the original approach (Turkevich et al., 2015) are compared with the experimental observation, as shown in Figure 37. A better agreement was reached with the modified method, when CNF concentration is less than 220 g m^{-3}. In addition, P_{max} values of other carbonaceous

material (Turkevich et al., 2015) were also plotted in Figure 37. It was found that the improved approach was applicable for most of the carbonaceous nanomaterial, especially at low concentrations. However, this model overestimated the maximum overpressure at high concentrations for graphite, graphene, MWCNT, and carbon black. Therefore, more efforts are needed for a better estimating model.

7.6 Influential Factors for CNF Explosions' $[dP/dt]_{max}V^{1/3}$

In the process of the CNFs' explosions, there are at least two major sub-processes: the combustion of CNFs in the burning zone, and the flame propagation from burning zone to unburnt zone. The whole process can be treated as the time evolution of these two sub-processes. The effects of influential factors on the value of $[dP/dt]_{max}V^{1/3}$ during these two sub-processes will be discussed in the next section.

Influential factors in the burning zone

In the burning zone, the pressure increase rate is mainly caused by gas expansion when temperature increases according to the ideal gas law (ignoring the changes in the number of moles of gases) and heat transfer between hot CNF agglomerates and gas:

$$\frac{dP}{dt} = \frac{N_{gas}R}{V} \times \frac{dT_{gas}}{dt} = \frac{R \times A_{CNF} \times q}{V \times c_{v,gas}} \quad (31)$$

where:

t is time (s);

q is the overall heat flux which is contributed by both convection and radiation (W m^{-2});

$c_{v,gas}$ is the heat capacity of gas ($J \cdot mol^{-1} \cdot K^{-1}$);

N_{gas} is the mole of gas in a certain volume (mole);

A_{CNF} is the total surface area of CNFs in the burning zone (m^2);

V is the volume of gas involved (m^3).

Therefore, in the burning zone, the pressure increase rate depends on the total surface area of CNFs when other variables are identical for different CNFs. Based on the equation below, milled CNFs have larger surface areas due to the decreased radius of CNF agglomerates (r):

$$A_{CNF} = 4\pi r^2 \times \text{Number}_{CNF} = 4\pi r^2 \times \frac{c_{CNF} \times V}{\frac{4}{3}\pi r^3 \times \rho_{CNF}} = \frac{3c_{CNF} \times V}{r \times \rho_{CNF}} \quad (32)$$

where:

c_{CNF} is the concentration of CNF suspended in air ($kg \cdot m^{-3}$);

ρ_{CNF} is the density of CNF agglomerates ($kg \cdot m^{-3}$).

Therefore, milled CNFs demonstrate stronger explosion violence due to their improved heat transfer effect in the burning zone.

Influential factors in the flame propagation process

In the process of flame propagation, the burning velocity of the dust explosion can be estimated by adopting the classical Mallard – Le Chatelier model for premixed

gases, with an additional term representing the thermal radiation (Eckhoff, 2003; Ogle, Beddow, Vetter, & Chen, 1984):

$$S_u = B + \left(B^2 + A\right)^{1/2} \tag{33}$$

$$B = \frac{1}{2}\left(\frac{\in \sigma}{\rho_u c_p}\right)\left(\frac{T_f^4 - T_0^4}{T_i - T_0}\right) \tag{34}$$

$$A = \frac{\lambda}{\rho_u c_p \tau}\left(\frac{T_f - T_i}{T_i - T_0}\right) \tag{35}$$

where:

S_μ is the burning velocity (m s^{-1});

ρ is the initial density of the gas phase (kg·m^{-3});

σ is the Stefan-Boltzmann constant (=5.66 ·10^{-8} J s^{-1} m^{-2} K^{-4});

$\in$ is the emissivity (unitless);

c_p is the heat capacity of gas at constant pressure (J kg^{-1} K^{-1});

T_f is the flame temperature (K);

T_i is ther ignition temperature (K);

T_0 is the initial temperature (K);

λ is the thermal conductivity (J s^{-1} m^{-1} K^{-1});

τ is the burning time of a dust particle (s).

For small CNF agglomerates, whose burning time is governed by the surface reaction rate, the combustion time can be calculated (Bouillard et al., 2010):

$$\tau_b = \frac{\rho_s d_p}{2k_1 \left(P_{tot} MW_{gas} / RT_s \right) \left(MW_C / MW_{O_2} \right) Y_{O_2,s}} \quad (36)$$

where:

k_1 : Kinetic constant of combustion, m s^{-1}

T_s : Temperature at the particle surface (K)

ρ_s, ρ_g : Density of solid particle and air (kg m^{-3})

d_p : Diameter of particle (μm)

$Y_{O_{2,\infty}}$: Oxygen mass fraction in air, 0.233

MW_{O_2}, MW_C : Molecular weight of oxygen and carbon

The combination of these two equations demonstrates that smaller CNF agglomerates after milling have a faster laminar burning velocity due to reducing the burning time of every particle, and innerted CNFs with promoted graphite perfection have a slower laminar burning velocity due to decreasing the combustion rate (k_1) and increasing the ignition temperature (T_i).

7.7 Estimated Laminar Burning Velocity

Though the three-zone model (A.E. Dahoe & de Goey, 2003) of dust explosion is more practical than the thin-flame model, considering that the flame thickness can be negligible comparing to the vessel radius, this study adopts the following estimation

formulas (A E Dahoe, Zevenbergen, Lemkowitz, & Scarlett, 1996) using the thin flame model:

$$\frac{m_u}{m_0} = \frac{P_e - P}{P_e - P_0} \tag{37}$$

Where

m_u is the mass of unburn material (kg);

m_0 is the mass of the initial material (kg);

P_e is the final pressure after explosion (N m^{-2});

P_0 is the initial pressure (N m^{-2}).

$$\frac{dm_u}{dt} = -4\pi r_f^2 \rho_u S_u \tag{38}$$

Where

r_f is the location of the thin flame front (m);

ρ_u is the density of the unburnt mixture (kg m^{-3});

S_u is the burning velocity (m s-1).

Then the pressure change rate can be written as:

$$\frac{dP}{dt} = -\frac{P_e - P_0}{m_0}\frac{dm_u}{dt} \tag{39}$$

And r_f can be expressed as:

$$r_f = \left[\frac{V_0 - \frac{m_u R T_u}{P}}{\frac{4}{3}\pi} \right]^{\frac{1}{3}} \tag{40}$$

For an adiabatic compress:

$$\frac{T_u}{T_0} = \left(\frac{P}{P_0} \right)^{\frac{\gamma-1}{\gamma}} \tag{41}$$

where:

T_u is the temperature of unburnt mixture (K);

T_0 is the initial temperature (K);

γ is the specific heat ratio, which equals to C_p/C_v.

Then the density of unburn mixture (ρ_u) can be written as:

$$\rho_u = \frac{m_0}{V_0} \frac{P}{P_0} \frac{T_0}{T} = \frac{m_0}{V_0} \left(\frac{P}{P_0} \right)^{\frac{1}{\gamma}} \tag{42}$$

Therefore, the pressure rise rate reaches the maximum value and it can be corrected with the laminar burning velocity:

$$\left(\frac{dP}{dt} \right)_{max} = \frac{3\left(P_{max} - P_0\right)}{R_{vessel}} \left[1 - \left(\frac{P_0}{P} \right)^{\frac{1}{\gamma}} \frac{P_{max} - P}{P_{max} - P_0} \right]^{\frac{2}{3}} \left(\frac{P}{P_0} \right) S_u \tag{43}$$

where

P_{max} is maximum pressure during the explosion (bar);

R_{vessel} is radius of the 36-L vessel (m);

The pressure profiles of CNF explosions were extracted from the LabVIEW program. Table 18 listed the parameters needed for estimating the laminar burning velocity.

Table 18. Pressure parameters

#	**Ignition**		**The maximum slope**			**P_{max}**	
	t_0 (ms)	P_0 (bara)	t (ms)	P (bara)	$[dP/dt]_{max}$ (bar ms^{-1})	t_{max} (ms)	P_{max} (bar)
1	233.2	1.07	243.3	4.97	0.1075	342.8	6.79
2	--	0.9	--	--	--	--	--
3	--	0.9	--	--	--	--	--
4	238.4	1.1	271	2.33	0.158	323.4	7.13
5	199	1.1	251.9	3.77	0.0627	356.4	5.84
6	175.6	1.06	187.1	3.68	0.0762	338.8	6.35
7	224	1.1	262.7	4.53	0.1793	294.4	7.09
8	253.6	1.06	260.8	3.92	0.1608	321.8	6.45
9	254.6	1.06	296.7	4	0.126	344.8	6.52

In addition, the total flame speed, which is the speed of the flame front relative to an observer or fixed geometries (the pressure transducer on the vessel wall for the experiments), can be written as (Eckhoff, 2003):

$$S_f = S_u + S_g \tag{44}$$

It explains that the flame speed (S_f) is the combination of laminar burning velocity (S_u) and the gas velocity component caused by the expansion and buoyancy of the combustion product gases.

Therefore, the flame speed can be estimated by

$$S_f = \frac{R_{vessel}}{t_{max} - t_0} \tag{45}$$

where

t_{max} is the time when the maximum overpressure is reached;

t_0 is the time when the ignitor is triggered.

The result of the laminar burning velocity and flame speed of these CNFs were plotted in Figure 38. All these behaviors occurred at a concentration of 125 g ṁ$^{-3}$.

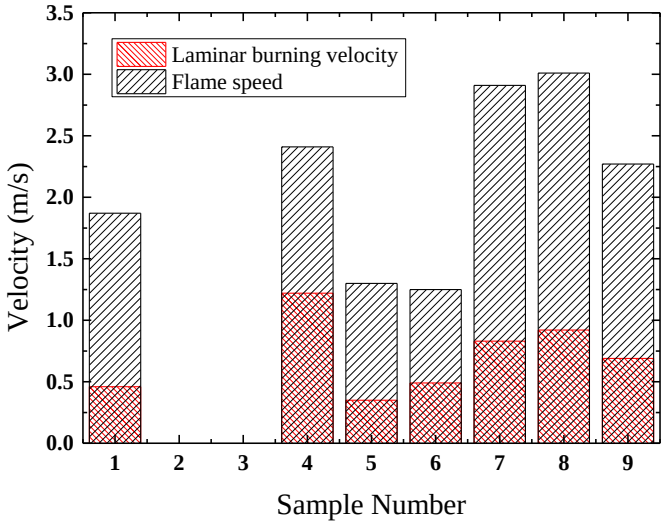

Figure 38. Laminar burning velocity and flame speed of CNFs at 125 g ṁ$^{-3}$

It should be noted that these results are estimated from the pressure profile. While currently no experimental data is available for either laminar burning velocity or flame speed of carbon nanofibers, it is not possible for the author to validate the results. While the burning velocity of coal at similar concentration was reported between 0.2 -

0.3 m s^{-1}, there is a high possibility that this model overestimates the burning velocity, but within a reasonable range.

Future work on obtaining experimental results of laminar burning velocity of dust explosion would further validate these results.

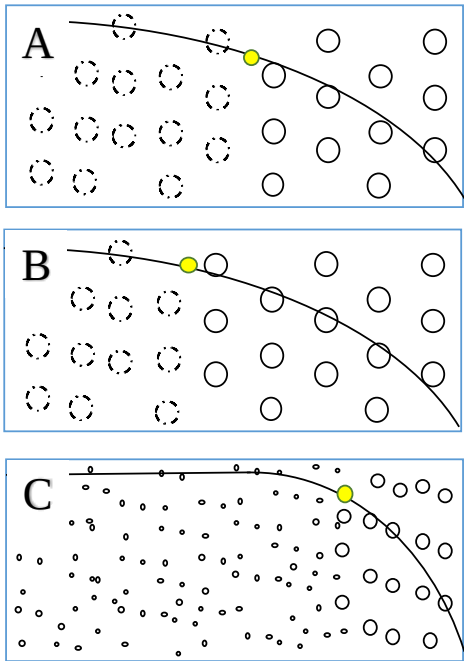

Figure 39. Heterogeneous dust explosion models for: (A) pristine CNFs (non-annealed, unmilled); (B) annealed CNFs with promoted graphite perfection; (C) milled CNFs with smaller agglomerates. The darkness of colors and the solid line indicate the temperature profile from burnt zone to unburnt zone. The yellow dot demonstrates the temperature needed for combustion.

A heterogeneous dust explosion model was applied in previous research to explain the effects of Fe-NPs and smaller agglomerates on promoting the ignition

process (J. Zhang et al., 2015). A similar model was proposed for the flame propagation process to explain the influential factors on $[dP/dt]_{max}V^{1/3}$.

In Figure 39, the circles represent dust particles – the dashed particles are burning while the solid ones remained unburnt. Both the background color (red for high temperature, blue for low temperature) and the solid line indicate the temperature – distance profile. Particles in the unburnt zone are mainly heated by the radiative energy and convective heat. At the same distance from the flame front, smaller agglomerates have a higher temperature as indicated in the solid line in Figure 39-C. The yellow dots are the ignition temperatures. Figure 39-B shows CNFs with promoted graphite perfection require a high temperature to ignite.

Compared with non-annealed CNFs (Figure 39-A), CNFs with promoted graphite perfection (Figure 39-B) have fewer agglomerates reaching the required ignition temperature. Therefore, the pressure increase rate caused by the heat released from combustion was lower than the non-annealed CNFs. On the other hand, milled CNFs have more agglomerates reaching the required ignition temperature. As a result, more heat is released from combustion.

7.8 Conclusion

This study identified the explosion violence for commercially available CNFs. They are categorized as St-1 class combustible dust, whose deflagration index is lower than 200 bar·m s^{-1}. In addition, this study finds the processing methods often applied to CNFs - milling and annealing - have different impacts on explosion violence. Factors

influencing CNF explosion maximum overpressure P_{max} (bar) and the deflagration index value $[dP/dt]_{max}V^{1/3}$ (bar·m·s^{-1}) were studied via explosibility tests. It was concluded that P_{max} of CNFs at low concentration, *e.g.* 125 g m^{-3}, were affected by graphite perfection while the deflagration index values $[dP/dt]_{max}V^{1/3}$ were affected by both agglomerate size and graphite perfection. Concentration of CNFs plays a similar role as with micro-size particle explosion behavior. This study also proposed an improved estimation method for the maximum overpressure, as well as demonstrations of influential factors on $[dP/dt]_{max}V^{1/3}$.

CHAPTER VIII

SUMMARY AND FUTURE WORK

8.1 Summary

This dissertation reported the results of a combustion and explosion study of carbon nanofibers (CNFs) after various production processes. This study characterized the morphology of CNFs with a scanning electron microscope, the particle size distributions with Spraytec laser scattering and Beckman Coulter, and the thermal stability with thermogravimetric analysis. Explosibility tests were performed in a customized 36-L dust explosion vessel and a minimum ignition energy apparatus (MIKE 3). Combining the characterization tests, explosibility tests, and theoretical analysis, this study provided an improved understanding about combustion and explosion risk of CNFs after different production processes - milling duration, and annealing at 1500 ℃ or 3000 ℃.

1. The sample morphology was observed by Scanning Electronic Microscope (SEM), showing that rather than exist as individual fibers, CNFs tended to agglomerate together and form micro-sized ellipsoid agglomerates. In addition, the milling process effectively reduced the CNF agglomerate size from approximately 30 μm to less than 10 μm and even smaller; longer mill time produces smaller agglomerates. The milling process also reduced the length of a considerable portion of fibers from about 10 μm to 5 μm or even shorter, although long fibers still existed. The reduced length to diameter ratio may contribute to smaller agglomerates after the milling process.

2. The morphology of carbon nanofibers dispersed through the 36-L dust explosion vessel was also studied. It was found that a significant quantity of the agglomerates were broken after the dispersion, resulting in carbon nanofibers as single fibers loosely attached with others. However, it also showed that some large agglomerates with a diameter of 30 μm still exist. However, most of the fibers were still as long as before dispersion. Therefore, a brief conclusion can be made that the effect of the dispersion process was to break the agglomerates but not to shorten single fibers. Also, this effect suggests that the explosibility results obtained from the 36-L vessel are worse than actual scenarios.
3. The particle size distribution study with both Spraytec and Beckman Coulter showed that most particles were larger than 30 μm before milling. After milling, many particles were broken, reducing their size to approximately 10 μm. Additional milling time led to the formation of more particles smaller than 10 μm. Meanwhile, the milling process widened the CNF agglomerate particle size distribution due to the generation of smaller particles and co-existence of large particles. In addition, all the samples showed multi-modal distribution behavior rather than a normal distribution. The milling process also increased the number of modals. It was possible that the CNFs formed not only primary agglomerates, but also secondary, or even tertiary agglomerates. Both analysis methods confirmed this result. The particle size obtained with the Beckman Coulter was smaller than that of the Spraytec, and closer to that found in the SEM images.

4. During the MIE tests, it was observed that the black CNF cloud filled the entire vertical tube and no sign of light was observed after the spark was released from the electrodes. Therefore, the MIE was determined to be above 1000 mJ for all concentrations. CNFs need relatively high initial energy to be ignited, which means it is safe from electrostatic discharge.
5. This study identified the thermal stability for commercially available CNFs. In general, CNFs have high thermal stability, which requires high temperature (> 500 ℃) to react with air. In addition, this study finds the processing methods often applied to CNFs – milling and annealing – have different impacts on thermal stability. The annealing process, which improved graphite perfection of CNFs increased the observed T_{onset}, and $T_{oxidation}$. CNF annealing at 1500 ℃ and 3000 ℃ showed nearly identical promotion of the annealing effects. The milling process also had an effect on CNFs thermal stability. For annealed samples, the milling process had a significant effect on their thermal stability, resulting in onset temperatures reduced by 80-100 ℃. However, the milling process had insignificant effect on non-annealed CNFs. In addition, the duration of milling played only a negligible role onset temperature reduction.
6. This research identified the MECs for various CNFs after different treatments: short/long milling periods and variable annealing temperatures. Minimum explosible concentration of CNFs varied from 105 g m^{-3} to greater than 300 g m^{-3}. Relatively high MECs indicate that CNFs are not very explosive; however, its explosibility can be significantly increased if milled or the presence of other

metal nanoparticles even in a small amount. It shows that the agglomerate size rather than the size of a single fiber determines the explosibility, and smaller CNF agglomerates together with metal nano particles which influence the explosion significantly. CNFs also present a good study material to determine dust explosion mechanism because of the controllable agglomerate size and iron content.

7. This study identified the explosion violence for commercially available CNFs. In general, the maximum overpressure was about 8 bar. CNFs are categorized as a St-1 class combustible dust, whose deflagration index is lower than 200 bar·m·s^{-1}. In addition, this study found the processing methods often applied to CNFs – milling and annealing – have different impacts on explosion violence. Factors influencing the maximum CNF explosion overpressure P_{max} (bar) and the deflagration index value $[dP/dt]_{max}V^{1/3}$ (bar·m·s^{-1}) were studied via explosiblity tests. It was concluded that P_{max} of CNFs at low concentration, *e.g.* 125 g·m^{-3}, were affected by graphite perfection, while the deflagration index values $[dP/dt]_{max}V^{1/3}$ were affected by both agglomerate size and graphite perfection. Concentration of CNFs plays a similar role as with micro-size particle explosion behavior.
8. This study also proposed an improved estimation method for the maximum overpressure of carbonaceous nanomaterial based on the two-film combustion theory. Instead of assuming only carbon monoxide was produced during CNF explosions, the modified method agreed more with the experimental data at low

concentration with the assumption that both carbon monoxide and carbon dioxide were produced.

9. A qualitative heterogeneous model based on heat transfer was also proposed to explain the effect of agglomerate size, Fe-NPs, and graphite degree on combustion and explosion: smaller agglomerates with larger specific surface area led to faster temperature rise; pyrophoric Fe-NPs could be ignited remotely with a favorable penetration topology of CNF agglomerates and therefore promote the heating of unburnt CNFs and facilitate the overall combustion and explosion process; CNFs with lower graphite degree required lower temperatures to initiate the combustion and explosion.

8.2 Future Work

8.2.1 Study of particle size and dispersion effect on the explosibility of nanomaterials

Experimental investigations of the particle agglomerate break-up in the flow passing through a nozzle at various velocities has been conducted. The investigation shows that the distribution of effective particle sizes shifts systematically towards smaller particles as the effective air velocity increases (Eckhoff, 2013).

When particles become smaller, the Van der Waals' forces increase. However, it is not prudent to ignore the dispersion's impact on agglomeration. This study collected CNF samples (sample 1 and 7 as representatives) after the 36-L vessel dispersion process under the same conditions as the explosibility testing and analyzed them by SEM. Results are shown in Figure 11 and Figure 12 in Section 3.4.2.

Progress in understanding the effect of particle size and dispersion on the explosibility of nanomaterials can be made, if the following are done:

1. A study using a combination of CFD simulations and experimental tests to investigate the effect of dispersion systems on nano-particle agglomeration. Previous research regarding dispersion effects focused on creating a uniform dust cloud inside the vessel. However, this study has shown that nanoparticle agglomerates were significantly affected after dispersion. The source of this de-agglomeration can be either the mechanical force of compressed air, or the shear force created by the nozzle and other parts of the dispersion system. A systematic study to find the key factors affecting agglomeration would be very valuable in developing a modified dispersion system for nano-materials, leading to more accurate explosibility measurements. To achieve this goal, a study using FLUENT CFD simulations, with experiments for verification, can be applied to a few candidate dispersion systems and industrially relevant combustible nanoparticles.
2. A comprehensive study of the effect of particle size and distribution on dust explosion characteristics such as MIE, K_{St}, and P_{max}. In this research, the explosibility of milled samples was enhanced due to their increased specific surface area of smaller agglomerates. However, in order to develop quantitative models to describe the effect of agglomerate size on explosibility, additional work needs to be conducted, including: observation of particle size distribution through more sophisticated methods, and measurements of dust characteristics

and parameters such as MIE, K_{St}, and P_{max} – some of which are functions of particle size. Currently, most equipment that observes the particle distribution is meant to ensure the dust cloud is uniform inside the vessel. Most methods assume that particle size distribution remains the same during dispersion. However, as we observed, agglomerate sizes changed significantly after dispersion. This will affect the uniformity of the dust clouds. Therefore, more sophisticated methods facilitate more accurate measurement of the agglomerate size distributions at different locations inside the vessel. A better dispersion system resulting in reduced agglomerate breakage of nanomaterials could provide more consistent and accurate explosibility results. Then the resulting explosibility data on nanomaterials (MIE, K_{St}, P_{max}) are more meaningful for developing safety guidelines in labs and industries.

8.2.2 Study of the laminar burning velocity

Laminar burning velocity is another parameter used to characterize the burning and explosion behavior of combustible dusts. However, this is an even rarer study than the explosibility of nanomaterials. Two possible approaches to this study are:

1. Equip the 36-L dust explosion vessel with an array of thermal transmitters. Most of the theories on estimating laminar burning velocity require temperature profiles during the explosion.
2. The other way is to measure the laminar burning velocity directly via high speed camera and image processing methods. However, the camera usually catches the

flame speed instead of the laminar burning velocity. A correlation between these speeds is needed.

8.2.3 Study of factors influencing nanomaterials' explosion

In this study, the influential factors of iron nanoparticles in CNFs, the graphite degree of CNFs, and the agglomerate size, were studied for their effect on the dust explosion characteristics. A semi-quantitative model was developed to explain the importance of the heat transfer processes during combustion and explosions. A more comprehensive study should be undertaken to further improve our understanding of these processes and their roles in the dust explosion. Proposed efforts include:

1. Study of impure materials or dust mixtures. In our study, the iron nanoparticles in the CNFs promoted the dust explosion process. The pyrophoricity of iron nanoparticles and the structure of CNF agglomerates contribute to the effect. It would be interesting to see if a mixture of Fe-NPs and CNFs would have similar results. In addition, it would be beneficial for academia and industry to test other materials and impurity effects.
2. Study of temperature profiles during explosions. While the heat transfer is the limiting factor in igniting an explosion of CNFs, an explosion involves, other processes including kinetic reactions and mass transfer. When the material and their properties change, other processes can become the limiting factor. Installation of temperature transducers in our 36-L dust explosion vessel could help provide insight into temperature development during a dust explosion.

3. Material characterizations, like thermogravimetric analysis (TGA) and differential scanning calorimetry (DSC) can provide more understanding about the properties of combustible nanomaterials.

REFERENCES

Abbasi, T., & Abbasi, S. a. (2007). Dust explosions-Cases, causes, consequences, and control. *Journal of Hazardous Materials*, *140*(1-2), 7–44. http://doi.org/10.1016/j.jhazmat.2006.11.007

Ajayan, P. M., Terrones, M., de la Guardia, a, Huc, V., Grobert, N., Wei, B. Q., … Ebbesen, T. W. (2002). Nanotubes in a flash--ignition and reconstruction. *Science (New York, N.Y.)*, *296*(April), 705. http://doi.org/10.1126/science.296.5568.705

Amyotte, P. R., Chippett, S., & Pegg, M. J. (1988). Effects of turbulence on dust explosions. *Progress in Energy and Combustion Science*, *14*(4), 293–310. http://doi.org/10.1016/0360-1285(88)90016-0

Andrews, R., Jacques, D., Qian, D., & Dickey, E. C. (2001). Purification and structural annealing of multiwalled carbon nanotubes at graphitization temperatures. *Carbon*, *39*(11), 1681–1687. http://doi.org/10.1016/S0008-6223(00)00301-8

ASTM. (2004). Standard Test Method for Iron in Trace Quantities Using the 1,10-Phenanthroline Method.

ASTM. (2012a). *ASTM E 1226: Standard Test Method for Explosibility of Dust Clouds*.

ASTM. (2012b). ASTM E1491: Standard Test Method for Minimum Autoignition Temperature of Dust Clouds.

ASTM. (2012c). ASTM F739 - 12e1 Standard Test Method for Permeation of Liquids and Gases through Protective Clothing Materials under Conditions of Continuous Contact.

ASTM. (2013a). *ASTM E 2019: Standard Test Method for Minimum Ignition Energy of a Dust Cloud in Air*.

ASTM. (2013b). ASTM E2021: Standard Test Method for Hot-Surface Ignition Temperature of Dust Layers.

ASTM. (2014). *ASTM E 1515: Standard Test Method for Minimum Explosible Concentration of Combustible Dusts*.

ASTM. (2015). *ASTM E 2931: A new standard for the limiting oxygen concentration of combustible dusts*.

Babrauskas, V. (2003). *Ignition handbook: principles and applications to fire safety engineering, fire investigation, risk management and forensic science*. Fire Science Publishers.

Bartknecht, W. (1987). Staubexplosionen: Ablauf u. Schutzmaßnahmen; 26 Tab.

Bartknecht, W. (2012). *Dust explosions: course, prevention, protection*. Springer Science & Business Media.

Blair, A. S. (2007). Dust explosion incidents and regulations in the United States. *Journal of Loss Prevention in the Process Industries*, *20*(4-6), 523–529. http://doi.org/10.1016/j.jlp.2007.03.012

Boilard, S. P., Amyotte, P. R., Khan, F. I., Dastidar, A. G., & Eckhoff, R. K. (2013). Explosibility of micron- and nano-size titanium powders. *Journal of Loss Prevention in the Process Industries*, *26*(6), 1646–1654. http://doi.org/10.1016/j.jlp.2013.06.003

Botelho, G., & Wang, K. (2015). More than 500 injured in explosion at Taiwan water park. Retrieved October 20, 2015, from http://www.cnn.com/2015/06/27/asia/taiwan-water-park-explosion/

Bouillard, J., Vignes, a, Dufaud, O., Perrin, L., & Thomas, D. (2010). Ignition and explosion risks of nanopowders. *Journal of Hazardous Materials*, *181*(1-3), 873–80. http://doi.org/10.1016/j.jhazmat.2010.05.094

Bradley, B. Y. D., Lau, A. K. C., & Lawes, M. (1992). Flame stretch rate as a determinant of turbulent burning velocity, *Philosophical Transactions of the Royal Society of London A: Mathematical, Physical and Engineering Sciences*, 338(1650), 359–387.

Burke, S., & Schumann, T. (1931). The mechanism of combustion of solid fuel. In *Proc. 3rd Intern. Conf. Bituminous Coal*.

Cashdollar, K. L. (1996). Coal dust explosibility. *Journal of Loss Prevention in the Process Industries*, *9*(1), 65–76.

Cashdollar, K. L. (2000). Overview of dust explosibility characteristics. *Journal of Loss Prevention in the Process Industries*, *13*(3-5), 183–199. http://doi.org/10.1016/S0950-4230(99)00039-X

Cashdollar, K. L., & Hertzberg, M. (1987). *Industrial Dust Explosions: Symposium on Industrial Dust Explosions : Pittsburgh, Pennsylvania, 10-13 June 1986*. Astm International.

Castellanos, D., Carreto-Vazquez, V. H., Mashuga, C. V., Trottier, R., Mejia, A. F., & Mannan, M. S. (2014). The effect of particle size polydispersity on the explosibility characteristics of aluminum dust. *Powder Technology*, *254*, 331–337. http://doi.org/10.1016/j.powtec.2013.11.028

Castellanos, D., Lewandowski, A., Mejia, A. F., Carreto, V., Mashuga, C., Rangwala, A. S., … Mannan, M. S. (2014). In fl uence of Particle Size and Crystalline Level on the E ffi ciency of Dust Explosion Inhibitors. *Industrial & Engineering Chemistry Research*, *53*(28), 11527-11537.

Castellanos, D., Skjold, T., van Wingerden, K., Eckhoff, R. K., & Mannan, M. S. (2013). Validation of the DESC Code in Simulating the Effect of Vent Ducts on Dust Explosions. *Industrial & Engineering Chemistry Research*, *52*(17), 6057–6067. http://doi.org/10.1021/ie4004943

Crowl, D. A., & Louvar, J. (2001). *Chemical process safety: fundamentals with applications*. Pearson Education.

CSB. (2011). *AL Solutions, Inc., New Cumberland, WV Metal Dust Explosion and Fire*.

CSB. (2012). Hoeganaes Corporation Fatal Flash Fires - Investigations | the U.S. Chemical Safety Board. Retrieved February 3, 2016, from http://www.csb.gov/hoeganaes-corporation-fatal-flash-fires/

CSB. (2015). US Ink Fire - Investigations | the U.S. Chemical Safety Board. Retrieved February 3, 2016, from http://www.csb.gov/us-ink-fire/

Dahoe, A. E., & de Goey, L. P. H. (2003). On the determination of the laminar burning velocity from closed vessel gas explosions. *Journal of Loss Prevention in the Process Industries*, *16*(6), 457–478. http://doi.org/10.1016/S0950-4230(03)00073-1

Dahoe, A. E., Zevenbergen, J. F., Lemkowitz, S. M., & Scarlett, B. (1996). Dust explosions in spherical vessels: the role of flame thickness in the validity of the 'cube-root law'." *Journal of Loss Prevention in the Process Industries*, 9(1) 33-44

Dastidar, A. G. (2005). Evaluation of dust and hybrid mixture explosion potential in process plants. *Process Safety Progress*, 24(4), 294-298.

Dastidar, A. G., Nalda-Reyes, B., & Dahn, C. J. (2005). Evaluation of dust and hybrid mixture explosion potential in process plants. *Process Safety Progress*, 24(4), 294–298. http://doi.org/10.1002/prs.10097

Denkevits, A., & Dorofeev, S. (2005). Dust explosion hazard in ITER: Explosion indices of fine graphite and tungsten dusts and their mixtures. *Fusion Engineering and Design*, *75-79*, 1135–1139. http://doi.org/10.1016/j.fusengdes.2005.06.032

Eckhoff, R. K. (2003). *Dust Explosions in the Process Industries: Identification, Assessment and Control of Dust Hazards: Third Edition*. *Dust Explosions in the Process Industries: Identification, Assessment and Control of Dust Hazards: Third Edition*. Gulf professional publishing.

Eckhoff, R. K. (2011). Are enhanced dust explosion hazards to be foreseen in production, processing and handling of powders consisting of nano-size particles? In *Journal of Physics: Conference Series* (Vol. 304, p. 012075). IOP Publishing.

Eckhoff, R. K. (2012). Does the dust explosion risk increase when moving from μm-particle powders to powders of nm-particles? *Journal of Loss Prevention in the Process Industries*, *25*(3), 448–459. http://doi.org/10.1016/j.jlp.2011.11.011

Eckhoff, R. K., Parker, S., & Gruvin, B. (1986). Ignitability and Explosibility of Silicon Dust Clouds Influence of Dust Fineness. *Journal of The Electrochemical Society*, *133*(12), 2631–2637.

Garcia-Agreda, A., & Benedetto, A. Di. (2011). Dust/gas mixtures explosion regimes. *Powder Technology*, *205*(1), 81–86.

Glor, M. (1985). Hazards due to electrostatic charging of powders. *Journal of Electrostatics*, *16*(2-3), 175–191. http://doi.org/10.1016/0304-3886(85)90041-5

Glor, M. (2001). Overview of the occurrence and incendivity of cone discharges with case studies from industrial practice. *Journal of Loss Prevention in the Process Industries*, *14*(2), 123–128. http://doi.org/10.1016/S0950-4230(00)00037-1

Graaf, D., & Brennst-Warme-Kraft, J. G. . (1965). No Title, *17*, 227.

Haase, H. (1977). *Electrostatic hazards: their evaluation and control*. Wiley-VCH.

Held, E. Van der. (1961). I3. The reaction between a surface of solid carbon and oxygen. *Chemical Engineering Science*, *14*(1), 300–312.

Hertzberg, M., Zlochower, I. A., & Cashdollar, K. L. (1988). Volatility model for coal dust flame propagation and extinguishment. *Symposium (International) on Combustion*, *21*(1), 325–333. http://doi.org/10.1016/S0082-0784(88)80260-1

Holbrow, P., Wall, M., Sanderson, E., Bennett, D., Rattigan, W., Bettis, R., … Hill, H. (2010). *Fire and explosion properties of nanopowders*. Buxton, UK.

Huang, W., Wang, Y., Luo, G., & Wei, F. (2003). 99.9% Purity Multi-Walled Carbon Nanotubes By Vacuum High-Temperature Annealing. *Carbon*, *41*(13), 2585–2590. http://doi.org/10.1016/S0008-6223(03)00330-0

Huang, Y., Risha, G. A., Yang, V., & Yetter, R. A. (2007). Combustion of bimodal nano/micron-sized aluminum particle dust in air. *Proceedings of the Combustion Institute*, *31*(2), 2001–2009. http://doi.org/10.1016/j.proci.2006.08.103

Jiang, J., Liu, Y., & Mannan, M. S. (2014). A correlation of the lower fl ammability

limit for hybrid mixtures. *Journal of Loss Prevention in the Process Industries*, *32*, 120–126. http://doi.org/10.1016/j.jlp.2014.07.014

Jiang, J., Liu, Y., Mashuga, C. V., & Mannan, M. S. (2015). Validation of a new formula for predicting the lower flammability limit of hybrid mixtures. *Journal of Loss Prevention in the Process Industries*, *35*, 52–58. http://doi.org/10.1016/j.jlp.2015.03.008

Jong, K. De, & Geus, J. (2000). Carbon nanofibers: catalytic synthesis and applications. *Catalysis Reviews*, *42*(4), 481–500.

Kalkert, N., & Schecker, H. (1979). Theoretische Überlegungen zum Einfluß der Teilchengröße auf die Mindestzündenergie von Stäuben. *Chemie Ingenieur Technik*, *51*(12), 1248–1249.

Kauffman, C. (1982). Agricultural dust explosions in grain handling facilities. *Fuel-Air Explosions, University of Waterloo Press*, 305–347.

Keane, T., Leng, D., & Prausnitz, J. (1985). Industrial & engineering chemistry fundamentals. *Journals Department*, *202*, 872–4600.

Kemsley, J. N. (2008). Explosion Injures Student - Accident Involved Nanostructured Explosive Materials. Retrieved October 20, 2015, from http://cen.acs.org/articles/86/web/2008/02/Explosion-Injures-Student.html

Krietsch, A., Scheid, M., Schmidt, M., & Krause, U. (2015). Explosion behaviour of metallic nano powders. *Journal of Loss Prevention in the Process Industries*, *36*, 237–243. http://doi.org/10.1016/j.jlp.2015.03.016

Liu, F., Zhang, X., Cheng, J., Tu, J., Kong, F., Huang, W., & Chen, C. (2003). Preparation of short carbon nanotubes by mechanical ball milling and their hydrogen adsorption behavior. *Carbon*, *41*(13), 2527–2532. http://doi.org/Doi: 10.1016/s0008-6223(03)00302-6

Liu, Y., Gao, X., Qian, W., Wang, Y., & Wei, F. (2011). Architectural and mechanical performances of carbon nanotube agglomerates characterized by compaction response. *Powder Technology*, *211*(2-3), 226–231. http://doi.org/10.1016/j.powtec.2011.04.024

Liu, Y., Qian, W., Zhang, Q., Cao, A., Li, Z., Zhou, W., … Wei, F. (2008). Hierarchical agglomerates of carbon nanotubes as high-pressure cushions. *Nano Letters*, *8*(5), 1323–7. http://doi.org/10.1021/nl0733785

Ma, X., Liu, L., Aronhime, N., & Zachariah, M. (2011). Ignition catalyzed by unsupported metal nanoparticles. *Energy & Fuels*, *25*(9), 3925–3933.

Mannan, S. (2005). *Lees Loss Prevention in the Process Industries*. *Federal Register* (Vol. 1). http://doi.org/10.1016/B978-0-12-397189-0.00014-8

Monthioux, M., No é, L., & Dussault, L. (2007). Texturising and structurising mechanisms of carbon nanofilaments during growth. *Journal of Materials Chemistry*, *17*(43), 4611–4618.

Moure-Eraso, R. (2014). The Danger of Combustible Dust. Retrieved March 17, 2015, from http://www.nytimes.com/2014/08/23/opinion/the-danger-of-combustible-dust.html?_r=1

Neufeld, P. D., Jansen, A. R., & Aziz, R. A. (1972). No Title. *The Journal of Chemical Physics*.

NFPA. (2012a). *NFPA 655: Standard for Prevention of Sulfur Fires and Explosions*.

NFPA. (2012b). *NFPA 664: Standard for the Prevention of Fires and Explosions in Wood Processing and Woodworking Facilities*.

NFPA. (2013a). *NFPA 61: Standard for the Prevention of Fires and Dust Explosions in Agricultural and Food Processing Facilities*.

NFPA. (2013b). *NFPA 654: Standard for the Prevention of Fires and Dust Explosions from the Manufacturing, Processing, and Handling of Combustible Particulate Solids*.

NFPA. (2014). *NFPA 484: Standard for Combustible Metals*.

NFPA, D. (2012c). 54-National Fuel Gas Code. *National Fire Protection Association*.

Nie, S., Han, X., Xu, H., Ding, Q., Wei, M., & Wu, W. (2015). The treatment and management of mass casualty in 2014 Kunshan explosion. *Wanfang Data*.

Ogle, R. A., Beddow, J. K., Vetter, A. F., & Chen, L.-D. (1984). A thermal theory of laminar premixed dust flame propagation. *Combustion and Flame*, *58*(1), 77–79. http://doi.org/10.1016/0010-2180(84)90081-6

Oner, E. (2007). Thermogravimetric Analysis. Retrieved from http://www.uzaktanegitimplatformu.com/UEP/uep_ylisans/ey2/uep_ey2.htm

OSHA. (2007). CPL 03-00-006 - Combustible Dust National Emphasis Program. Retrieved February 4, 2016, from https://www.osha.gov/pls/oshaweb/owadisp.show_document?p_table=DIRECTIVES&p_id=3729

OSHA. (2008). CPL 03-00-008 - Combustible Dust National Emphasis Program

(Reissued). Retrieved February 4, 2016, from https://www.osha.gov/pls/oshaweb/owadisp.show_document?p_table=DIRECTIVES&p_id=3830

Piccinno, F., & Gottschalk, F. (2012). Industrial production quantities and uses of ten engineered nanomaterials in Europe and the world. *Journal of Nanoparticle Research*, *14*(9), 1–11.

Pyrograf. (2012). Graphitic Carbon Nanofibers - Properties and Applications of Pyrograf III. Retrieved February 9, 2016, from http://www.azonano.com/article.aspx?ArticleID=3072#2

Rengasamy, S., Eimer, B. C., & Shaffer, R. E. (2009). Comparison of nanoparticle filtration performance of NIOSH-approved and CE-marked particulate filtering facepiece respirators. *Annals of Occupational Hygiene*,*53*(2), 117-128.

SAWS. (2014). *Incident investigation of Kunshan explosion*.

Smits, J., Wincheski, B., & Namkung, M. (2003). Response of Fe powder, purified and as-produced HiPco single-walled carbon nanotubes to flash exposure. *Materials Science and Engineering: A*, *358*(1), 384–389.

Turkevich, L. a., Dastidar, A. G., Hachmeister, Z., & Lim, M. (2015). Potential explosion hazard of carbonaceous nanoparticles: Explosion parameters of selected materials. *Journal of Hazardous Materials*, *295*, 97–103. http://doi.org/10.1016/j.jhazmat.2015.03.069

Turns, S. R. (2000). *An introduction to combustion: concepts and applications*. *System* (Vol. 499). http://doi.org/10.1016/j.ijhydene.2008.07.121

van der Wel, P. G. J., van Veen, J. P. W., Lemkowitz, S. M., Scarlett, B., & van Wingerden, C. J. M. (1992). An interpretation of dust explosion phenomena on the basis of time scales. *Powder Technology*, *71*(2), 207–215. http://doi.org/10.1016/0032-5910(92)80010-T

VDI-Richtlinien. (1990). Staubbr ¨ande und Staubexplosionen Gefahren-Beurteilung-Schutzma ßnahmen. In *Beuth Verlag GmbH*. Berlin.

Vignes, a., Dufaud, O., Perrin, L., Thomas, D., Bouillard, J., Jan ès, a., & Valli ères, C. (2009). Thermal ignition and self-heating of carbon nanotubes: From thermokinetic study to process safety. *Chemical Engineering Science*, *64*(20), 4210–4221. http://doi.org/10.1016/j.ces.2009.06.072

Vorderbrueggen, J. B. (2011). Imperial sugar refinery combustible dust explosion investigation. *Process Safety Progress*, *30*(1), 66–81.

http://doi.org/10.1002/prs.10445

Wang, N. (2012). *Boron Composite Nanoparticles for Enhancement of Bio-Fuel Combustion*. Louisiana State University.

Worsfold, S. M., Amyotte, P. R., Khan, F. I., Dastidar, A. G., & Eckhoff, R. K. (2012). Review of the Explosibility of Nontraditional Dusts. *Industrial & Engineering Chemistry Research*, 120125112424001. http://doi.org/10.1021/ie201614b

Wu, H.-C. (2010). Explosion Characteristics of Aluminum Nanopowders. *Aerosol and Air Quality Research*, 38–42. http://doi.org/10.4209/aaqr.2009.06.0043

Wu, H.-C., Chang, R., & Hsiao, H. (2009). Research of minimum ignition energy for nano titanium powder and nano iron powder. *Journal of Loss Prevention in the Process Industries*, *22*(1), 21–24.

Wu, H.-C., & Wu, J. (2008). *Study of explosion characteristics of industrial nano dust used in domestic*.

Zhang, H., Wang, J., Zhang, C., Wang, Z., & Wang, S. (2011). Dangerous, an explosion of polyaniline nanomaterials. *Synthetic Metals*, *161*(5-6), 544–547. http://doi.org/10.1016/j.synthmet.2010.12.032

Zhang, J., Chen, H., Liu, Y., Elledge, H., Mashuga, C. V., & Mannan, M. S. (2015). Dust Explosion of Carbon Nanofibers Promoted by Iron Nanoparticles. *Industrial & Engineering Chemistry Research*, *54*(15), 3989–3995. http://doi.org/10.1021/acs.iecr.5b00341